The role of Polo-like kinase 2 in early meiotic chromosome motion in *Caenorhabditis elegans*

Anja Boskovic

Department of Biology
McGill University, Montreal

November 2016

A thesis submitted to McGill University in partial fulfilment of the requirements of the degree of Master of Science

Table of Contents

List of Figures and Tables

Chapter I

Chapter II

Abstract

Meiosis is a series of cell divisions which ensures that the DNA content of a cell is reduced by half in preparation for fertilization. Any defect in the meiotic machinery could give rise to chromosomal aneuploidy, which can be lethal or result in severe developmental abnormalities in the ensuing progeny. Upon meiotic onset in the nematode *Caenorhabditis elegans*, *cis*-acting regions at one end of each chromosome, termed pairing centres (PC), recruit PC proteins and associate with the inner nuclear envelope protein, SUN-1. The Polo-like kinase, PLK-2, localizes to the PC proteins and facilitates phosphorylation of the S12 residue on SUN-1. SUN-1 proceeds to self-oligomerize into distinct foci which further coalesce with one another into larger patches. Through its C-terminal domain, SUN-1 associates with ZYG-12, to transmit forces from the cytoskeleton to the PCs of chromosomes, thus promoting dynamic chromosome end motion. Disruption in the association between SUN-1 and ZYG-12 in *sun-1(jf18)* mutants results in an annulment in chromosome end motion, and consequent high levels of embryonic lethality. To further investigate the impact of PLK-2 on chromosome motion, and to improve our understanding of the important factors of chromosome motion, fusion proteins of PLK-2 and its mutants tagged with the fluorescent protein mCherry were constructed. We found that PLK-2 kinase activity is essential for dynamic chromosome motion. In its absence, chromosomes are limited to small jittery movements and interact with greatly reduced frequency. We also provided evidence that the coalescing of SUN-1/ZYG-12 foci is not required for chromosome motion. However, mobile chromosomes are not sufficient for accurate chromosome pairing. In *plk-2(vv44)* mutants, chromosomes are movement-competent, but have difficulty in locating their homolog and in forming durational cohesive patches with other chromosomes. In order to further understand how PLK-2 regulates and

coordinates homology search, we collaborated with MRC Clinical Sciences to conduct a quantitative phosphoproteomics experiment which compared the phosphoproteomes of wild type animals and *plk-2* mutants. Using the resulting datasets, we identified 126 potential PLK-2 phosphorylation target sites for further analysis and provided evidence for 2 possible PLK-2 docking motifs.

Résumé

La méiose est une série de divisions cellulaires qui garantit que la teneur en ADN d'une cellule soit réduite de moitié en vue de la fécondation. Tout défaut dans le mécanisme de la méiose pourrait donner lieu à une aneuploïdie chromosomique, qui peut être mortelle ou entraîner des anomalies graves du développement de la progéniture. Dès le début de la méiose chez les nématodes Caenorhabditis elegans, des régions à effet cis a une extrémité de chaque chromosome, appelés centres d'appariement (PC), recrutent des protéines de PC qui s'associent avec une protéine de l'enveloppe nucléaire interne; SUN-1. La kinase polo-like, PLK-2, se trouve avec les protéines de PC et facilite la phosphorylation du résidu S12 sur SUN-1. SUN-1 procède à l'auto-oligomérisation en des foyers distincts qui coalescent avec d'autre afin d'en former des plus grands. Grâce à son domaine terminal C, SUN-1 associé avec ZYG-12, pour transmettre les forces du cytosquelette aux PC des chromosomes, favorisant ainsi le mouvement dynamique des extrémités des chromosomes. Perturbation dans l'association entre SUN-1 et ZYG-12 dans le mutant *sun-1(jf18)* se traduit par une annulation du mouvement des extrémités des chromosomes, qui conduis a des niveaux élevés de létalité embryonnaire. Pour étudier davantage l'impact des PLK-2 sur le mouvement des chromosomes, et d'améliorer notre compréhension des facteurs importants dans le mouvement des chromosomes, des protéines de fusion de PLK-2 et de ses mutants marquées avec la protéine fluorescente mCherry ont été construits. Nous avons constaté que l'activité kinase de PLK-2 est essentielle pour le mouvement dynamique des chromosomes. En son absence, les chromosomes sont limités à de petits mouvements nerveux et interagissent bien moins souvent. Nous avons également fourni des preuves que l'auto-oligomérisation de SUN-1 / ZYG-12 n'est pas nécessaire pour le mouvement des chromosomes. Cependant, les

chromosomes mobiles ne sont pas suffisants pour un appariement précis des chromosomes. Dans *plk-2(vv44)* mutants, les chromosomes ont un mouvement compétent, mais ont de la difficulté à trouver leur homologue ainsi que dans la formation de foyers de cohésion duratifs avec d'autres chromosomes. Afin de mieux comprendre comment PLK-2 régule et coordonne la recherche d'homologie, nous avons collaboré avec les Sciences Cliniques MRC afin de mener une expérience phosphoprotéomique quantitative qui a comparé les phosphoproteomes des animaux de type sauvages et de mutants PLK-2. En utilisant les ensembles de données obtenus, nous avons identifié 126 cibles potentielles de phosphorylation par PLK-2 pour une analyse plus approfondie et avons fourni des preuves de l'existence de 2 motifs d'aammarage pour PLK-2.

Acknowledgements

While in the valley of a Masters one often feels like they are Sisyphus, alone and trying to push a boulder up a hill only to have it roll back down. In truth, I had others beside me helping me. Without their invaluable support this body of work would not exist and my time spent pushing the boulder of scientific inquiry wouldn't have been half as pleasant.

I would like to start by thanking my supervisor Dr. Monique Zetka, who took a risk taking on a computational student in her classical biology lab. Since then, she has helped motivated me through my roadblocks, ensured I had all the support, tools and funding I needed to do my work and was endlessly patient while I was learning my craft. My time spent doing this work would not have been half as pleasant if it weren't for the environment she has crafted and curated for our success. Additionally, Dr. Monique Zetka came up with the project and asked the questions which inspired the strategy undertaken for the progression of the research. Thank you Monique, for everything.

I would also like to thank the other members of my committee, Dr. Gary Brouhard and Dr. Craig Mandato, who provided feedback on my Chapter I experiments and contributed insight on the analysis of fluorescence images.

I would like to thank Dr. Jon Sakata and the QCBS R workshops for planting the seeds for my statistical sophistication. Without their help this paper would've been full of inappropriate *t*-tests.

Thanks to Dr. Michael Hallett, Dr. Vanessa Dumeaux and the students of the McGill BCI lab for their guidance and feedback on the work in Chapter II. Thank you for instilling in me the discipline to investigate every aspect of my data and the importance of understanding all of the tools I use on a deep level. They also provided assistance in the method of analysis that was chosen and helped guide my literature review.

A special thanks goes to my collaborator and partner in Biology Dr. Sara Labella. Dr. Sara Labella was a PhD student when she started working with me and taught me everything I know about wet lab work. She instilled in me a humility and appreciation for the difficulty and complexity of wet lab work. It's not an over-exaggeration to say the work wouldn't exist without her, because it was thanks to her skill in creating fusion constructs that the genotypes I worked with even existed. Dr. Sara Labella was also the one who isolated and first began to characterize the allele *plk-2(vv44)*. Her work was the backend of my own analysis. This can be most directly seen in the number of times I cited Labella et al., 2011 and Labella, 2012. Additionally, she has emotionally supported me every step of the way and encouraged me to cherish my time off of work. To her I owe a debt of gratitude. Grazi Sara. <3

I would like to thank the other past and present members of the Zetka lab. My fellow Masters students, Hanh Nguyen and Camille Delouche, provided feedback, support and company during those long days in the lab. Older students Jasmin Hanafi and Aleksandar Vujin provided advice in navigating my Masters. Dr. Annina Spilker always ensured there was a smile on my face. They are all my cherished friends with whom I hope to still engage with many years in the future. No future workplace will ever live up to the high expectations you guys set.

I would like to thank the undergrad I mentored Julyan Barouch, who kept me on my toes by writing all his code in Java (use R or Python Julyaaaaaaan) and who worked me in the early stages of Chapter II. I wish him the best of luck in the continuation of his studies.

I would like to extend gratitude to Dr. Elke Küster-Schöck who was a member of the CIAN microscopy facility while I was working on my Masters. Her company and assistance during those dark and stormy nights spent imaging and analyzing images using Imaris kept me sane. She taught me how to use both the software and the microscope and always provided help when I ran into problems with either.

I would like to additionally thank Dr. Richard Roy and the other members of the Roy Lab who provided me with side Bioinformatic projects to play with and who provided feedback on my work and its presentation during lab meetings.

I would like to extend gratitude to fellow student Melanie Segado, who is my Beverly Crusher. She directly helped with the reviewing of Chapter II but on top of that the Monday breakfasts with her were a comforting part of my routine.

Last but certainly not least are the non-scientists in my life. Thank you to my family for supporting my decision to attend McGill University for my Masters and for providing me with emotional and financial assistance. Without that support none of this would have happened. No words are sufficient to apologize for the stress I have put you through or to thank you for all the love and support you have provided me unconditionally. Thank you for everything and thank you for believing in me and for always expecting the best.

I would like to extend gratitude to my dearest Mano Majumdar who is my centre, and whose influence can be directly seen in the typeface chosen for this thesis. His dedication to style and excellence helped with the design of Figure 8A in Chapter I and Table 8 in Chapter II. Not seen in this thesis is the joy he brought me and the hours spent helping me keep calm and carry on. Everyone should have an engineer that helps them navigate through the Red Alerts of life. Thank you for being the engineering officer to my science officer.

That’s all, folks!

Contribution of Authors

Dr. Monique Zetka proposed the original research question and reviewed the thesis. Dr. Monique Zetka, Dr. Sara Labella and I came up with the successive follow-up research questions and I came up with the avenues to answer the questions. I have produced all of the writing, collected all of the data in Chapter I, created all of the figures, and performed all of the statistical and computational analyses other than the initial processing of the mass spectrometry data. Dr. Sara Labella and I produced the movies that were analyzed. Dr. Sara Labella mapped and cloned the *plk-2(vv44)* allele. She constructed all of the mutant worm strains (further details are in Labella, 2012). She performed the *syp-1(RNAi)* experiment. I performed the *syp-2(RNAi)* experiment. MRC Clinical Science Center performed the mass spectrometry experiment and processed the raw data. Details of their contribution are in the "Mass Spectrometry" section in the Methods of Chapter II. Dr. Michael Hallett confirmed that I should focus on the fold change as a method of comparison in Chapter II. He also recommended using the Fisher's exact test for analysis of Docking Motif Enrichment. Chapter I and II were both reviewed by Aleksandar Vujin. Chapter I was reviewed by Dr. Sara Labella. Chapter II was reviewed by Melanie Segado.

Chapter I

PLK-2 kinase activity is required for dynamic chromosome motion

Introduction

Overview of meiotic chromosome segregation

Meiosis is a series of two reductional cell divisions in which one diploid parental cell produces four haploid daughter cells in preparation for fertilisation. This involves one DNA replication event, followed by the segregation first of homologous chromosome pairs, and then sister chromatid pairs. Unlike the sister chromatids, homologous chromosomes are not physically linked at meiotic onset, but rather are independently scattered throughout the nucleus (Oliveira and Nasmyth, 2010). Accurate chromosome segregation relies on the occurrence of a series of tightly regulated steps during the extended prophase of meiosis I. In leptotene, chromosomes must first find their homolog and align in close proximity for long enough to initiate pairing (Reviewed in Zickler, 2006 and Colaiácovo, 2006). By the end of zygotene, a proteinaceous structure (the synaptonemal complex) will have formed along the axis of the homologs. This process, called synapsis, further stabilizes the association between homologs (Page and Hawley, 2004). By pachytene, double-strand breaks have formed along the chromosome (Mets and Meyer, 2009). Most of these breaks are repaired as non-crossovers. In *Caenorhabditis elegans* nematodes, one double-strand break per chromosome undergoes homologous recombination to form the obligate crossover during pachytene (Barnes et al., 1995; Mets and Meyer, 2009; Nottke et al., 2011). This process allows homologs to exchange genetic material, which permits the formation of novel gene combinations, thus contributing to biological diversity. The chiasmata are the physical linkages resulting from crossovers which hold the homologs together in a bivalent conformation once the synaptonemal complex disassembles by the end of diplotene. As bivalents, the homologs are able to orient towards opposite poles along the metaphase plate, which aids in proper chromosome segregation

(Östergren, 1951; Nicklas, 1994). Failure to accurately segregate chromosomes results in aneuploidy of the gametes and therefore aneuploid embryos. In most organisms, chromosomal aneuploidy may result in the formation of tumours and/or severe developmental abnormalities (Torres et al., 2008). While *C. elegans* nematodes may still be viable while subjected to some degree of genetic imbalance (Hodgkin, 2005), most of the time autosomal chromosome mis-segregation is lethal for the embryo. X chromosome mis-segregation results in a high incidence of male worms, which are usually rare in the predominantly hermaphrodite population (Hodgkin et al., 1979). While much research has gone into the study of the general steps required for accurate chromosome segregation, many of the details of coordination and regulation of each step remain an open question. Previous research by Sara Labella has involved the discovery of a key protein involved in regulating homology search and recognition, PLK-2 (Labella et al., 2011; Labella, 2012). In this thesis, I provide further evidence and characterization of PLK-2's role in the chromosome dynamics required for successful homology search.

Introduction to the meiotic bouquet

In premeiotic nuclei, chromosomes are immobile and randomly positioned throughout the nucleus (MacQueen and Villeneuve, 2001). For most eukaryotes, in early leptotene, chromosomes mobilize and the telomeres associate with the inner nuclear envelope (NE). By late leptotene, the telomeres have moved along the NE and polarized towards one end of the nuclear periphery (Scherthan et al., 1996). Since the late 1800s, biologists have witnessed this bundling of the telomeres in early prophase in cytological studies of the flatworm *Dendrocoelum lacteum* and have termed it the "chromosomal bouquet" (reviewed in Scherthan, 2001; Zickler and Kleckner, 1998). The meiotic bouquet has been observed in many organisms,

and is considered to be a conserved feature of meiosis across kingdoms. Bouquet formation has been shown to be actin and/or microtubule dependent depending on the organism (Trelles-Sticken et al., 2005; Sato et al., 2009). Meiosis-specific adaptor proteins which mediate the telomere association with the NE have also been identified (Conrad et al., 2008; Phillips and Dernburg 2006; Chikashige et al., 2006). Despite the amount of currently known molecular details, the role of the chromosomal bouquet in pairing remains an outstanding question. However, it has been shown in yeast that loss of bouquet formation results in increased mis-segregation and reduced levels of genetic recombination (Cooper, 2000; Yamamoto and Hiraoka, 2001). The bouquet has been theorized to assist in homology search by limiting the search space and hence contributing to the efficiency of pairing (Loidl, 1990; Roeder, 1997; Schlecht et al., 2004). It has also been hypothesized that the dynamic movements of the meiotic bouquet may prevent the entanglement and accidental pairing of heterologous chromosomes (Koszul and Kleckner, 2009). In *C. elegans*, there exists an alternate form of the bouquet. Instead of the telomeres, *cis*-acting regions at one end of each chromosome cluster and associate with the inner NE (Rose et al., 1984; Sanford and Perry, 2001). Despite the fact that in *C. elegans* the meiotic chromosomes adopt a configuration which differs from the meiotic bouquet, both the bouquet and the polarization of *C. elegans* chromosomes have the same predicted function of assisting in chromosome pairing. This allows us to take advantage of multiple benefits of using the *C. elegans* model system. By studying meiotic chromosome motion in *C. elegans*, we will improve our understanding of the role of the bouquet in homologous chromosome pairing in other eukaryotic organisms.

The *C. elegans* model system

The model organism used in this study is the nematode *C. elegans.* Due to the fact that *C. elegans* is transparent, it is ideal for live-imaging microscopy. In both males and hermaphrodites, the adult gonads contain germ cell nuclei at all stages of meiotic prophase. These stages are organized temporally and spatially along the distal-proximal axis within the gonads (Crittenden et al., 1994). This means that we can easily locate and focus on nuclei in the leptotene-zygotene stage, the period when homology search and pairing takes place. The leptotene-zygotene nuclei are positioned in the region of the gonad termed the Transition-Zone (TZ) (Hirsh et al., 1976; Crittenden et al., 1994). A final advantage of using *C. elegans* is that it only has 6 chromosome pairs. This makes chromosome behaviour easier to track and characterize.

Overview of prophase I in *C. elegans*

Over the course of homology search, chromosome ends come in close proximity to one another and homology assessment occurs. Pairing refers to the meeting and the local stabilization of the alignment of homologous chromosomes (Peoples et al., 2002). In *C. elegans* a region of oligonucleotide repeats located at one end of each chromosome associates with the inner NE (Rose et al., 1984; Sanford and Perry 2001). These *cis*-acting regions have been termed pairing centres (PCs) and they are fundamental in initially stabilizing pairing (McKim et al., 1988; Villeneuve, 1994). Their discovery involved the exchange of these regions between two non-homologous chromosomes which led to crossover suppression in those regions (Rosenbluth and Baillie, 1981). Later it was found that mutations in the X chromosome PC resulted in decreased levels of homolog crossing over between X chromosomes and high levels of X chromosome nondisjunction (Villeneuve, 1994). A family of four zinc-finger C_2H_2 proteins

(ZIM-1, 2, 3 and HIM-8) localize to the PCs and are termed PC proteins (Phillips and Dernburg, 2006). ZIM-1 localizes to chromosome II and III, ZIM-2 to chromosome V, ZIM-3 to chromosome I and IV and HIM-8 to the X chromosome. Interaction between matching PC proteins would not be sufficient in identifying homologous chromosome partners, since both ZIM-1 and ZIM-3 bind to two different chromosomes. In the absence of a PC protein, the respective chromosomes fail to pair.

Synapsis is the process by which a proteinaceous structure, the synaptonemal complex (SC), forms between two chromosome pairs. In *C. elegans* and *Drosophila melanogaster,* pairing is genetically separate from synapsis. While SC assembly is coordinated with pairing (Phillips et al., 2005), it can form along the axis of a pair of heterologous chromosomes in *C. elegans* (Leu et al., 1998; Tsubouchi and Roeder, 2002; Couteau and Zetka, 2005; Martinez-Perez and Villeneuve, 2005; Penkner et al., 2007; Baudrimont, 2010). Additionally, in mutants in which proteins that are required for the formation of the SC are knocked out, the PCs are sufficient to transiently stabilize homologous chromosome alignment in the PC region (Moreau et al., 1985; Loidl et al., 1994; Weiner and Kleckner, 1994; Nag et al., 1995; MacQueen et al., 2002, 2005). However, synapsis is required in order to stably pair along the full length of the chromosome. In the absence of all of the PC proteins, synapsis does not occur (Phillips and Dernburg 2006; Phillips et al., 2005).

The SC is composed of proteins which align along the chromosomal axis (the axial elements), and the central region (transverse elements) between the paired homologous chromosomes during leptotene-zygotene. Its full assembly can be seen with immunostaining. It appears as a zipper-like structure between chromosomes (MacQueen et al., 2002). Prior to homolog pairing, HIM-3 and HTP-1/2/3 begin assembling along the axes of chromosomes. These axial

elements are important in coordinating pairing with synapsis. In the absence of HTP-1/2, chromosomes fail to properly cluster and chromosomes precociously synapse with a heterologous partner. In the absence of HTP-3, HIM-3 fails to localize to the meiotic chromosomal axes. In *him-3* null mutants, synapsis is defective and chromosomes fail to synapse (Zetka et al., 1999; Couteau et al., 2004; Couteau and Zetka, 2005; Goodyer et al., 2008). The transverse elements of the SC (SYP-1/2/3/4) localize between the axes of paired homologs. Each of the SYP proteins is required for the assembly of the full complex. Knocking out any of the SYP proteins effectively abrogates synapsis (MacQueen et al., 2002; Colaiácovo et al., 2003; Smolikov et al., 2007, 2009).

Synapsis is important for the promotion of recombination and crossovers (Colaiácovo, 2003). The synapsed chromosomes undergo multiple double-strand breaks, initiated by SPO-11, from which one obligate crossover per chromosome pair forms (Mets and Meyer, 2009; Nottke et al., 2011). This crossover triggers the asymmetric disassembly of the SC in late pachytene, which allows for the formation of the chromosome bivalent structure (Nabeshima et al., 2005). In some organisms, problems in recombination impact the progression of earlier meiotic events, such as pairing. In *C. elegans*, knocking out key proteins involved in recombination does not impact pairing.

Factors important in chromosome motion during prophase I

Forces applied by the cytoskeleton and associative motor proteins have a conserved role in dynamic chromosome motion (Alsheimer, 2008; Hiraoka and Dernburg, 2009; Koszul and Kleckner, 2009; Sato et al., 2009; Wynne et al., 2012). SUN-1 and ZYG-12 are transmembrane proteins which span the NE and connect the cytoplasmic cytoskeletal network with chromosomes (Tzur et al., 2006; Minn et al., 2009, Sato et al., 2009). When meiosis begins, the

PCs associate with SUN-1 (Alsheimer, 2008; Hiraoka and Dernburg, 2009). SUN-1 then interacts through its C-terminal SUN domain with the C-terminal KASH domain of the outer NE protein ZYG-12 (Malone et al., 2003; Padmakumar, 2005; McGee et al., 2006; Minn et al., 2009). In the *sun-1(jf18)* mutant, SUN-1 is unable to retain ZYG-12 in the outer NE, therefore disrupting the link between SUN-1 and ZYG-12. In this mutant, chromosomes remain randomly distributed throughout the nucleus (Penkner et al., 2007, 2009) and chromosome speed sharply decreases (Baudrimont et al., 2010; Wynne et al., 2012), showing that cytoskeletal force transduction through the SUN/KASH domain proteins is essential for dynamic chromosome end motion in TZ nuclei. Imaging of the gonads of worms which express SUN-1::GFP has revealed that in mitotic precursor cells, SUN-1 is uniformly dispersed around the NE (Penkner et al., 2009). Phosphorylation of SUN-1 at Serine 12, upon entrance into meiotic prophase, results in SUN-1 focussing into distinct foci, which mobilize and further cluster into larger patches in a limited part of the NE (Penkner et al., 2009; Sato et al., 2009; Labella et al., 2011). These clusters of SUN-1/ZYG-12 patches have been shown to co-localize with PC proteins (Penkner et al., 2007, 2009; Sato et al., 2009). The patches are dynamic and have been used to infer chromosome end motion. Earlier studies showed that SUN-1/ZYG-12 undergo at least two distinct modes of motions. SUN-1/ZYG-12 mostly perform small diffusive movements that result in very small displacements. However, 10-15 % of the time, SUN-1/ZYG-12 move long distances in one direction, resulting in larger displacements (Baudrimont et al., 2010; Wynne et al., 2012). During these movements, SUN-1 has been shown to jump from speeds of 40-160 nm/s to speeds of 160-260 nm/s (Baudrimont et al., 2010); ZYG-12 has been shown to increase from an average speed of 125 nm/s to average peak speeds of 400 nm/s (Wynne et al., 2012). Using HIM-8 fluorescent transgenes, it has been shown that these modes of speed are also

undergone by the PCs of X chromosomes. X chromosome PCs spend 79 % of the time moving at an average speed of 82 nm/s and then 21 % of the time undergo what was termed processive chromosome motions (PCMs) that have an average speed of 120 nm/s (Wynne et al., 2012). These large increases in movement have been shown to be dynein-dependent (Wynne et al., 2012) and are thought to be the result of motor proteins pulling along a cytoskeletal track (Baudrimont et al., 2010; Wynne et al., 2012). During pachytene, dephosphorylation of SUN-1 triggers re-dispersion of SUN-1 foci and patches in concert with re-dispersion of chromosome ends (Penkner et al., 2009).

Previous studies in our lab have found evidence that the protein Polo-like kinase 2 (PLK-2) is a key player in homologous chromosome pairing and in meiotic chromosome motion (Labella et al., 2011; Labella, 2012). PLK-2 is a member of the polo kinase family; it is recruited by ZIMs/HIM-8 to the PCs. The PCs then localize to SUN-1 in the inner NE, and PLK-2 mediates the phosphorylation of Serine 12 on SUN-1 (Labella et al., 2011). This results in two distinct outcomes. First, it initially aggregates SUN-1 into foci in the periphery. It then allows these foci to coalesce into larger patches which promote chromosome homology assessment. The movement of the chromosomes during the homology search is driven by the cytoskeletal microtubule network connected to the chromosomes via SUN-1/ZYG-12 (Penkner et al., 2009; Sato et al., 2009; Baudrimont et al., 2010; Wynne et al., 2012).

We wished to further characterize the role of PLK-2 in regulating early meiotic chromosome dynamics. Previously, the motion of all of the chromosome ends had only been indirectly inferred through the tagging of X chromosomes and NE proteins. Through, the use of PLK-2 fluorescent transgenes, we were able to tag the PCs of chromosomes and directly track chromosome ends in the TZ of *C. elegans* germline. We utilized alleles which led to the

expression of PLK-2 and SUN-1 mutant proteins in order to investigate the impact of PLK-2 kinase activity and NE reorganization on various factors of chromosome motion during homology search. In doing so, we've uncovered some of the important parameters of chromosome motion and provided evidence for how they are regulated by PLK-2 kinase activity.

Experimental Procedures

Plates and culture

The *C. elegans* strains were kept on solid NGM within plates. The solid NGM was made using 20 g agar, 0.55 g Tris HCl, 0.25 g Tris base, 3.1 g bacto-peptode and 0.008 g cholesterol. The mixture was increased to a total volume of 1 L using distilled H_2O. The solution was then autoclaved for sterilization, poured into plates and left to cool until solid.

The LB liquid culture medium for the bacterial strains used to feed the nematodes was made using 10 g bacto-tryptone, 5 g yeast extract, 10 g NaCl and increased to a total volume of 1 L with distilled H_2O. The solution was then autoclaved for sterilisation.

Transgenic worm strains

EZ332: plk-2(tm1395) I; ttTi5604 vvls15 II; unc119(ed3) III; vvls15[Ppie-1::mCherry::plk-2, unc-119(+)]

EZ333: plk-2(tm1395 I; uTi5605 vvls16 II; unc119(ed3) III; vvls16[Ppie-1::mCherry::plk-2(vv44), unc-119(+)]

EZ347: plk-2(tm1395) I; ttT5605 vvls18 II; unc-119(ed3) III; vvls18[Ppie-1::mCherry::plk-2(K65M), unc-119(+)]

EZ349: plk-2(tm1395) I; ttTi5605 vvls16 II; unc-119(ed3) III; sun-1(jf18)/nt1 (IV; V) vvls16[Ppie-1::mCherry::plk-2(vv44), unc-119(+)]

EZ371: plk-2(vv44) I; him-8(tm611) IV; ttTi5605 vvls17 II; unc119(ed3) III; H2B::GFP vvls[Ppie-1::mCherry::hm-8::unc54ter, unc-119(+)]

EZ373: him-8(tm611) IV; ttTi5605 vvls17 II; unc-119(ed3) III; H2B::GFP vvls17[Ppie-1::mCherry::him-8::unc54ter, unc-119(+)]

These strains were constructed by Sara Labella (Labella, 2012).

For simplicity, in this thesis **EZ332** is referred to as *plk-2::mCherry*; **EZ333** as *plk-2(vv44)::mCherry*; **EZ347** as *plk-2(K65M)::mCherry*; **EZ371** as *plk-2(vv44)::mCherry; sun-1(jf18)*; **EZ371** as *him-8::mCherry*; **EZ373** as *plk-2(vv44); him-8::mCherry*. In Figures, *mCherry* is abbreviated to *mCh.*

Time-lapse microscopy

In preparation for microscopy, young adult worms were mounted on 2 % agarose pads in 5 mM levamisole on microscopy slides. The levamisole would paralyze the worms so they wouldn't move around on the agarose. The pad was covered with a coverslip and sealed with nail polish at the corners.

Time lapses were recorded with a Spinning-disc confocal microscope (Leica DMI 6000B inverted microscope equipped with a Quorum WaveFX spinning Disc and EM CCD camera) using a 63x objective (NA 1.4 – 0.6 DIC Oil).

The transition zone (TZ) nuclei were identified using markers which allowed the visualization of chromosome clustering. With *plk-2::mCherry, plk-2(vv44)::mCherry, plk-2(K65M)::mCherry* and *plk-2(vv44)::mCherry; sun-1(jf18)* strains, the TZ nuclei were identified by a combination of their position within the gonad and by a background mCherry signal which delineated the nuclei. With *him-8::mCherry* and *plk-2(vv44); him-8::mCherry* strains, the TZ nuclei were marked using H2B::GFP.

These nuclei were then observed for the localization and movement of the mCherry signal. 5 minute and 8 seconds movies of the TZ nuclei were assembled from time-lapse images taken every 7 seconds (with *plk-2::mCherry, plk-2(vv44)::mCherry, plk-2(K65M)::mCherry* and *plk-2(vv44)::mCherry; sun-1(jf18)* worms) or every 12 seconds (with *him-8::mCherry* and *plk-2(vv44; him-8::mCherry* worms*)* with 0.5 µm spaced Z-stacks. The longer timelapse of the latter was due to those strains having two different fluorescent proteins, GFP and mCherry.

These movies were limited to a duration of ~5 minutes because the image quality was compromised by photo bleaching.

4D tracking

The images were aligned using **Imaris** software *(***Bitplane***)*. The positions of a nucleus over time in each section of the gonad were used to align the dataset during that section's analysis. This was to control for movement of the nematode during recording. Nuclei were ascertained based on H2B::GFP or mCherry background fluorescence and then modelled as a sphere through manual use of the **Imaris (Bitplane)** *Spots* tool. Alignment was then performed using the *Correct for Drift* tool to apply a translational shift. This minimized the movement of the nuclei.

After alignment, the PLK-2::mCherry or HIM-8::mCherry signal was detected and tracked using the *Spots* tool. These tracks were then edited manually to eliminate inappropriate connections and tracks were connected when two signals overlapped into one signal and separated when a signal split into two separate signals.

Data about the "spot's" distance covered, velocity, fluorescence intensity was then downloaded from **Imaris (Bitplane)** and processed using custom Python (v3.5.2) scripts (https://github.com/damedebugger/Thesis).

RNAi feeding

Bacterial clones which were used for RNAi feeding were obtained from the Ahringer *C. elegans* RNAi bacterial library. The bacterial clones were cultured in 3 mL of LB liquid culture medium. 300 µg of ampicillin was added in order to select for the bacteria that contained the RNAi vector. They were then left overnight in a rocker at 37°C. Plates were made which contained solid NGM with added 50 µg/mL ampicillin, for additional selection, and 1 mM IPTG, to induce RNAi expression. Then the RNAi bacteria were streaked onto the plates in a sterilized environment. For each experiment, we created 3 plates which were streaked with a bacterial clone which carried an empty L4440 vector as negative a control. Plates were left overnight at room temperature in order to induce dsRNA.

Synchronized L1 worms were placed on each RNAi plate. After 3 days, worms had developed into adults and were subsequently imaged.

Distance between a pair of X chromosomes

Distances between the two X chromosomes in a nucleus were evaluated using **Imaris (Bitplane).** Nematode strains with a *him-8::mCherry* and *H2B::GFP* construct were used. Individual nuclei were identified using the H2B::GFP signal, which is a histone marker which delineates the DNA content of the nucleus. Within the confines of individual nuclei, the two X chromosome signals were marked by HIM-8::mCherry, a pairing centre protein which localizes to the X chromosome ends during prophase I. The *Distance* tool with the Line parameter selected was used to mark and connect the centres of each of the two HIM-

8::mCherry signals delineated by a nucleus. The distances between these two points were downloaded from **Imaris** and processed with a custom Python (v3.5.2) script (https://github.com/damedebugger/Thesis).

Statistics

Statistical tests were run using R (*v3.3.1*). To construct generalized linear models, the *glm* function from the **stats** package (R Core Team, 2015) was used. The multiple comparisons tests were run using the *glht* function from the **multcomp** package (Hothorn, et al., 2008). Student's *t*-tests were run using the *t.test* function from the **stats** package (R Core Team, 2015). Negative binomial generalized linear mixed effect models were run with the *glmer.nb* function from the **lme4** package (Bates et al., 2015).

Statistics code is located in https://github.com/damedebugger/Thesis.

Results

PLK-2 kinase activity is required for PC driven processive chromosome motions during prophase I

We had isolated a mutant allele of *plk-2* which we termed *plk-2(vv44).* This allele expresses a form of PLK-2 containing a proline to leucine substitution at amino acid 197 in the activation loop of the kinase domain. *plk-2(vv44)* mutants have high embryonic lethality (54.3 %) and high incidence of males in the surviving progeny (15.4 %) due to autosomal and X-chromosome non-disjunction, respectively (Labella et al., 2011). In the transition zone (TZ) nuclei of *plk-2(vv44)* worms, SUN-1/ZYG-12 remain uniformly distributed around the nuclear envelope (NE) and fail to aggregate into foci and cluster (Labella, 2012). Previous studies have inferred the motion of all 12 chromosomes through the utilization of SUN-1::GFP and ZYG-12::GFP (Baudrimont et al., 2010; Wynne et al., 2012). If SUN-1 is an effective proxy for chromosome motion, this would mean that in *plk-2(vv44)* mutants chromosome motion is abrogated.

In order to directly investigate PLK-2's role in early prophase chromosome end motion, we constructed transgenic lines which expressed fusion proteins of PLK-2 and PLK-2^{vv44} tagged with mCherry. Since PLK-2^{vv44} localized appropriately, both PLK-2::mCherry and PLK-2^{vv44}::mCherry could be used as robust markers for pairing centres (PCs). This effectively marks the end of each chromosome which drives and initiates pairing (Labella, 2012). We then used a spinning-disc confocal microscope to make 3D time-lapse images of chromosome end movement in the nuclei in the TZ of *plk-2::mCherry* and *plk-2(vv44)::mCherry* worms. In *plk-2::mCherry* worms the fluorescent signals appeared as aggregates of varying dimensions which were dynamic and moved along the NE periphery (Figure 1A). These aggregates interacted, coalesced into larger patches and then separated into independent foci over the course of

leptotene/zygotene. The movement resembled what was previously observed using SUN-1 and ZYG-12 fluorescent tags (Baudrimont et al., 2010; Wynne et al., 2012). On preliminary observation in *plk-2(vv44)::mCherry* animals the chromosome ends were mobile and occasionally coalesced into larger patches (Figure 1B). This finding was in contradiction of the previous hypothesis that the self-oligomerization of SUN-1/ZYG-12 into patches is necessary for the facilitation of chromosome movement (Wynne et al., 2012). The pairing defect in *plk-2(vv44)::mCherry* worms (Labella et al., 2011) is not due to a complete loss of chromosome end motion. Additionally, it is clear that SUN-1/ZYG-12 fluorescent markers do not necessarily accurately reflect PC motion in meiotic mutants.

In order to more definitively compare the differences in chromosome end dynamics between *plk-2::mCherry* and *plk-2(vv44)::mCherry* early meiotic nuclei, we proceeded to track the chromosome end movement using **Bitplane**'s particle tracking software which is part of the **Imaris** program (Figure 2). In *plk-2::mCherry* nuclei, chromosomes clustered in a crescent pattern along one side of the NE periphery. In *plk-2(vv44)::mCherry* animals we saw much more phenotypic diversity. In some nuclei, the chromosome ends simply oscillated around their starting location, covering a small search space. In these nuclei, there appeared to be fewer interactions between the chromosome ends, and the track pattern was more circular than crescent shaped. In other nuclei, the chromosome ends appeared to partially assume the crescent shaped trajectory pattern. Therefore, even though the chromosomes in *plk-2(vv44)::mCherry* worms are moving, the pattern of movement is not the same as in wild type early meiotic nuclei.

PLK-2^{vv44} can still phosphorylate the non-physiological substrate casein *in vitro* which means that the *plk-2(vv44)* allele is not a complete loss-of-function allele (Labella et al., 2011). We

wondered how PLK-2 kinase activity contributed to homologous chromosome pairing. To that end, we constructed an additional strain termed *plk-2(K65M)::mCherry,* which expresses a kinase-dead form of PLK-2 tagged with mCherry. PLK-2^{K65M} has an amino acid change from lysine to methionine in position 65. This residue is located in the ATP binding motif. It has been shown to be essential for Polo kinase activity (Lee et al. 1995). *plk-2(K65M)::mCherry* mutants had a more severe embryonic lethality (91.7 %) and high incidences of males in the surviving progeny (29.4 %) phenotype than *plk-2(vv44)::mCherry* (embryonic lethality: 54.3 %; incidence of males in the surviving progeny: 15.4 %) (Labella et al., 2011). When we tracked the chromosome end motion in the germline of this strain (Figure 2), we noticed that chromosome movement had sharply decreased. In the absence of PLK-2 kinase activity, early-prophase chromosome motion is reduced to slight jiggling, resulting in a complete abrogation of chromosome clustering. In most nuclei, the chromosome tracks showed no overlap, and hence no chromosome interactions. Therefore, PLK-2 kinase function is important in facilitating proper chromosome motion. Additionally, we can conclude that the *plk-2(K65M)::mCherry* nuclei do not phenocopy *plk-2(vv44)::mCherry* nuclei with respect to chromosome end motion.

In *plk-2(vv44)::mCherry* worms, the SUN-1/ZYG-12 proteins remain uniformly distributed around the nucleus, as opposed to clustering around the PC of the chromosomes (Labella et al., 2011). We wanted to test whether the residual motion seen in *plk-2(vv44)::mCherry* nuclei is still due to force transduction from the cytoskeleton through the NE proteins to the chromosome ends. To that end, we constructed the *plk-2(vv44)::mCherry; sun-1(jf18)* strain, in which the inner NE protein SUN-1 is unable to retain the outer NE protein ZYG-12 and hence the association between the chromosome ends and the cytoskeleton is lost (Penkner et al.,

2007; Sato et al., 2009). In the leptotene-zygotene nuclei of *plk-2(vv44)::mCherry; sun-1(jf18)* worms, chromosome ends behaved similarly to what we saw in the *plk-2(K65M)::mCherry* animals (Figure 2). Key differences include that there appeared to be many more fluorescent foci in *plk-2(vv44)::mCherry; sun-1(jf18)* nuclei than there were in *plk-2(K65M)::mCherry* nuclei. The dynamics of the chromosome ends also appear to be slightly weaker in *plk-2(vv44)::mCherry; sun-1(jf18)* worms. Therefore, chromosome motion in *plk-2(vv44)::mCherry* nuclei is dependent on chromosome end association with the NE envelope proteins and force transduction from the cytoskeleton.

Previous studies have noted that perturbations to proteins involved in pairing or cytoskeletal proteins or motors can effect chromosome end speed (Baudrimont et al., 2010; Wynne et al., 2012). We used the displacement over time data from the chromosome tracks to calculate the impact of PLK-2 and SUN-1 mutations on the speed distribution of chromosome ends during early prophase (Figure 3A). Wild type chromosome ends moved at an average speed of 61.5 nm/s with a standard deviation of 47.6 nm/s. We noticed that the chromosome end speed distribution of *plk-2::mCherry* worms took on a Maxwellian shape, similar to what Baudrimont et al. (2010) noticed using SUN-1::GFP (Figure S1A). We confirmed the existence of at least two types of speeds; 85 % of the time chromosome ends moved at an average speed of 46.2 nm/s, while the other 15 % of the time chromosome ends jumped to an average speed of 148.83 nm/s. We determined these "peak speeds" from the tail end of the Maxwellian speed distribution. These movements result in two types of motions; one where the chromosome end motion does not show a large net displacement and another where there is rapid motion in one direction, resulting in a larger displacement (Figure 3B). We favour the idea that these are the processive chromosome motions (PCMs) defined by Wynne et al. (2012). In *plk-2(vv44)::mCherry* worms,

there was a significant reduction in the speed to a mean of 49.8 nm/s and a standard deviation of 34.4 nm/s (gamma distribution, $p < 2*10^{-16}$, followed by a Tukey Contrasts, $p < 0.001$) (Figure 3A). We noted the existence of PCM in these mutants, however the average peak speed of chromosome ends was lower than in wild type at 139.52 nm/s. Additionally, chromosome ends in *plk-2(vv44)::mCherry* mutants were only undergoing PCMs 7 % of the time (Figure S1B). We conclude that the self-oligomerizing of SUN-1/ZYG-12 proteins into patches is not necessary for the existence PCM per se, however it greatly promotes peak speeds of higher magnitude and quantity. There was a further significant reduction in speed of chromosome movement in germlines which expressed the kinase-dead form of PLK-2 to an average of 31.3 nm/s and standard deviation of 21.8 nm/s (gamma distribution, $p < 2*10^{-16}$, followed by a Tukey Contrasts, $p < 0.001$) (Figure 3A). The difference in chromosome end speed between *plk-2(K65M)::mCherry* worms and *plk-2(vv44)::mCherry; sun-1(jf18)* worms was slighter with the chromosomes in the latter attaining an average speed of 26.3 nm/s and a standard deviation of 18.7 nm/s. In *plk-2(K65M)::mCherry* and *plk-2(vv44)::mCherry; sun-1(jf18)* mutants, PCMs were largely absent. Distributions did not have a substantial tail. Chromosome ends in both mutants underwent speeds associated with wild type PCMs less than 1 % of the time (Figures S1C, D). Therefore, both PLK-2 kinase activity and the association of chromosome end with the cytoskeleton are key in PC-driven chromosome motion during early prophase.

In *plk-2(vv44)::mCherry* worms, chromosome ends often undergo precocious synapsis between non-homologous chromosome pairs (Labella et al., 2011). Therefore, we wished to evaluate if the decrease in chromosome speed could be partly explained by the premature loading of the synaptonemal complex (SC). To test this, we abrogated formation of the SC in *plk-2(vv44)::mCherry* animals by feeding them *syp-2(RNAi).* We did not find a significant change in

speed compared to unfed *plk-2(vv44)::mCherry* animals (gamma distribution, $p < 2*10^{-16}$, followed by a Tukey Contrasts, $p > 0.05$) (mean = 49.5 nm/s, sd = 34.0 nm/s) (Figure 3A). Additionally, we did not find any change in the proportion or magnitude of peak speeds. Chromosome ends in *plk-2(vv44)::mCherry; syp-2(RNAi)* worms underwent PCM 6.5 % of the time. They had an average magnitude of 141.18 nm/s (Figure S1E). Therefore, the reduction of chromosome end speed in *plk-2(vv44)::mCherry* worms is not due to precocious synapsis.

In *plk-2* mutants chromosome ends interact less often during homology search

On preliminary viewing, there appeared to be differences in the number of chromosome end patches per nucleus. We wished to know whether PLK-2 kinase activity was essential for aggregate formation. To assess this, we quantified the distinct fluorescent signal counts (Table 1). We found that in *plk-2::mCherry* worms, the early prophase nuclei contained on average less than 6 chromosome end aggregates per nuclei (mean = 4.9, standard deviation = 1.0). This is consistent with previous evidence that homologous PCs pair early in prophase and that chromosomes interact with both homologous and heterologous partners in the earliest meiotic stages. In the *plk-2(vv44)::mCherry* nuclei, the aggregate count was significantly higher and greater than 6 (mean = 6.4, standard deviation = 1.3) (Poisson regression model, $p < 0.001$, followed by a Tukey Contrasts, $p < 0.001$). This verified that there was less aggregate formation occurring in nuclei which express PLK-2^{vv44}::mCherry compared to the wild type protein; though some chromosome clustering does occur since we didn't see signals representing 12 individual chromosome ends. In *plk-2(K65M)::mCherry* worms the count per nucleus was similar to *plk-2(vv44)::mCherry* animals (mean = 5.8, standard deviation = 2.1). This was a surprising result considering the more pronounced movement and pairing defect. Further investigation would be needed to uncover the mechanism behind this. In *plk-2(vv44)::mCherry;sun-1(jf18)*

worms, the count per nucleus was significantly higher (mean = 10.5, standard deviation = 1.2) (Poisson regression model, $p < 0.001$, followed by a Tukey Contrasts, $p < 0.001$). Therefore, without cytoskeletal force, the individual chromosome ends hardly coalesce and remain independent.

For proper homology assessment to occur, it is crucial for chromosome ends to be able to move into close proximity with one another. It is then important for heterologous chromosomes to disentangle in order to prevent non-homologous pairing. We decided to further look into the interaction and separation dynamics of PCs in each of the strains and to see how the changes in PLK-2 kinase activity and removal of the transduction of force from the cytoskeleton through the NE may have impacted it. In order to evaluate this, we counted the number of times two fluorescent signals coalesced into a single one (Figure 4A). We additionally investigated the number of times a single track would separate into two or more tracks (Figure 4B). In wild type nuclei, chromosome ends interacted a median of 6 times in a single nucleus over a 5 minute window. The range of interactions went from a minimum of 1 per nucleus to a maximum of 14. The median number of separation events was 5.5 times per nucleus, with a range from 1 to 10 per nucleus. This meant, on average, there are the same number of separations as there are aggregations. In *plk-2(vv44)::mCherry* worms, the median significantly dropped to 2 interactions per nucleus (quassi-Poisson regression model, $p < 0.05$, followed by a Tukey Contrasts, $p < 0.001$) with a corresponding median of 2 separation events per nucleus over a 5 minute window (Poisson regression model, $p < 0.05$, followed by a Tukey Contrasts, $p < 0.001$). A high proportion of nuclei exhibited no interactions at all over the course of 5 minutes. However, a notable proportion managed to achieve 4-8 interactions per nucleus. This shows that nuclei expressing PLK-2^{vv44} have a decrease in chromosome end

interaction but not an abrogation. In *plk-2(vv44)::mCherry* worms, the ratio of the average number of fusion to separation events did not change. In *plk-2(K65M)::mCherry* and *plk-2(vv44)::mCherry; sun-1(jf18)* worms, the medians dropped significantly down to 0 (Interaction: quassi-Poisson regression model, $p < 0.05$, followed by a Tukey Contrasts, $p < 0.001$; Separation: Poisson regression model, $p < 0.05$, followed by a Tukey Contrasts, $p < 0.00001$). In *plk-2(vv44)::mCherry; sun-1(jf18)* animals, the chromosomes never interacted or separated. In *plk-2(K65M)::mCherry* animals there were a few nuclei that exhibit a range of 1 to 4 interaction and separation events, though most exhibited 0. Even though *plk-2(K65M)::mCherry* nuclei appear to have clusters of patches, these patches are much less dynamic than in *plk-2::mCherry* and *plk-2(vv44)::mCherry* worms. This shows that PLK-2 kinase activity and chromosome end interaction with the cytoskeleton are important for the promotion of chromosome interactions and separations.

In order to verify whether precocious synapsis could be restricting *plk-2(vv44)::mCherry* chromosome ends from interacting, we counted the number of encounters between chromosome ends in *plk-2(vv44)::mCherry* worms which were fed *syp-2(RNAi).* We found no significant difference in the number of interactions compared to *plk-2(vv44)::mCherry* worms which were not fed *syp-2*(RNAi) (quasi-Poisson regression model, $p < 0.05$, followed by a Tukey Contrasts, $p > 0.05$) (Figures 4A, B). Therefore, it is not precocious synapsis which results in the decrease in chromosome end interactions in *plk-2(vv44)::mCherry* mutants.

Wynne et al. (2012) provided evidence that X chromosomes are not biased towards moving closer together. They theorized that chromosome motion is random, and that the large bursts in speed and displacement are required to increase the probability of random interaction. We were interested in whether the average chromosome speed within a nuclei is correlated with

the number of times chromosomes within that nuclei interacted or separated. We performed a generalized linear mixed model fit by maximum likelihood with a negative binomial distribution to assess whether the average speed of chromosomes in the nucleus contributed to the frequency of chromosome interactions in the nucleus, while controlling for the genotype of the worm as a random effect. We found a significant correlation of average chromosome speeds with the frequency of interactions and splitting events while controlling for the effect of worm genotype ($p < 0.001$ for both frequency of interactions and frequency of splitting events). Therefore, PLK-2 kinase activity likely contributes to the frequency of chromosome aggregations and separations through its influence of chromosome end motion.

Phosphorylation by PLK-2 and the self-oligomerization of SUN-1/ZYG-12 proteins into patches contributes to more cohesive PC patches

In the absence of NE reorganization, *plk-2(vv44)::mCherry* chromosome ends are able to move, cluster and separate. We considered that the role of SUN-1/ZYG-12 aggregation might be to constrain movement so that homologous chromosomes are in close proximity for a long enough duration in order to perform homology assessment and progress to more stable linkages. Therefore, we proceeded to investigate the differences in the ability to form cohesive chromosome patches between chromosome ends in nuclei expressing different forms of PLK-2. We evaluated the lengths of time two patches remained together in the 5 minute window, and assessed the frequency the various coalescence times (Figure 5). In wild type TZ nuclei, chromosome aggregates had remained clustered on average for 59.70 seconds. In comparison, there was a significant drop in average coalescence time in *plk-2(vv44)::mCherry* mutants to 28.64 seconds, showing that early-prophase chromosomes in *plk-2(vv44)::mCherry* worms were less competent in maintaining patch cohesion (quasi-Poisson regression model $p < 0.01$,

followed by a Tukey Contrasts model, $p < 0.0001$). Additionally, we also looked at the few interaction events in *plk-2(K65M)::mCherry* TZ nuclei. They had a slightly lower average cohesion time of 19.95 seconds. Therefore, SUN-1/ZYG-12 self-oligomerization is not only essential for the establishment of dynamic patches that disperse and interchange frequently to allow the separation of non-homologous chromosomes, but also for locally concentrating the patches to facilitate homolog assessment. This provides support to the theory that the role of SUN-1/ZYG-12 aggregation around PCs in wild type meiosis is to help hold chromosome ends together in a cluster for longer periods.

PCMs correlate with chromosome disentanglement

Despite the agreement in the literature about the existence of at least two phases of chromosome motion, there is currently no consensus on the biological role of peak speeds (Baudrimont et al., 2010; Wynne et al., 2012). We sought out to investigate the role of PCM in homology search in wild type worms. Additionally, we wanted to compare our findings with PCMs in *plk-2(vv44)::mCherry* mutants, whose chromosomes achieved fewer peak speeds and whose peak speeds were of a lower magnitude. We investigated what chromosomes ends were doing when they were moving at a peak speed. If the chromosome which was undergoing PCM was splitting off from a chromosome cluster, it was characterized as a "splitting event". If the faster movement of a chromosome resulted in the aggregation of a chromosome cluster, it was characterized as a "fusion event". We found that most of the time, in the same proportion in both *plk-2::mCherry* and *plk-2(vv44)::mCherry* worms, a large increase in displacement was correlated with a splitting or fusion event (Figure 6A). This adds support to the idea of Baudrimont et al. (2010) that when chromosomes entangle or pull on each other, tension is

created. The force of the microtubules pulling on the chromosomes increases this tension, resulting in an increase in potential energy and a consequent increase in speed.

In order to address the hypothesis that the tensions involved in chromosome separations result in an increase in speed, we next decided to investigate the splitting events themselves. We assessed whether splitting events correlated with PCM (Figure 6B). We found that within wild type nuclei, 53 % of the foci involved in a splitting event reached peak speeds. This is of particular significance since wild type chromosomes undergo PCM only 15 % of the time (Figure S1A). High tension chromosome separations were resulting in peak speeds half the time. In *plk-2(vv44)::mCherry* mutants, the situation was slightly different. Aggregates were splitting into foci at a lower speed much more frequently than in wild type nuclei (chi-square test, $p < 0.001$). 89 % of the splitting events were not associated with a peak speed. We hypothesized that chromosome aggregates in *plk-2(vv44)::mCherry* mutants weren't able to reach higher speeds and levels of tension and hence possibly weren't able to successfully untangle from unfavourable pairings.

The X chromosome pairs in *plk-2(vv44)* mutants have difficulties in moving closer together

A question still remained on the underlying cause of the pairing defect in *plk-2(vv44)::mCherry* worms. Were the chromosome ends in *plk-2(vv44)::mCherry* worms failing to recognize their homologous partner? Or were chromosomes unable to find their homologous partner? The latter would mean that the polarized configuration of the chromosomes is essential for proper homologous chromosome pairing, and isn't merely a mechanism to increase pairing efficiency. To begin investigating this further, we made and crossed a transgenic line of *him-8::mCherry* worms with *plk-2(vv44)* mutants. HIM-8 is the PC protein that localizes to the *C.*

elegans X chromosome upon meiotic onset. This allowed us to track the process of homologous chromosome pairing of one specific pair of chromosome ends. In wild type germlines, the X chromosome ends started off in random positions in the nuclei. They proceeded to move rapidly towards one another. The fluorescent foci representing the X chromosomes would begin to overlap until they fused into a single focus. By the end of the 5 minute recording, 100 % of the nuclei showed a single fluorescent signal which represented the successfully paired X chromosomes (*Data not shown;* Wynne et al., 2012*).* In *plk-2(vv44); him-8::mCherry* mutants, at the end of the movie, the X chromosome ends were in various configurations (Figures 7A, S2). We measured the distance between the HIM-8::mCherry foci. Foci less than 0.7 µm apart were inferred to be paired (MacQueen et al., 2002). In 67 % percent of nuclei, the X chromosome pairs were more than 1.5 µm apart and appeared to be moving independently from one another. By the end of the 5 minute recording, in 95 % of these nuclei, the X chromosomes remained more than 1.5 µm apart. This suggests that in *plk-2(vv44)* mutants, the X chromosomes take a longer time to find each other than in wild type. In *him-8::mCherry* worms with PLK-2^{WT}, 5 minutes was sufficient time for the X chromosomes to find one another. This adds support to the hypothesis that the pairing defect is due to homologous chromosomes being unable to find each other within the nucleus. In 16 % of the total nuclei the chromosome ends did manage to attain a distance of close to 0.7 µm (< 1.5 µm; > 0.7 µm), but in only 15 % of these nuclei did the X chromosomes manage to get within pairing distance after 5 minutes, despite being close enough to do so (Figure S3). This suggests that a mechanism may exist which controls the establishment of a more intimate association, which occurs less frequently in *plk-2(vv44)* mutants. In these nuclei, the X chromosome PCs would sometimes move in concert, but they would not initiate the shuffling typical of pairing. We termed this

conformation "the align conformation". Only 17 % of the X chromosome pairs were within pairing distance at the start of the movie and of those, only 85 % remained paired by the end of the movie. Therefore, due to decreased levels of phosphorylation by PLK-2, chromosome ends in *plk-2(vv44)* mutants are encountering difficulty at three stages. Some of them can't find their homolog due to a decreased level of clustering. Other X chromosome pairs are close enough that their inertia is sufficient to reach the proximal distance required for pairing but aren't initiating pairing. Lastly, even when X chromosome pairs do manage to get within pairing distance they aren't always able to maintain the coalescence.

The low percentage of X chromosomes pairs moving within pairing distance in a *plk-2(vv44)* background is not due to precocious synapsis

We hypothesized that the "align conformation" was possibly due to synapsis precociously zipping up the chromosomes to heterologous partners. Even though the X chromosome ends were close, they were potentially already in a stable pairing and hence couldn't initiate pairing with their homologous partner. In order to investigate this, we performed *syp-1*(RNAi) on the *plk-2(vv44); him-8::mCherry* worms. We found no significant change in observed phenotypes (chi-square test, $p > 0.05$) (Figures 7A, S2). We further decided to quantify the distance between the X chromosomes in a *plk-2(vv44)* background, with and without performing *syp-1*(RNAi) (Figure 7B). We found no significant difference in the distances between the X chromosomes (*plk-2(vv44)*: mean = 2.00 µm, sd = 1.04 µm; *plk-2(vv44); syp-1(RNAi):* mean = 1.83 µm, sd = 1.07 µm) (2-tailed *t*-test, $p > 0.05$). Therefore, precocious synapsis is not the underlying cause of the presence of the "align conformation" and the low percentage of X chromosome pairs within pairing distance in a *plk-2(vv44)* background.

We then wished to evaluate if X chromosomes were on average moving closer together or further apart. In order to assess this, we looked at the change in distance between X chromosomes over time (Figure 8). We found that in *plk-2(vv44)* worms, the median change in distance lay very close to 0 and that this didn't significantly change after treatment with *syp-1(*RNAi) (2-tailed *t*-test, $p > 0.05$). Therefore, the X chromosomes aren't predominantly moving closer together or further apart in a *plk-2(vv44)* background.

Discussion

An outstanding question in the meiosis field is how chromosome motion during homology search promotes accurate homologous chromosome pairing. Previous studies have approached this question by indirectly inferring the movement of all of the chromosomes during homology search through the use of SUN-1, ZYG-12 and HIM-8 fluorescent protein constructs (Baudrimont et al., 2010; Wynne et al., 2012). We sought to directly track the motion of all of the pairing centres (PCs) during leptotene-zygotene; through the use of PLK-2 fluorescent constructs, we were able to visualize and quantify aspects of chromosome end movement during homology search in wild type and mutant backgrounds and compare it with what was observed by Baudrimont et al. (2010) and Wynne et al. (2012). We additionally investigated the role of PLK-2, synaptonemal complex (SC) and the nuclear envelope (NE) protein bridge in regulating chromosome motion.

We confirmed that chromosome ends cluster towards one side of the nucleus, in a crescent-shaped trajectory, and frequently coalesce together into transient aggregates which they later separate from. Chromosome end speeds took on a Maxwellian distribution, as observed by Baudrimont et al. (2012). Despite the SUN-1/ZYG-12 protein bridge failing to enrich at the chromosome attachment plaque of chromosome PCs in *plk-2(vv44)::mCherry* mutants, this does not abrogate chromosome motion, showing that SUN-1 clustering is not essential for chromosome motion and that tagged SUN-1 or ZYG-12 is not a sufficient indicator of chromosome behaviour in meiotic mutants. This brings into question the results of Baudrimont et al. (2010) and Wynne et al. (2012), who used SUN-1::GFP and ZYG-12::GFP respectively as a proxy for chromosome motion in meiotic mutants. However, the SUN-1/ZYG-12 protein bridge is required for the dynamic movement in *plk-2(vv44)::mCherry* germline; in

its absence the chromosomes show a much more pronounced movement defect. In *plk-2(vv44)::mCherry* germline, chromosomes precociously synapse with heterologous partners. However, removal of synapsis through the use of *syp-2(RNAi)*, did not alter the phenotype in any way. This agrees with Wynne et al. (2012) but contradicts with Baudrimont et al. (2010); it appears that synapsis does not play a large role in chromosome motion.

Our results support the existence of the processive chromosome motions (PCMs), first observed by Baudrimont et al. (2010) and further expanded upon by Wynne et al. (2012); we identified them from the tail end of the wild type Maxwellian speed distribution. These PCMs were observed less frequently in *plk-2(vv44)* nuclei but were largely absent in germline which expressed a kinase-dead form of PLK-2. This supports the idea PLK-2^{vv44} is not a kinase-dead protein, since PLK-2^{K65M} results in a much more severe phenotype. In *plk-2(K65M)* nuclei, chromosome movement sharply decreases and chromosomes rarely interact, showing that PLK-2 kinase activity is required for dynamic chromosome motion.

We found a significant relationship between higher average chromosome speeds in a nucleus and more frequent chromosome interactions in that nucleus. This is slightly in conflict with Wynne et al. (2012), which theorized that higher chromosome motions don't bring chromosomes closer together any more frequently than slower ones. Our result that chromosome separations from aggregates were associated with PCM, supported Baudrimont et al. (2010)'s theory that high speeds are the consequence of the higher tensions in aggregates which contain multiple chromosomes. In *plk-2(vv44)* nuclei, chromosomes had attained PCM less frequently and the correlation between PCM and separation from chromosome aggregates was weaker. Chromosomes rarely interacted with each other, and when they did they were not able to form highly-cohesive patches.

In *plk-2(vv44)* germline, 67 % of TZ nuclei showed X chromosomes located further than 1.5 µm away from each other at the start of recording. In only 5 % of these nuclei did the X chromosome pairs decrease the distance between them to less than 1.5 µm by the end of the 5 minute movie. This implies that the homologous chromosomes aren't able to locate one another. This differs from wild type germline (Wynne et al., 2012) where most nuclei show a single foci representing the associated X chromosomes by the middle of the TZ. Our results agreed with Wynne et al. (2012) that synapsis did not play a role in X chromosome motion. Performing *syp-1(RNAi)* did not dramatically alter the X chromosome movement phenotype in *plk-2(vv44)* nuclei.

There were some unexpected differences in phenotype between *plk-2(K65M)::mCherry* and *plk-2(vv44)::mCherry; sun-1(jf18)* mutants. In both strains, PCs rarely interacted with one another and chromosome movement had sharply decreased to the same degree. However, in *plk-2(K65M)::mCherry* mutants we saw some large patches of chromosomes while in *plk-2(vv44)::mCherry; sun-1(jf18)* worms we saw 10-12 independent foci, which correspond to the 12 chromosome ends, and no patches. Currently, we favour the idea that residual cytoskeletal forces in *plk-2(K65M)::mCherry* mutants had resulted in some chromosome aggregates which, due to weaker chromosome motion, chromosomes weren't able to separate from. However, the support for this is limited and further experiments will need to be done in order to investigate this difference between the two strains.

In *plk-2(vv44)* nuclei, X chromosomes move away from each other at the same rate as they move closer together; they seem to move independently. Surprisingly, this is similar to what Wynne et al. (2012) observed with X chromosomes in wild type nuclei, yet X chromosomes in wild type nuclei find their partner much more efficiently and chromosomes interact much

more frequently with other. It could be that due to the limiting of the search space in wild type nuclei, through the polarization of chromosome ends, these random interactions are more likely to result in chromosomes finding their homolog. Whereas in *plk-2(vv44)* nuclei, chromosomes fail to polarize and are less likely to randomly bump into other chromosomes, and consequently their homolog. Further experiments will need to be run to quantify the differences in the search space covered by chromosome ends *plk-2(vv44)* mutants versus wild type.

Additionally, of interest is that even when X chromosome manage to get close enough to initiate pairing, they sometimes get stuck in what we termed an "align conformation". This "align conformation" is not due to precocious synapsis between a heterologous chromosome partners as evidenced by experiments where we performed *syp-1*(RNAi) and didn't see a decrease in the number of nuclei which had X chromosomes "aligned". Further investigation is required to assess whether this "align conformation" is of biological significance.

In conclusion, we undertook to record and analyse movies of the TZ nuclei of *plk-2::mCherry* worms and worms which carried a mutant allele of *plk-2*. The general aspects of wild type chromosome end motion which we quantified using PLK-2::mCherry as a marker are similar to what was previously found using SUN-1/ZYG-12 and HIM-8 as markers (Wynne et al., 2012; Baudrimont et al., 2010). Additionally, we have characterized some of the contribution of PLK-2, the SC, and the NE protein bridge to chromosome motion. In the absence of PLK-2 kinase activity, pronounced chromosome motion is lost and chromosomes are limited to small jittery movements. We have found no contribution of synapsis to chromosome movement in a *plk-2(vv44)* mutant background. We have found that the aggregation of the NE protein bridge

correlates with more frequent occurrences of PCM, higher amount of chromosome interactions and longer-term chromosome cohesion.

Our results can help provide some insight into how changes in chromosome motion impact pairing in combination with the previous work done by Baudrimont et al. (2010) and Wynne et al. (2012). One primary hypotheses is that SUN-1/ZYG-12 aggregation is necessary to hold chromosomes together for a longer period of time. In *plk-2(vv44)::mCherry* nuclei, chromosomes were less cohesive than in *plk-2::mCherry* nuclei. This constraint on chromosome motion may be important in order to allow time for homology assessment or for the recruitment of proteins required for pairing. We favour the idea posited by Baudrimont et al. (2010) that perhaps the aggregation of SUN-1/ZYG-12 patches is necessary for the concentration of cytoskeletal forces. In the absence of those forces, there is less tension between homologous chromosomes. This tension might be required for homology assessment. We have shown that in *plk-2(vv44)* nuclei, there are fewer PCM and the relationship between separating chromosome aggregates and PCM is weaker. Another idea which is supported by our findings is that in a *plk-2(vv44)* background, chromosomes do not efficiently locate their homologous partner. The clustering of SUN-1/ZYG-12 patches could be limiting the search space between homologous chromosome pairs in order to ensure a higher probability that they'll find each other by random chance. This would mean that the polarized configuration of the chromosomes is essential for accurate homologous chromosome pairing, and isn't merely a mechanism to increase pairing efficiency. Another possibility is that due to a decrease in PLK-2 mediated phosphorylation, a protein which facilitates homologous chromosome identification is not being activated at sufficient functional levels.

For future directions, it would be interesting to characterize the movement behaviour of an autosomal chromosome pair in *plk-2(vv44)* animals. The X chromosomes pair earlier and more efficiently than the autosomal chromosomes in *C. elegans*. Analysis should be repeated with a tagged version of ZIM-2 as a marker, which would exclusively tag chromosome V, in a *plk-2(vv44)* background. This would allow us to more definitively track and compare the relationship between two homologous chromosomes in a wild type and *plk-2(vv44)* background.

It would also be interesting to further investigate the align conformation. A statistical analysis should be performed to assess whether the align conformation occurs more often than would be considered by chance. Since there is a limited 3D space for chromosome ends to manoeuvre in, it is possible that they are positioned close together by random chance and that some manage to further move within pairing distance through Brownian motion and some don't. To further assess whether there is a biological component to the align conformation, it would be interesting to perform a targeted genetic knockdown screen or EMS screen, to see if perturbations in expression of a specific protein result in changes in the rate of appearance of the align conformation. If there is a protein which requires PLK-2 contribution in order for the chromosome ends to move closer together, a screen should reveal that.

We have decided to interpret differences in chromosome motion between strains as differences in chromosome speed. However, a fluorescent signal which moved in the same direction in the interval between image acquisitions would be interpreted as moving faster than one which changed directions over the course of the interval, even if they were moving at a constant speed. Wynne et al. (2012) argue that to clearly differentiate PCMs from diffusive motion requires multiple images per second. There are limits of accomplishing that in *C.*

elegans due to the size of the nematode germline nuclei, however it would be interesting to obtain movies with shorter time points in order to better characterize the differences in chromosome motion between the various strains.

It would also be interesting to discover the direct targets of PLK-2. Currently, we do not know the mechanism behind its regulation of chromosome motion. Uncovering the downstream proteins may aid in further understanding the *plk-2(vv44)* and *plk-2(K65M)* mutant phenotype.

Finally, it would also be of special interest to answer the question of whether homology assessment occurs by a tension mechanism or a molecular one.

References:

Alsheimer, M. (2008). The dance floor of meiosis: evolutionary conservation of nuclear envelope attachment and dynamics of meiotic telomeres Meiosis (Vol. 5, pp. 81-93): Karger Publishers.

Barnes, T., Kohara, Y., Coulson, A., & Hekimi, S. (1995). Meiotic recombination, noncoding DNA and genomic organization in Caenorhabditis elegans. Genetics, 141(1), 159-179.

Bates, D., Maechler, M., Bolker, B., & Walker, S. (2015). Fitting Linear Mixed-Effect Models using lme4. Journal of Statistical Software, 67(1), 1-48. doi:18637/jss.v067.io1.

Baudrimont, A., Penkner, A., Woglar, A., Machacek, T., Wegrostek, C., Gloggnitzer, J., Fridkin, A., Klein, F., Gruenbaum, Y., & Pasierbek, P. (2010). Leptotene/zygotene chromosome movement via the SUN/KASH protein bridge in Caenorhabditis elegans. PLoS Genet, 6(11), e1001219.

Chikashige, Y., Tsutsumi, C., Yamane, M., Okamasa, K., Haraguchi, T., & Hiraoka, Y. (2006). Meiotic proteins bqt1 and bqt2 tether telomeres to form the bouquet arrangement of chromosomes. Cell, 125(1), 59-69.

Colaiácovo, M. P. (2006). The many facets of SC function during C. elegans meiosis. Chromosoma, 115(3), 195-211.

Colaiácovo, M. P., MacQueen, A. J., Martinez-Perez, E., McDonald, K., Adamo, A., La Volpe, A., & Villeneuve, A. M. (2003). Synaptonemal complex assembly in C. elegans is dispensable for loading strand-exchange proteins but critical for proper completion of recombination. Developmental cell, 5(3), 463-474.

Conrad, M. N., Lee, C.-Y., Chao, G., Shinohara, M., Kosaka, H., Shinohara, A., Conchello, J.-A., & Dresser, M. E. (2008). Rapid telomere movement in meiotic prophase is promoted by NDJ1, MPS3, and CSM4 and is modulated by recombination. Cell, 133(7), 1175-1187.

Cooper, J. P. (2000). Telomere transitions in yeast: the end of the chromosome as we know it. Current Opinion in Genetics & Development, 10(2), 169-177.

Couteau, F., Nabeshima, K., Villeneuve, A., & Zetka, M. (2004). A component of C. elegans meiotic chromosome axes at the interface of homolog alignment, synapsis, nuclear reorganization, and recombination. Current Biology, 14(7), 585-592.

Couteau, F., & Zetka, M. (2005). HTP-1 coordinates synaptonemal complex assembly with homolog alignment during meiosis in C. elegans. Genes & Development, 19(22), 2744-2756.

Crittenden, S. L., Troemel, E. R., Evans, T. C., & Kimble, J. (1994). GLP-1 is localized to the mitotic region of the C. elegans germ line. Development, 120(10), 2901-2911.

Goodyer, W., Kaitna, S., Couteau, F., Ward, J. D., Boulton, S. J., & Zetka, M. (2008). HTP-3 links DSB formation with homolog pairing and crossing over during C. elegans meiosis. Developmental cell, 14(2), 263-274.

Hiraoka, Y., & Dernburg, A. F. (2009). The SUN rises on meiotic chromosome dynamics. Developmental cell, 17(5), 598-605.

Hirsh, D., Oppenheim, D., & Klass, M. (1976). Development of the reproductive system of Caenorhabditis elegans. Developmental biology, 49(1), 200-219.

Hodgkin, J. (2005). Karyotype, ploidy, and gene dosage.

Hodgkin, J., Horvitz, H. R., & Brenner, S. (1979). Nondisjunction mutants of the nematode Caenorhabditis elegans. Genetics, 91(1), 67-94.

Hothorn, T., Bretz, F., & Westfall, P. (2008). Simultaneous Inference in General Parametric Models. Biometrical Journal 50(3), 346-363.

Koszul, R., & Kleckner, N. (2009). Dynamic chromosome movements during meiosis: a way to eliminate unwanted connections? Trends in cell biology, 19(12), 716-724.

Labella, S. (2012). Characterization of the functions of Polo-like kinase 2 during meiotic chromosome pairing in C. elegans. (Biology), McGill University.

Labella, S., Woglar, A., Jantsch, V., & Zetka, M. (2011). Polo kinases establish links between meiotic chromosomes and cytoskeletal forces essential for homolog pairing. Developmental cell, 21(5), 948-958.

Lee, K. S., Yuan, Y., Kuriyama, R., & Erikson, R. L. (1995). Plk is an M-phase-specific protein kinase and interacts with a kinesin-like protein, CHO1/MKLP-1. Molecular and Cellular Biology, 15(12), 7143-7151.

Leu, J.-Y., Chua, P. R., & Roeder, G. S. (1998). The meiosis-specific Hop2 protein of S. cerevisiae ensures synapsis between homologous chromosomes. Cell, 94(3), 375-386.

Loidl, J. (1990). The initiation of meiotic chromosome pairing: the cytological view. Genome, 33(6), 759-778.

Loidl, J., Klein, F., & Scherthan, H. (1994). Homologous pairing is reduced but not abolished in asynaptic mutants of yeast. The Journal of cell biology, 125(6), 1191-1200.

MacQueen, A. J., Colaiácovo, M. P., McDonald, K., & Villeneuve, A. M. (2002). Synapsis-dependent and-independent mechanisms stabilize homolog pairing during meiotic prophase in C. elegans. Genes & Development, 16(18), 2428-2442.

MacQueen, A. J., Phillips, C. M., Bhalla, N., Weiser, P., Villeneuve, A. M., & Dernburg, A. F. (2005). Chromosome sites play dual roles to establish homologous synapsis during meiosis in C. elegans. Cell, 123(6), 1037-1050.

MacQueen, A. J., & Villeneuve, A. M. (2001). Nuclear reorganization and homologous chromosome pairing during meiotic prophase require C. elegans chk-2. Genes & Development, 15(13), 1674-1687.

Malone, C. J., Misner, L., Le Bot, N., Tsai, M.-C., Campbell, J. M., Ahringer, J., & White, J. G. (2003). The C. elegans hook protein, ZYG-12, mediates the essential attachment between the centrosome and nucleus. Cell, 115(7), 825-836.

Martinez-Perez, E., & Villeneuve, A. M. (2005). HTP-1-dependent constraints coordinate homolog pairing and synapsis and promote chiasma formation during C. elegans meiosis. Genes & Development, 19(22), 2727-2743.

McGee, M. D., Rillo, R., Anderson, A. S., & Starr, D. A. (2006). UNC-83 IS a KASH protein required for nuclear migration and is recruited to the outer nuclear membrane by a physical interaction with the SUN protein UNC-84. Molecular biology of the cell, 17(4), 1790-1801.

McKim, K. S., Howell, A. M., & Rose, A. M. (1988). The effects of translocations on recombination frequency in Caenorhabditis elegans. Genetics, 120(4), 987-1001.

Mets, D. G., & Meyer, B. J. (2009). Condensins regulate meiotic DNA break distribution, thus crossover frequency, by controlling chromosome structure. Cell, 139(1), 73-86.

Minn, I., Rolls, M. M., Hanna-Rose, W., & Malone, C. J. (2009). SUN-1 and ZYG-12, Mediators of Centrosome–Nucleus Attachment, Are a Functional SUN/KASH Pair in Caenorhabditis elegans. Molecular biology of the cell, 20(21), 4586-4595.

Moreau, P. J., Zickler, D., & Leblon, G. (1985). One class of mutants with disturbed centromere cleavage and chromosome pairing in Sordaria macrospora. Molecular and General Genetics MGG, 198(2), 189-197.

Nabeshima, K., Villeneuve, A. M., & Colaiácovo, M. P. (2005). Crossing over is coupled to late meiotic prophase bivalent differentiation through asymmetric disassembly of the SC. The Journal of cell biology, 168(5), 683-689.

Nag, D. K., Scherthan, H., Rockmill, B., Bhargava, J., & Roeder, G. S. (1995). Heteroduplex DNA formation and homolog pairing in yeast meiotic mutants. Genetics, 141(1), 75-86.

Nicklas, R. B. (1974). Chromosome segregation mechanisms. Genetics, 78(1), 205-213.

Nottke, A. C., Beese-Sims, S. E., Pantalena, L. F., Reinke, V., Shi, Y., & Colaiácovo, M. P. (2011). SPR-5 is a histone H3K4 demethylase with a role in meiotic double-strand break repair. Proceedings of the National Academy of Sciences, 108(31), 12805-12810.

Nottke, A. C., Beese-Sims, S. E., Pantalena, L. F., Reinke, V., Shi, Y., & Colaiácovo, M. P. (2011). SPR-5 is a histone H3K4 demethylase with a role in meiotic double-strand break repair. Proceedings of the National Academy of Sciences, 108(31), 12805-12810.

Oliveira, R. A., & Nasmyth, K. (2010). Getting through anaphase: splitting the sisters and beyond. Biochemical Society Transactions, 38(6), 1639-1644.

Östergren, G. (1951). The mechanism of co-orientation in bivalents and multivalents. Hereditas, 37(1-2), 85-156.

Padmakumar, V., Libotte, T., Lu, W., Zaim, H., Abraham, S., Noegel, A. A., Gotzmann, J., Foisner, R., & Karakesisoglou, I. (2005). The inner nuclear membrane protein Sun1 mediates the anchorage of Nesprin-2 to the nuclear envelope. J Cell Sci, 118(15), 3419-3430.

Page, S. L., & Hawley, R. S. (2004). The genetics and molecular biology of the synaptonemal complex. Annu. Rev. Cell Dev. Biol., 20, 525-558.

Penkner, A., Tang, L., Novatchkova, M., Ladurner, M., Fridkin, A., Gruenbaum, Y., Schweizer, D., Loidl, J., & Jantsch, V. (2007). The nuclear envelope protein Matefin/SUN-1 is required for homologous pairing in C. elegans meiosis. Developmental cell, 12(6), 873-885.

Penkner, A. M., Fridkin, A., Gloggnitzer, J., Baudrimont, A., Machacek, T., Woglar, A., Csaszar, E., Pasierbek, P., Ammerer, G., & Gruenbaum, Y. (2009). Meiotic chromosome homology search involves modifications of the nuclear envelope protein Matefin/SUN-1. Cell, 139(5), 920-933.

Peoples, T. L., Dean, E., Gonzalez, O., Lambourne, L., & Burgess, S. M. (2002). Close, stable homolog juxtaposition during meiosis in budding yeast is dependent on meiotic recombination, occurs independently of synapsis, and is distinct from DSB-independent pairing contacts. Genes & Development, 16(13), 1682-1695.

Phillips, C. M., & Dernburg, A. F. (2006). A family of zinc-finger proteins is required for chromosome-specific pairing and synapsis during meiosis in C. elegans. Developmental cell, 11(6), 817-829.

Phillips, C. M., Wong, C., Bhalla, N., Carlton, P. M., Weiser, P., Meneely, P. M., & Dernburg, A. F. (2005). HIM-8 binds to the X chromosome pairing center and mediates chromosome-specific meiotic synapsis. Cell, 123(6), 1051-1063.

R Core Team (2015). R: A language and environment for statistical computing. R Foundation for Statistical Computing, Vienna, Austria. URL https://www.R-project.org.

Roeder, G. S. (1997). Meiotic chromosomes: it takes two to tango. Genes & Development, 11(20), 2600-2621.

Rose, A., Baillie, D., & Curran, J. (1984). Meiotic pairing behavior of two free duplications of linkage group I in Caenorhabditis elegans. Molecular and General Genetics MGG, 195(1-2), 52-56.

Rosenbluth, R. E., & Baillie, D. L. (1981). The genetic analysis of a reciprocal translocation, eT1 (III; V), in Caenorhabditis elegans. Genetics, 99(3-4), 415-428.

Sanford, C., & Perry, M. D. (2001). Asymmetrically distributed oligonucleotide repeats in the Caenorhabditis elegans genome sequence that map to regions important for meiotic chromosome segregation. Nucleic acids research, 29(14), 2920-2926.

Sato, A., Isaac, B., Phillips, C. M., Rillo, R., Carlton, P. M., Wynne, D. J., Kasad, R. A., & Dernburg, A. F. (2009). Cytoskeletal Forces Span the Nuclear Envelope to Coordinate Meiotic Chromosome Pairing and Synapsis. Cell, 139(5), 907-919. doi:http://dx.doi.org/10.1016/j.cell.2009.10.039

Scherthan, H. (2001). A bouquet makes ends meet. Nature reviews Molecular cell biology, 2(8), 621-627.

Scherthan, H., Weich, S., Schwegler, H., Heyting, C., Härle, M., & Cremer, T. (1996). Centromere and telomere movements during early meiotic prophase of mouse and man are associated with the onset of chromosome pairing. The Journal of cell biology, 134(5), 1109-1125.

Schlecht, H. B., Lichten, M., & Goldman, A. S. (2004). Compartmentalization of the yeast meiotic nucleus revealed by analysis of ectopic recombination. Genetics, 168(3), 1189-1203.

Smolikov, S., Eizinger, A., Schild-Prufert, K., Hurlburt, A., McDonald, K., Engebrecht, J., Villeneuve, A. M., & Colaiácovo, M. P. (2007). SYP-3 restricts synaptonemal complex assembly to bridge paired chromosome axes during meiosis in Caenorhabditis elegans. Genetics, 176(4), 2015-2025.

Smolikov, S., Schild-Prüfert, K., & Colaiacovo, M. P. (2009). A yeast two-hybrid screen for SYP-3 interactors identifies SYP-4, a component required for synaptonemal complex assembly and chiasma formation in Caenorhabditis elegans meiosis. PLoS Genet, 5(10), e1000669.

Torres, E. M., Williams, B. R., & Amon, A. (2008). Aneuploidy: cells losing their balance. Genetics, 179(2), 737-746.

Trelles-Sticken, E., Adelfalk, C., Loidl, J., & Scherthan, H. (2005). Meiotic telomere clustering requires actin for its formation and cohesin for its resolution. The Journal of cell biology, 170(2), 213-223.

Tsubouchi, H., & Roeder, G. S. (2002). The Mnd1 protein forms a complex with hop2 to promote homologous chromosome pairing and meiotic double-strand break repair. Molecular and Cellular Biology, 22(9), 3078-3088.

Tzur, Y. B., Wilson, K. L., & Gruenbaum, Y. (2006). SUN-domain proteins:'Velcro'that links the nucleoskeleton to the cytoskeleton. Nature reviews Molecular cell biology, 7(10), 782-788.

Villeneuve, A. M. (1994). A cis-acting locus that promotes crossing over between X chromosomes in Caenorhabditis elegans. Genetics, 136(3), 887-902.

Weiner, B. M., & Kleckner, N. (1994). Chromosome pairing via multiple interstitial interactions before and during meiosis in yeast. Cell, 77(7), 977-991.

Wynne, D. J., Rog, O., Carlton, P. M., & Dernburg, A. F. (2012). Dynein-dependent processive chromosome motions promote homologous pairing in C. elegans meiosis. The Journal of cell biology, 196(1), 47-64.

Yamamoto, A., & Hiraoka, Y. (2001). How do meiotic chromosomes meet their homologous partners?: lessons from fission yeast. BioEssays, 23(6), 526-533. doi:10.1002/bies.1072

Zetka, M. C., Kawasaki, I., Strome, S., & Müller, F. (1999). Synapsis and chiasma formation in Caenorhabditis elegans require HIM-3, a meiotic chromosome core component that functions in chromosome segregation. Genes & Development, 13(17), 2258-2270.

Zickler, D. (2006). From early homologue recognition to synaptonemal complex formation. Chromosoma, 115(3), 158-174.

Zickler, D., & Kleckner, N. (1998). The leptotene-zygotene transition of meiosis. Annual review of genetics, 32(1), 619-697.

Figure 1

A

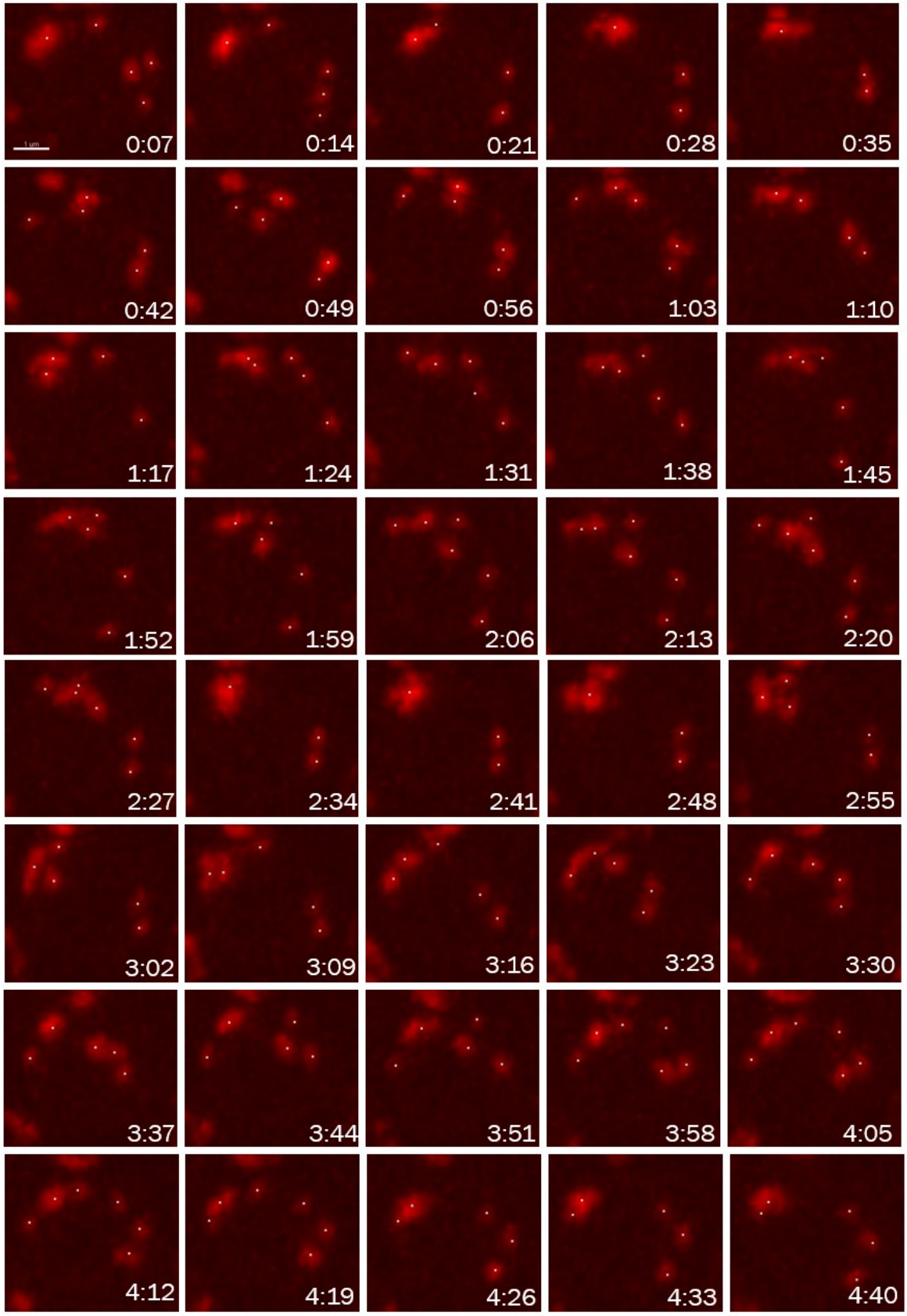
1 µm
0:07
0:14
0:21
0:28
0:35
0:42
0:49
0:56
1:03
1:10
1:17
1:24
1:31
1:38
1:45
1:52
1:59
2:06
2:13
2:20
2:27
2:34
2:41
2:48
2:55
3:02
3:09
3:16
3:23
3:30
3:37
3:44
3:51
3:58
4:05
4:12
4:19
4:26
4:33
4:40

B

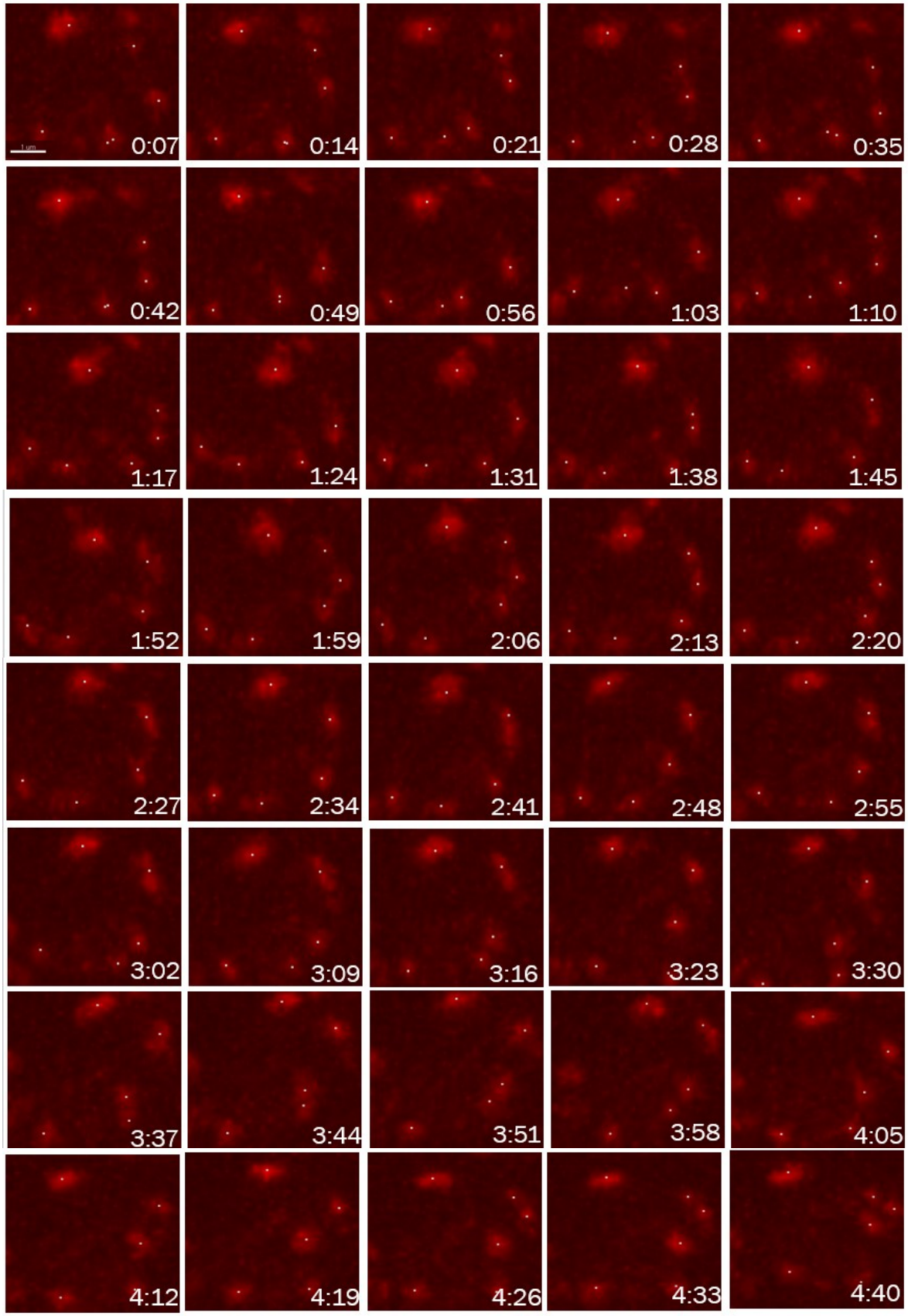
0:07
0:14
0:21
0:28
0:35
0:42
0:49
0:56
1:03
1:10
1:17
1:24
1:31
1:38
1:45
1:52
1:59
2:06
2:13
2:20
2:27
2:34
2:41
2:48
2:55
3:02
3:09
3:16
3:23
3:30
3:37
3:44
3:51
3:58
4:05
4:12
4:19
4:26
4:33
4:40

Figure 1. The aggregation of SUN-1 is not required for chromosome movement *per se*. However, chromosomes ends in *plk-2(vv44)::mCherry* mutants appear to move slower and to cluster less compared to wild type worms.

The PLK-2^{vv44} protein is the product of a mutation in the activation domain of PLK-2. SUN-1 remains uniformly distributed around the early-meiotic nucleus in *plk-2(vv44)* mutants and fails to aggregate. To assess the impact this has on chromosome motion, nuclei in the meiotic Transition Zone (TZ) of paralysed *C. elegans* animals which express (A) PLK-2::mCherry tag and (B) PLK-2^{vv44}::mCherry tag were imaged using a spinning disc confocal microscope. Thirteen 0.5 µm spaced Z-stacks were max-intensity projected for each 7 second interval. Each animal was recorded for 5 minutes and 8 seconds; only the first 4 minutes and 40 seconds are shown. The (A) PLK-2::mCherry and (B) PLK-2^{vv44}::mCherry fluorescent signals were tracked with the **Spot** tracking tool in **Imaris (Bitplane).** Since both constructs successfully localize to the Pairing Centre (PC) of chromosomes, this allowed us to assess TZ chromosome end dynamics. The dots in the fluorescent signals represent the distinct chromosome end clusters identified by the **Spot** tracking program. In (A) chromosome ends exhibit highly dynamic behaviour; they cluster, disperse and move rapidly. In (B) chromosome ends still move, albeit much more slowly. They cluster occasionally and then rapidly split apart. Scale bars, 1 µm.

Figure 2

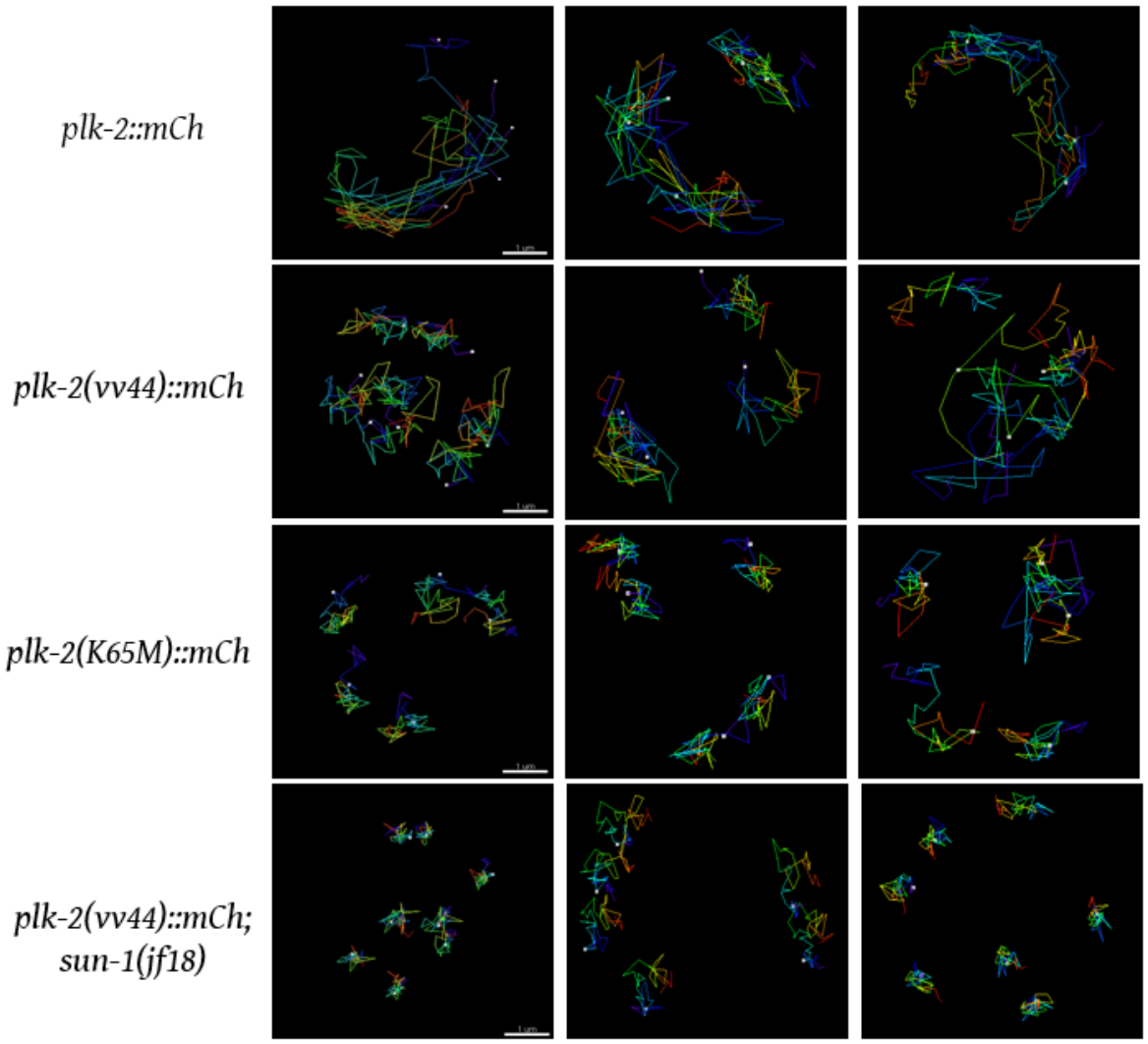

Figure 2. PLK-2 kinase activity is necessary for rapid chromosome end motion during Prophase I.

The *Spot* Tool in **Imaris (Bitplane)** software was used to track the PLK-2^{X}::mCherry fluorescent signals. Displacement tracks which represent the movement of PLK-2^{X}::mCherry marked chromosome end clusters in 3 TZ nuclei are shown for each indicated genotype. Tracks are coloured according to time point. The track goes from red to orange, to yellow, to green to blue to violet, where red represents the earliest time point and violet the latest. Movies were taken with a spinning disc confocal microscope and are 5 minutes and 8 seconds long with 7 second intervals of thirteen 0.5 µm spaced Z-stacks. PLK-2^{K65M} is a kinase-dead form of PLK-2, which involves a mutation in the ATP binding motif of PLK-2 (Lee et al. 1995). SUN-1^{JF18} is unable to retain ZYG-12 in the outer nuclear envelope, therefore abrogating the connection between the chromosome ends and the cytoskeleton (Penkner et al., 2007; Sato et al., 2009). In nuclei which express SUN^{JF18} and PLK-2^{vv44}, chromosome end movement is largely lost and only small diffusive motions are made. This is similar to what was observed previously in mutants which express only *sun-1(jf18)* (Baudrimont et al., 2010). In *plk-2(K65M)::mCherry* nuclei, this movement is a little bit more dynamic but is dramatically worse than in *plk-2(vv44)::mCherry* and *plk-2::mCherry* animals. The crescent pattern of the tracks seen in *plk-2::mCherry* nuclei is lost in the other strains. The tracks seem to overlap less often in the other strains than in *plk-2::mCherry* worms. They overlap more in *plk-2(vv44)::mCherry* mutants than in *plk-2(K65M)::mCherry* worms. *plk-2(vv44)* mutants show the most variability, having both long and shorter tracks. Scale bars, 1 µm.

Figure 3

A

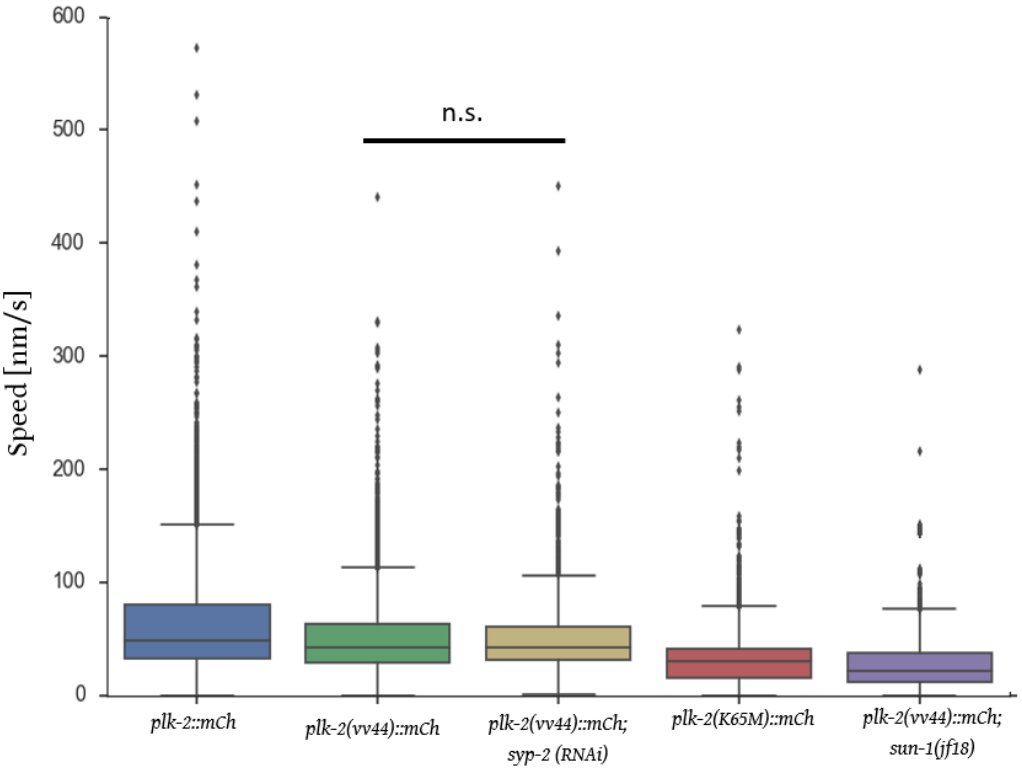
600
500
400
300
200
100
0
Speed [nm/s]
n.s.
plk-2::mCh
plk-2(vv44)::mCh
plk-2(vv44)::mCh; syp-2 (RNAi)
plk-2(K65M)::mCh
plk-2(vv44)::mCh; sun-1(jf18)

B

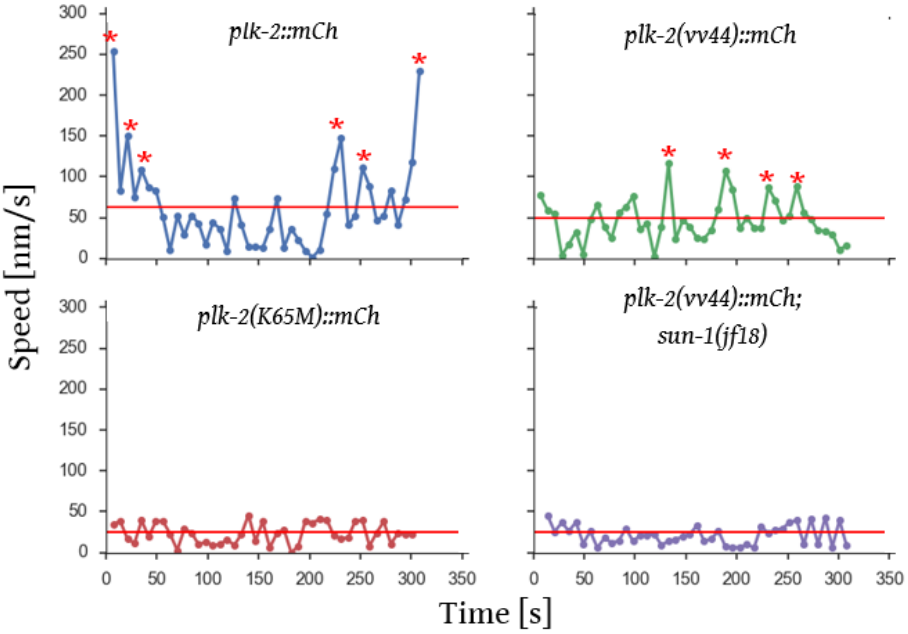
plk-2::mCh
plk-2(vv44)::mCh
plk-2(K65M)::mCh
plk-2(vv44)::mCh; sun-1(jf18)
Speed [nm/s]
Time [s]
0
50
100
150
200
250
300
350

Figure 3. Loss of PLK-2 kinase activity and chromosome-end association with the cytoskeleton results in a decrease in PC-driven chromosome motion speed during early prophase.

Displacements of PLK-2^X aggregates over 7 second intervals were used to calculate the speeds of chromosome end clusters. (A) The cumulative distribution of the speeds for each indicated genotype. A gamma regression provided support that the genotypes studied had an impact on chromosome end speed ($p < 2*10^{-16}$). The follow-up multiple comparisons of mean using Tukey Contrasts showed a significant difference of the speeds between each pair of strains ($p < 0.001$) except for between *plk-2(vv44); syp-2(RNAi)* and *plk-2(vv44)* mutants ($p > 0.05$). This shows that decreases in chromosome end speed in *plk-2(vv44)::mCherry* worms are not due to precocious synapsis. (n = 12 nuclei per worm, 3 animals per strain). (B) Displacement of distinct PLK-2^X::mCherry fluorescence signals over 7 second intervals were used to infer the speeds of chromosome end clusters. Shown is a 5 minute and 8 second speed snapshot of one of the chromosome end clusters for each indicated strain. The red bar is drawn at the average speed for that chromosome end cluster. The stars denote processive chromosome motions (PCM). PCM are dynein-dependent (Wynne et al., 2012) bursts in chromosome speed (Figure S1). *plk-2(vv44)::mCherry* mutant's chromosome ends are still competent at undergoing PCM, albeit less frequently and at a lower magnitude than in wild type worms. These movements are still due to linkage to the cytoskeleton and PLK-2 kinase activity since in *plk-2(vv44)::mCherry; sun-1(jf18)* and *plk-2(K65M)::mCherry* mutants respectively PCM stops occurring.

Table 1

Genotype	Mean ± SD Patch Count per Nucleus
plk-2::mCh	4.9 ± 1.0
plk-2(vv44)::mCh	6.4 ± 1.3
plk-2(K65M)::mCh	5.8 ± 2.1
plk-2(vv44)::mCh; sun-1(jf18)	10.5 ± 1.2

Table 1. *plk-2* mutants have a significantly higher average independent number of chromosome end hubs per nucleus, suggesting a decrease in chromosome end aggregate formation.

This table shows the mean number, plus or minus the standard deviation, of distinct fluorescent signals per nucleus for each indicated strain. The number of distinct fluorescent objects were a proxy for the number of chromosome end clusters detected by the spinning disc confocal microscope in a nucleus. An example of a nucleus that has 5 distinct fluorescent signals is seen in Figure 1A, timestamp 0:07. Lower ranges signify higher chromosome end clustering occurring in the nucleus. A Poisson regression model provided support for a significant contribution of genotype on patch count per nucleus ($p < 0.001$ for the model of patch count as a factor of genotype; $p < 0.001$ between all comparisons between genotypes in the Tukey contrasts that followed) ($n = 8$ nuclei per worm, 2 worms per genotype).

Figure 4

A

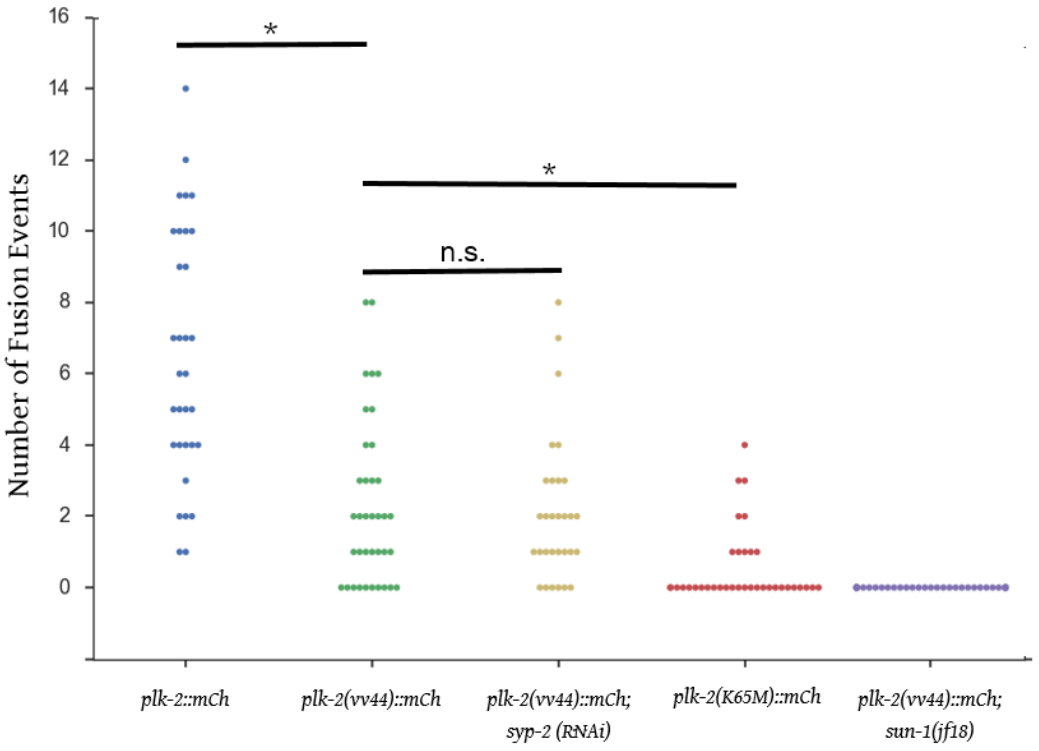
Number of Fusion Events
16
14
12
10
8
6
4
2
0
*
*
n.s.
plk-2::mCh
plk-2(vv44)::mCh
plk-2(vv44)::mCh; syp-2 (RNAi)
plk-2(K65M)::mCh
plk-2(vv44)::mCh; sun-1(jf18)

B

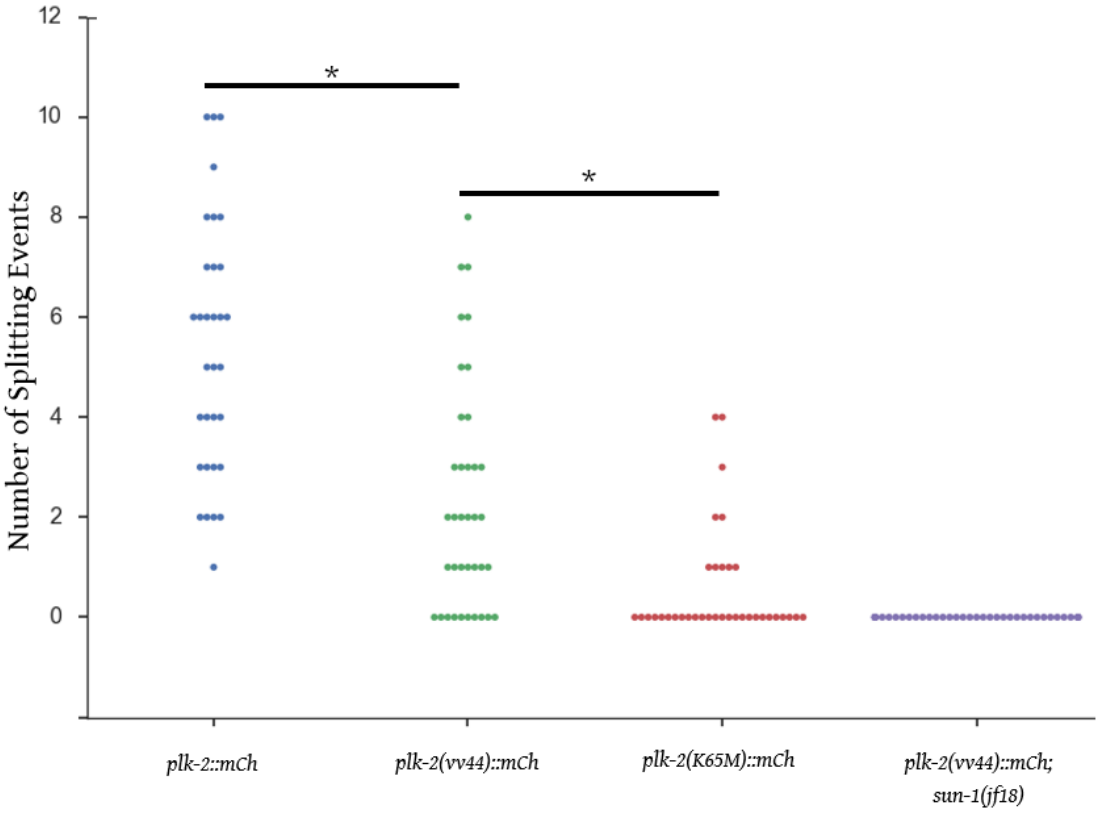
Number of Splitting Events
12
10
8
6
4
2
0
*
*
plk-2::mCh
plk-2(vv44)::mCh
plk-2(K65M)::mCh
plk-2(vv44)::mCh; sun-1(jf18)

Figure 4. PLK-2 kinase activity and the NE protein bridge have a significant contribution to the frequency of chromosome end interaction and separation.

(A) For each nuclei in the TZ, the number of times two or more fluorescent signals overlapped and could not be distinguished were counted as "fusion events". Chromosomes in these hubs were close enough to perform homology assessment. Each data point reflects one nucleus which had *y* number of fusion events. A quasi-Poisson regression provided support for the genotype impacting the number of interaction events in TZ nuclei ($p < 0.05$). The Tukey contrasts model that followed provided support for a difference in fusion events between wild type and *plk-2(vv44)::mCherry* animals ($p < 0.001$), and between *plk-2(vv44)::mCherry* and *plk-2(K65M)::mCherry* mutants ($p < 0.001$). It did not provide support for there being a difference between *plk-2(vv44)::mCherry* and *plk-2(vv44)::mCherry; syp-2(RNAi)* mutants ($p > 0.05$). This means that the decrease in chromosome interaction in *plk-2(vv44)::mCherry* mutants is not due to precocious synapsis. *plk-2(vv44)::mCherry; sun-1(jf18)* animals were not included in the statistical analysis because all of their TZ nuclei had 0 fusion events, and with their inclusion the model failed to converge. ($n = 12$ nuclei per worm, 3 animals per strain). (B) For each nuclei in the TZ, the number of times a single fluorescent signal separated into two or more fluorescent signals were counted as a "separation events". Each data point reflects one nucleus which had *z* number of separation events. A Poisson regression provided support for the genotype impacting the number of separation events in TZ nuclei ($p < 0.05$). The Tukey contrasts model that followed provided support for a difference in disentangling events between wild type and *plk-2(vv44)::mCherry* animals ($p < 0.0001$) and *plk-2(vv44)::mCherry* and *plk-2(K65M)::mCherry* ($p < 0.00001$) mutants. *sun-1(jf18)* animals were not included in the statistical analysis because all of their nuclei had 0 separation events, and with their inclusion the model failed to converge ($n = 12$ nuclei per worm, 3 animals per strain).

Figure 5

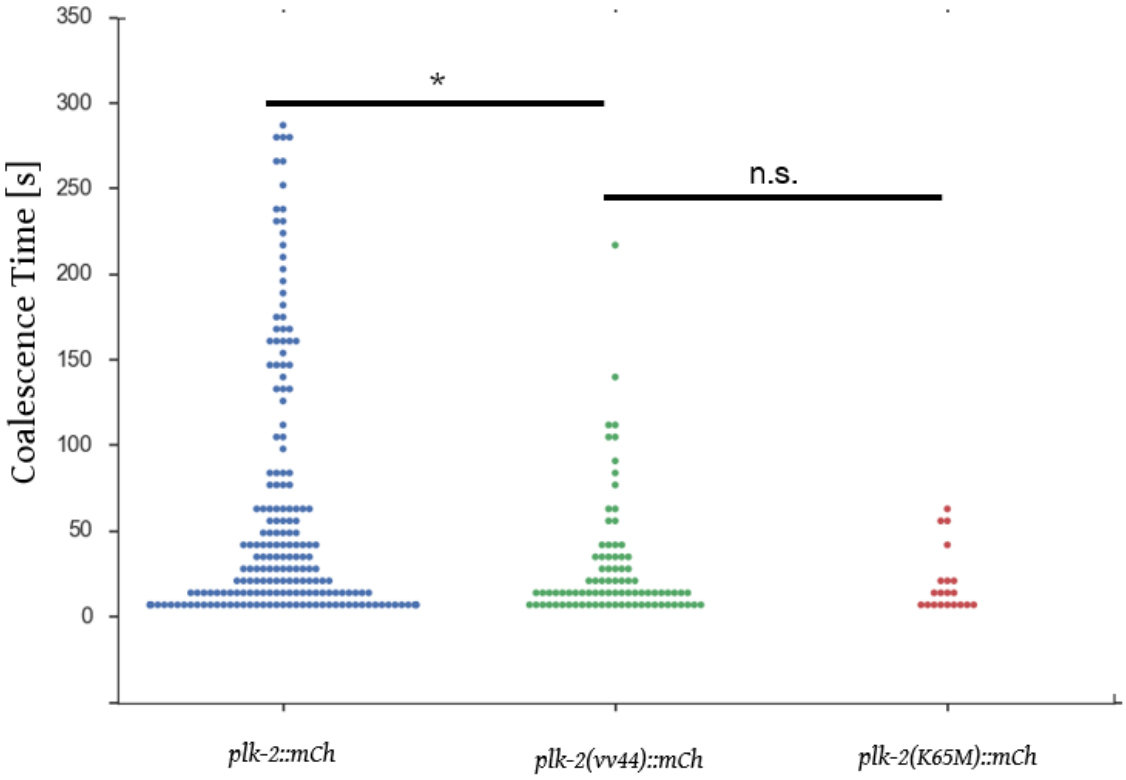
Coalescence Time [s]
350
300
250
200
150
100
50
0
*
n.s.
plk-2::mCh
plk-2(vv44)::mCh
plk-2(K65M)::mCh

Figure 5. PLK-2 kinase activity is essential for holding chromosome ends close together for longer durations.

When two or more fluorescent signals clustered into one larger signal, they were tracked until they separated. Each data point in the plot represents the length of time between one fusion and splitting event. The number of fusion and splitting events is different for each strain. A quasi-Poisson regression supported that there was a relationship between genotype and coalescence time ($p < 0.01$). A post-hoc Tukey contrasts model supported a difference between *plk-2::mCh* and *plk-2(vv44)::mCh* animals ($p < 0.0001$) but not between *plk-2(vv44)::mCh* and *plk-2(K65M)::mCh* ($p > 0.05$) animals ($n = 12$ nuclei per animal, 3 worms per strain).

Figure 6

A

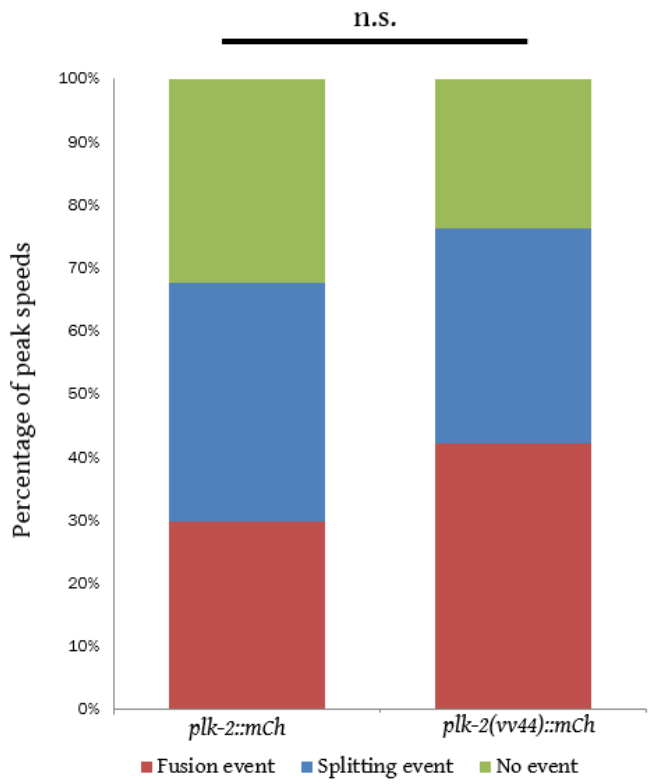
n.s.
100%
90%
80%
70%
60%
50%
40%
30%
20%
10%
0%
Percentage of peak speeds
plk-2::mCh
plk-2(vv44)::mCh
Fusion event
Splitting event
No event

B

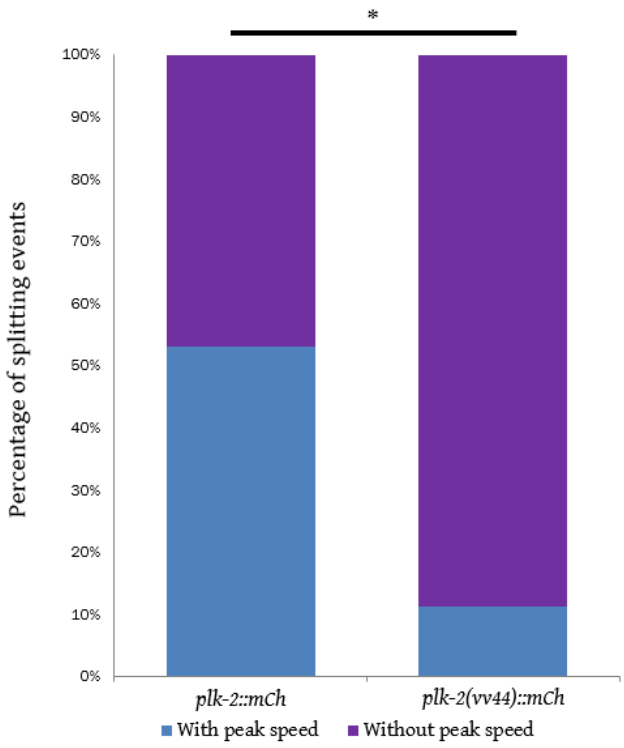
*
100%
90%
80%
70%
60%
50%
40%
30%
20%
10%
0%
Percentage of splitting events
plk-2::mCh
plk-2(vv44)::mCh
With peak speed
Without peak speed

Figure 6. Processive chromosome motions correlate with high-tension splitting and fusion events.

(A) The tracks and time points in which PCM occurred were identified (Figure S1). The event which was occurring during that time point was identified. If in the previous time point the fluorescent signal had been fused with another which it had split off from, it was characterized as a "splitting event". If in the next time point the fluorescent signal becomes fused with another it was characterized as a "fusion event". In both *plk-2::mCherry* worms and *plk-2(vv44)::mCherry* mutants, peak speeds were correlated with splitting events and fusion events in a similar proportion (chi-square test, $p > 0.05$) ($n = 111$ peak speeds sampled from 3 *plk-2::mCherry* worms; $n = 38$ peak speeds sampled from 3 *plk-2(vv44)::mCherry* worms). (B) Splitting events were assessed and evaluated if they correlated with a peak speed. In *plk-2::mCherry* worms, 53 % of the splitting events assessed correlated with peak speeds. In *plk-2(vv44)::mCherry* about 89 % of the splitting events didn't (chi-square test, $p < 0.001$) ($n = 81$ splitting events sampled from 3 *plk-2::mCherry* worms; $n = 71$ splitting events sampled from 3 *plk-2(vv44)::mCherry* worms).

Figure 7

A

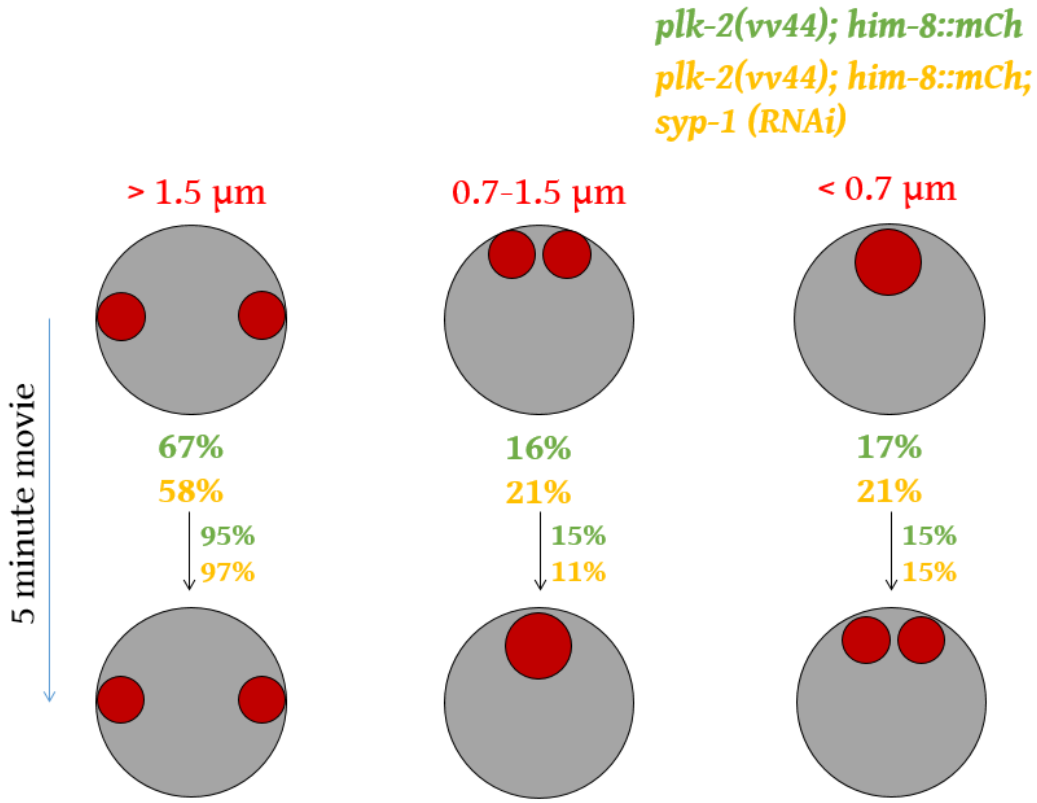
plk-2(vv44); him-8::mCh
plk-2(vv44); him-8::mCh; syp-1 (RNAi)
> 1.5 µm
0.7-1.5 µm
< 0.7 µm
5 minute movie
67%
58%
16%
21%
17%
21%
95%
97%
15%
11%
15%
15%

B

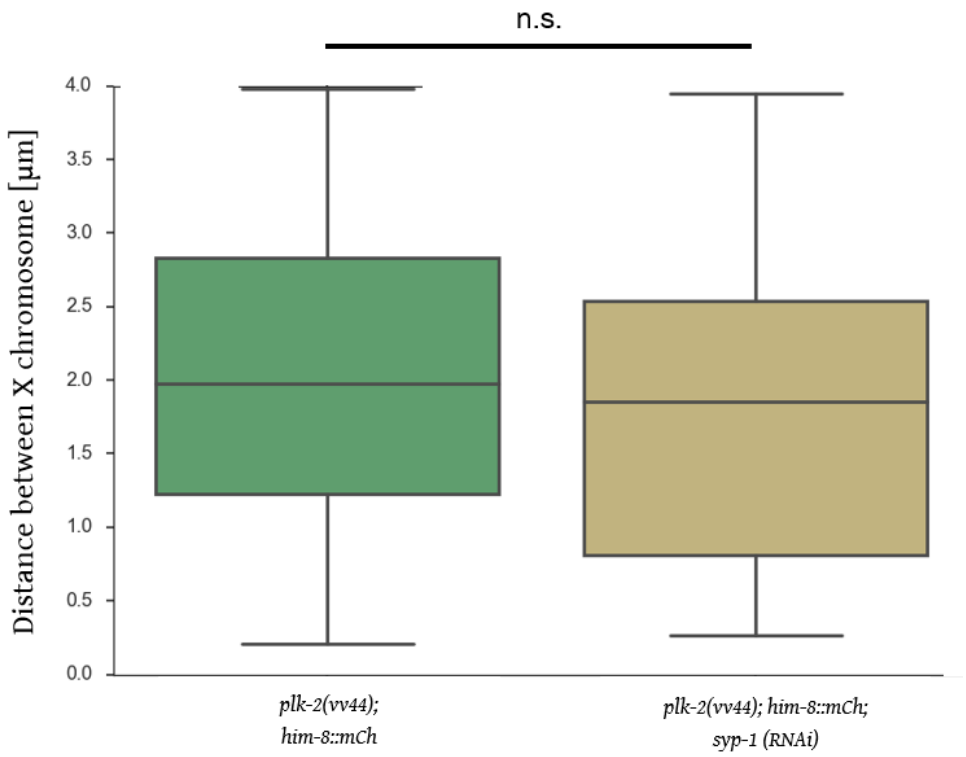
n.s.
Distance between X chromosome [µm]
4.0
3.5
3.0
2.5
2.0
1.5
1.0
0.5
0.0
plk-2(vv44); him-8::mCh
plk-2(vv44); him-8::mCh; syp-1 (RNAi)

Figure 7. The X chromosomes in *plk-2(vv44)* mutants have difficulty locating their homolog and then initiating and maintaining pairing with their homolog; this defect is not due to precocious entanglement with heterologous chromosomes due to synapsis.

(A) Representation of X chromosome behaviour in a strain expressing the PC protein HIM-8 tagged with mCherry fluorophore in *plk-2(vv44)* animals. The movement of the X chromosomes was tracked over a 5 minute period, acquiring images at 12 second intervals. The distance between the centres of the two HIM-8::mCherry foci was measured using the *Distance* tool in **Imaris (Bitplane).** Foci less than 0.7 µm apart were considered to be within pairing distance (MacQueen et al., 2002). In this mutation background, in 67 % of the nuclei the two X chromosomes were more than 1.5 µm apart at the beginning of the movie (Figure S2). Of these nuclei, 95 % of them had X chromosomes which remained at a distance greater than 1.5 µm during the 5 minutes recorded showing a complete lack of interaction. 16 % of the nuclei showed X chromosome pairs that were closer than 1.5 µm apart but further than 0.7 µm at the start of recording. In 85 % of these nuclei, the X chromosomes remained close enough to be able to get within pairing distance (Figure S3) and become a single focus but they didn't manage to in 5 minutes. This behaviour is not due to precocious synapsis impeding the final step of pairing (chi-square test, $p > 0.05$). When synapsis was removed with RNAi, 89 % of the nuclei with X chromosomes which were at a distance of 0.7 to 1.5 µm still remained in that proximity by the end of the recording. 17 % of the nuclei had X chromosomes closer than 0.7 µm at the beginning of the movie. For 15 % of the nuclei which showed X chromosomes that were closer than 0.7 µm, the distance between them increased to higher than 0.7 µm by the end of the movie showing that X chromosome ends cannot stay together even when they manage to coalesce. The results for *plk-2(vv44);him-8::mCherry* nuclei are shown in green. The

results for *plk-2(vv44);him-8::mCherry; syp-1(RNAi)* nuclei are shown in yellow (*n* = ~40 nuclei per worm, 3 animals per strain). (B) The distance between the centres of a pair of HIM-8::mCherry fluorescent signals was calculated with the *Distance* tool in **Imaris (Bitplane).** This was used to infer the distances between X chromosome PCs. The average distance between X chromosomes over the 5 minute recording for each nucleus was calculated and plotted. There is no significant difference between the distance between X chromosome distributions of *plk-2(vv44); him-8::mCherry* and *plk-2(vv44); him-8::mCherry; syp-1 (RNAi)* mutants (2-tailed *t*-test, $p > 0.05$) (*n* = 35 nuclei per worm, 3 animals per strain).

Figure 8

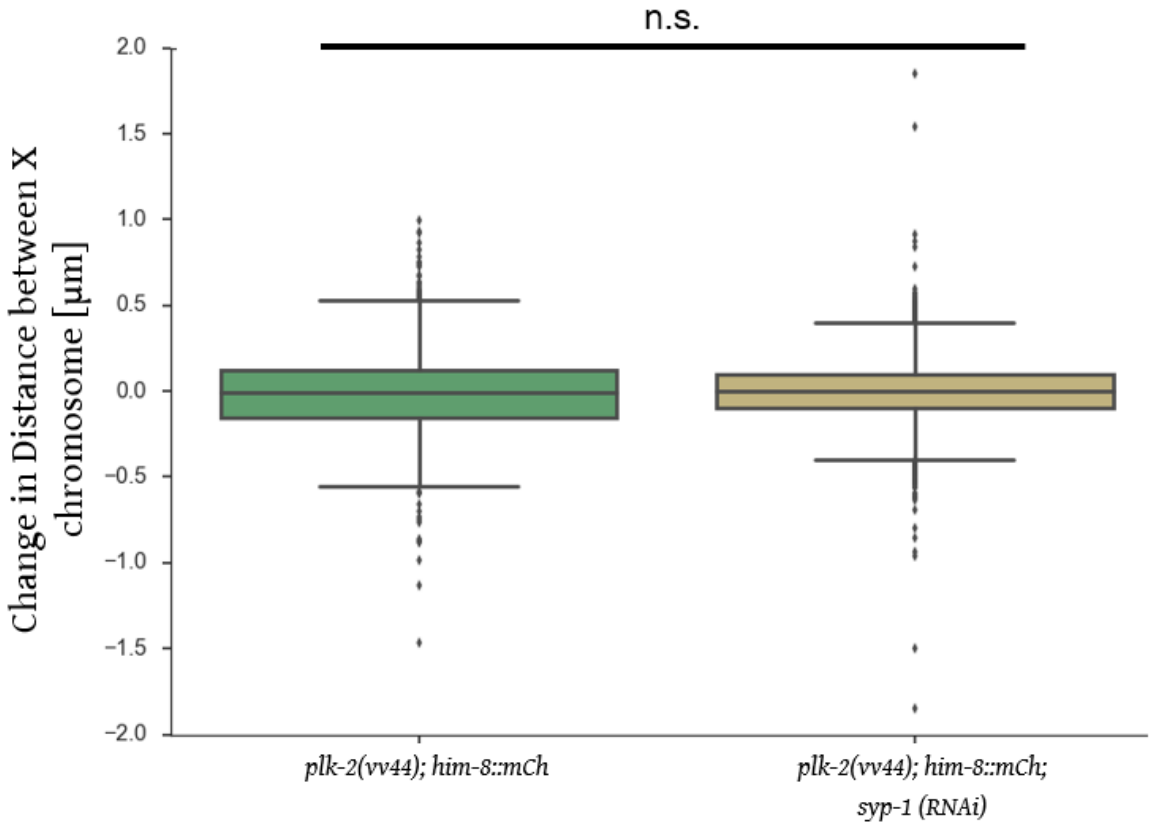
n.s.
Change in Distance between X chromosome [µm]
2.0
1.5
1.0
0.5
0.0
−0.5
−1.0
−1.5
−2.0
plk-2(vv44); him-8::mCh
plk-2(vv44); him-8::mCh; syp-1 (RNAi)

Figure 8. X chromosomes in a *plk-2(vv44)* background move independently from each other; removing synapsis does not alter this pattern.

The HIM-8::mCherry fluorescent signals were used to infer the position of the X chromosome PC. The change in distance between the X chromosomes over time was evaluated using the *Distance* tool in **Imaris (Bitplane).** A positive change in distance suggests the X chromosome PCs were moving further apart. A negative change in distance suggests that the X chromosome ends were moving closer together. The median change in distance is close to 0 in both *plk-2(vv44); him-8::mCherry* and *plk-2(vv44)::mCherry; him-8::mCherry; syp-1(RNAi)* mutants. There is no significant difference in change in X chromosome distance over time between *plk-2(vv44); him-8::mCherry* and *plk-2(vv44); him-8::mCherry; syp-1(RNAi)* mutants (2-tailed *t*-test, $p > 0.05$) ($n = 16$ nuclei per worm, 3 animals per strain; ~24 changes in distance per nucleus).

Supplemental Figures

Figure S1

A

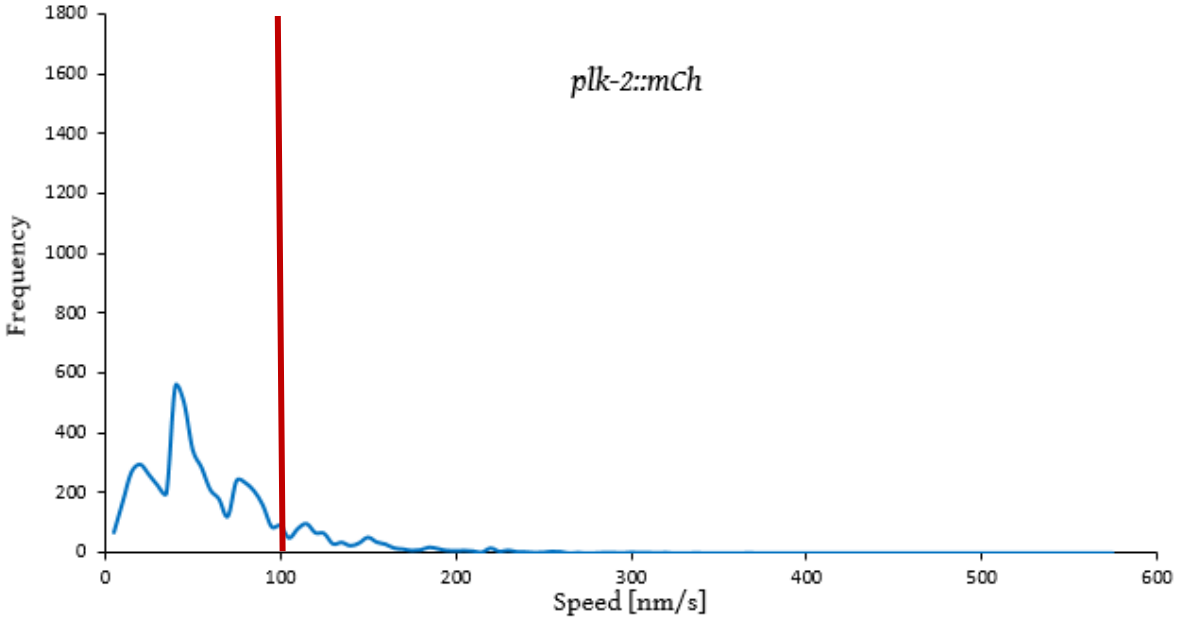

B

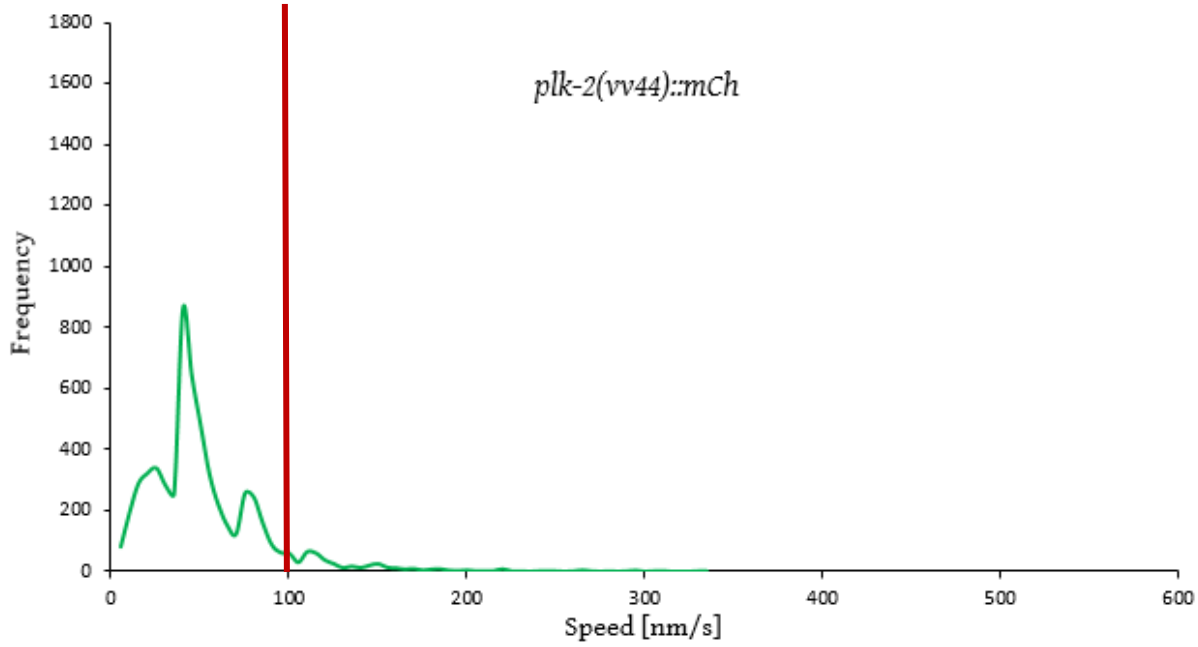

C

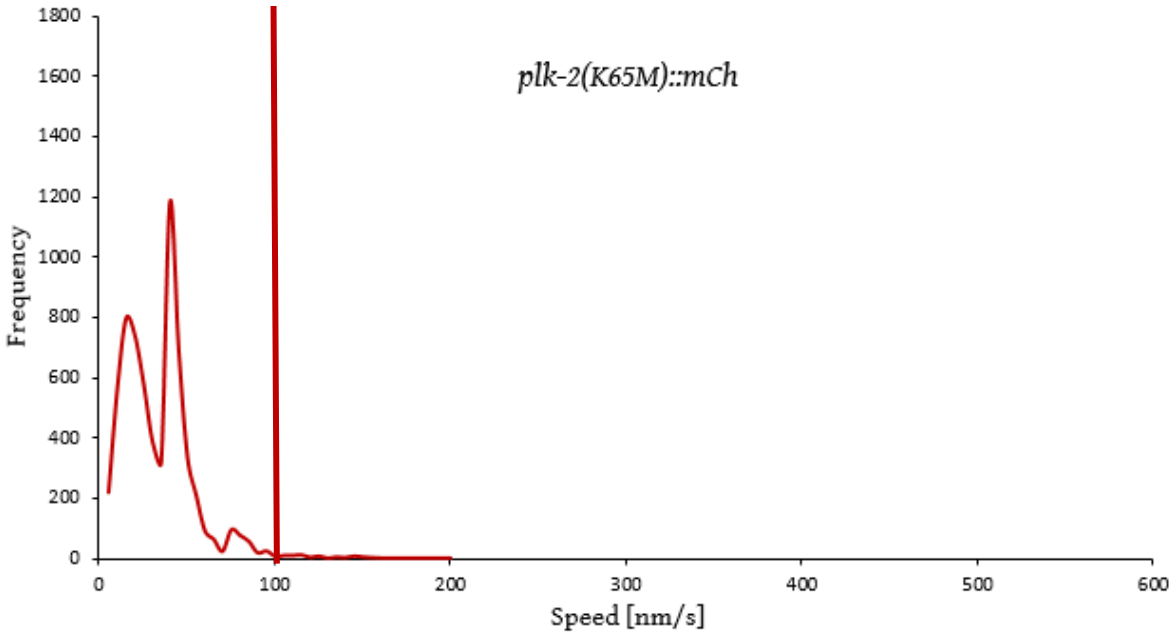
plk-2(K65M)::mCh
Frequency
Speed [nm/s]
0
200
400
600
800
1000
1200
1400
1600
1800
0
100
200
300
400
500
600

D

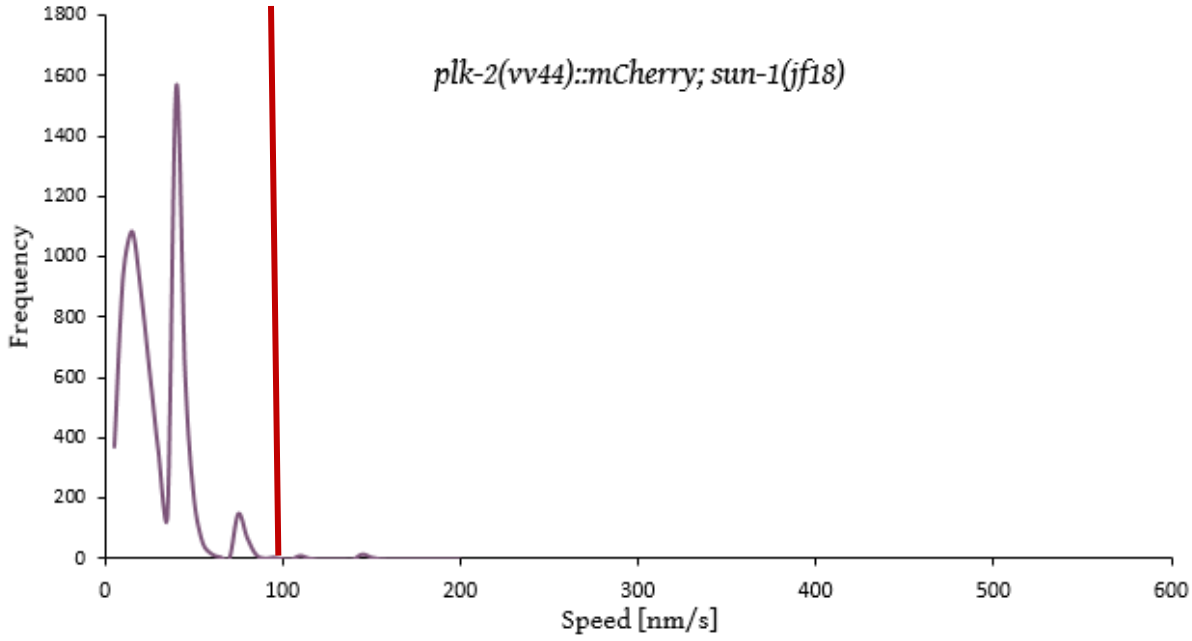
plk-2(vv44)::mCherry; sun-1(jf18)
Frequency
Speed [nm/s]
0
200
400
600
800
1000
1200
1400
1600
1800
0
100
200
300
400
500
600

E

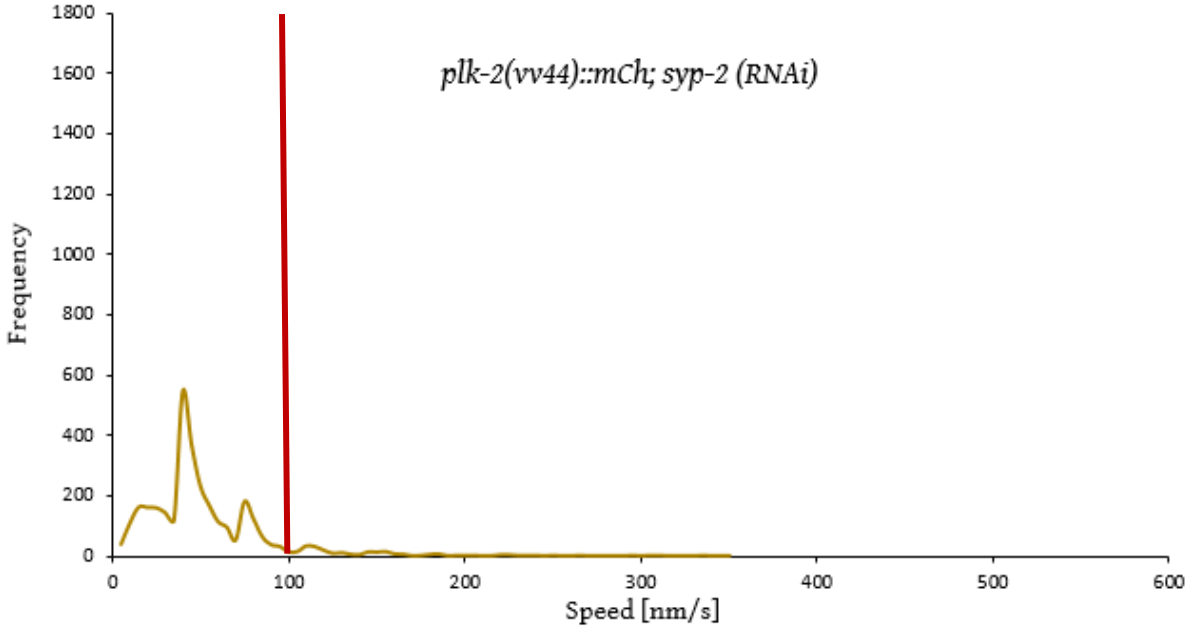
plk-2(vv44)::mCh; syp-2 (RNAi)
Frequency
1800
1600
1400
1200
1000
800
600
400
200
0
0
100
200
300
400
500
600
Speed [nm/s]

Figure S1, related to Figure 3. Polo-like kinase activity and force transduction by the cytoskeleton are necessary in order for chromosomes to undergo processive chromosome motions.

Displacements of the distinct PLK-2^{X}::mCherry fluorescence signals over 7 second intervals were measured with the *Spot* tool in **Imaris (Bitplane).** These measurements were used to infer the speeds of chromosome end clusters. Shown is the cumulative distribution of the speeds for (A) *plk-2::mCherry,* (B) *plk-2(vv44)::mCherry*, (C) *plk-2(K65M)::mCherry*, and (D) *plk-2(vv44)::mCherry; sun-1(jf18)* worms and (E) *plk-2(vv44)::mCherry; syp-2(RNAi)*. The red bars delineate the boundary at which we defined "peak speeds" (100 nm/s). Peak speeds were inferred from the tail end of the *plk-2::mChery* worm speed distribution as per Baudrimont et al. (2012). We consider these "peak speeds" to represent processive chromosome motions, as defined by Wynne et al. (2012). PCMs occurred 15 % of the time in wild type worms and occurred 7 % of the time in *plk-2(vv44)::mCherry* mutants. Proportion of peak speeds did not change upon feeding *plk-2(vv44)::mCherry* animals *syp-2* (RNAi). We did not detect the presence of substantial processive chromosome motions in worms which expressed PLK-2^{K65M}::mCherry or SUN-1^{jf18} in a *plk-2(vv44)::mCherry* background. This shows that the contribution of PLK-2 kinase activity and cytoskeletal force transduction through the NE are required for processive chromosome motions. (*n* =12 nuclei per worm, 3 animals per strain).

Figure S2

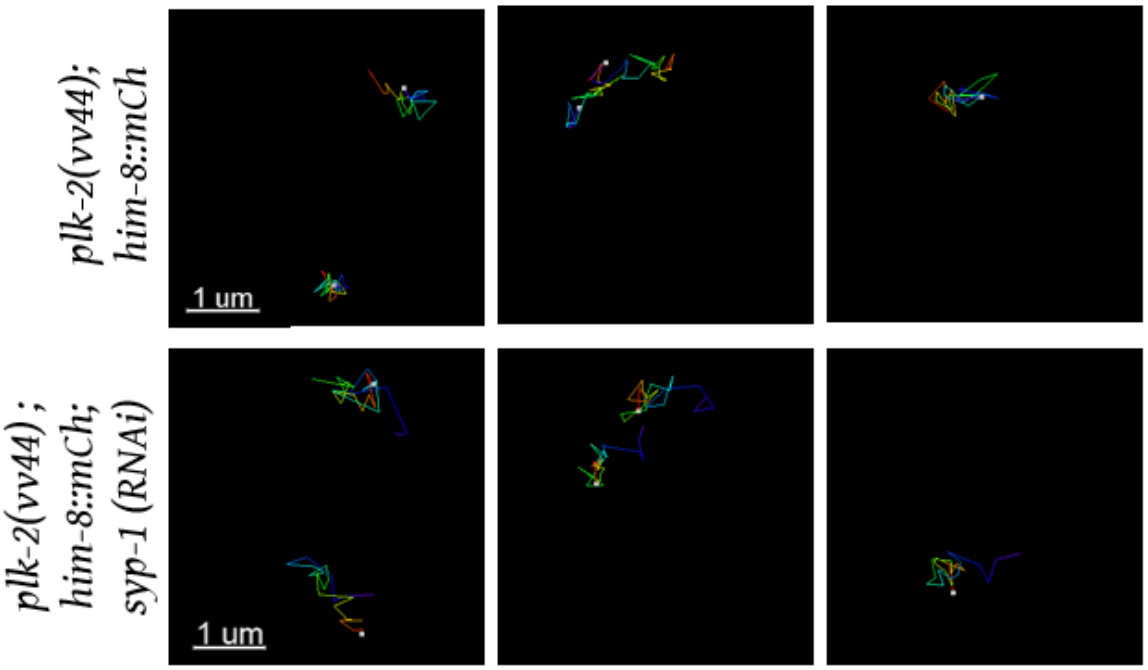

Figure S2, related to Figure 7. Chromosomes have difficulty finding their homologous partner in a *plk-2(vv44)::mCherry* background; abrogation of synapsis does not change X chromosome movement dynamics in a *plk-2(vv44)* background. Him-8::mCherry foci movement was tracked over time using the *Spot* tool in **Imaris (Bitplane).** Displacement tracks which represent the movement of X chromosome ends are shown for the two indicated genotypes. Tracks are coloured according to time point. The track goes from red to orange, to yellow, to green to blue to violet, where red represents the earliest time point and violet the latest. Movies are ~5 minutes long with 12 second intervals. Example of non-overlapping tracks are shown in the first column. They represent X chromosomes which did not interact over the course of the 5 minute movie (Figure 7A). Example of chromosome ends which are close but cannot bridge the gap are shown in the second column (Figure 7A). Example of the movement of a coalesced pair of X chromosomes is shown in the third column (Figure 7A). Scale bars, 1 μm

Figure S3

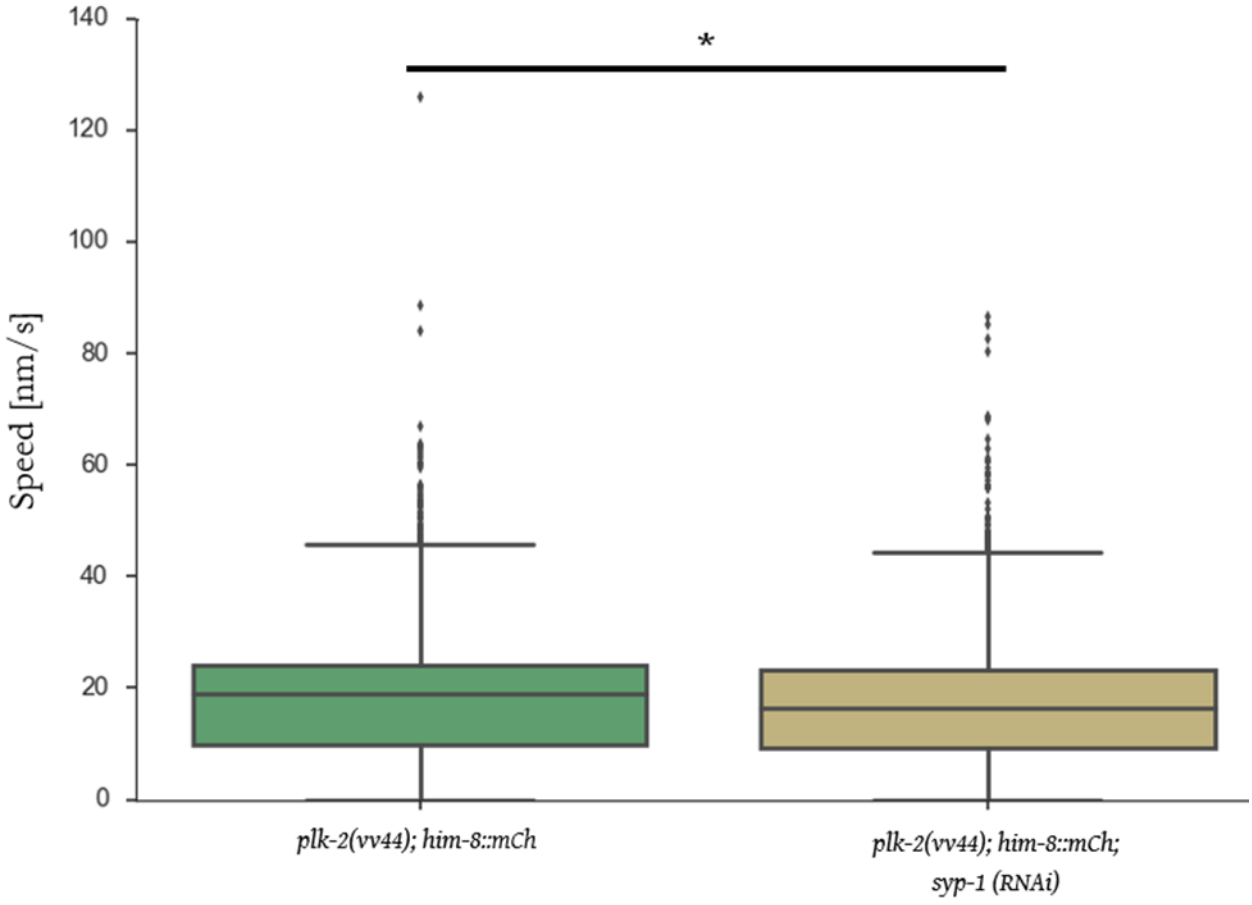
Speed [nm/s]
140
120
100
80
60
40
20
0
*
plk-2(vv44); him-8::mCh
plk-2(vv44); him-8::mCh;
syp-1 (RNAi)

Figure S3, related to Figure 7. The average speed of X chromosomes is high enough, that chromosomes which are less than 1.5 µm apart should be able to move within pairing distance by the end of a 5 minute movie.

Displacements of HIM-8 fluorescent markers over 12 second time points were measured with the *Spot* tool in **Imaris (Bitplane)**. These measurements were used to infer the speeds of X chromosome PCs. Shown is the cumulative distribution of X chromosome end speed in a *plk-2(vv44); him-8::mCherry* background. There is a slight significant drop in X chromosome PC speed between *plk-2(vv44); him-8::mCherry* animals, average speed of 18.78 nm/s, and *plk-2(vv44); him-8::mCherry; syp-1 (RNAi)* mutants, average speed of 17.73 nm/s (2-tailed *t*-test, $p < 0.05$) ($n = 16$ nuclei per worm, 3 animals per strain).

Chapter II

Identifying putative PLK-2 targets involved in early meiotic chromosome motion

Introduction

PLK-2 is a key coordinator of meiotic chromosome motion

Upon meiotic onset, one end of each chromosome associates with the inner nuclear periphery (Alsheimer, 2008; Hiraoka and Dernburg, 2009). PLK-2 localizes to these pairing centres (PCs), and facilitates the phosphorylation of the inner nuclear envelope (NE) protein, SUN-1 (Penkner et al., 2009; Labella et al., 2011). SUN-1, and ZYG-12 which is embedded in the outer NE, then aggregate into distinct foci. These foci then coalesce into larger patches in the vicinity of the chromosome PCs (Penkner et al., 2009; Sato et al., 2009; Labella et al., 2011). Force is transduced from the cytoskeleton through the SUN-1/ZYG-12 protein bridge, resulting in dynamic chromosome end motion (Penkner et al., 2007, 2009; Baudrimont et al., 2010; Wynne et al., 2012). Chromosomes proceed to find and align with their homologous partner. In the absence of PLK-2 kinase activity, SUN-1 and ZYG-12 fail to aggregate and instead remain uniformly distributed around the TZ nuclear periphery and the late prophase I nuclei exhibit high levels of heterologous chromosome pairing (Labella et al., 2011).

In Chapter I, we provided evidence that PLK-2 is a key regulator of chromosome motion during prophase I. Namely, that in *plk-2* mutants chromosome speed sharply decreases and chromosome PCs interact less frequently with each other. Further investigation of how PLK-2 coordinates these events through its kinase domain would contribute to our understanding of how chromosomes locate and accurately identify their homologous partner.

Identification of possible PLK-2 docking motifs

PLK-2 is a member of the polo-like family of kinases. Proteins in this family are characterized by an N-terminal serine/threonine kinase domain and a C-terminal polo-box domain. The polo-box domain is required for correct subcellular localization and for binding to target

proteins (Cheng et al., 2003). In this family, PLK-1 is the most studied, due to its essential role in many events during mitosis (Petronczki et al., 2008).

In *C. elegans* during meiotic prophase, PLK-1 and PLK-2 have some functional redundancies. PLK-2 has a higher affinity than PLK-1 to several of its meiotic targets. In a *plk-2* null background, PLK-1 localizes to chromosome PCs and facilitates phosphorylation of PLK-2 NE substrates, such as S12 on SUN-1 (Labella, 2012). The fact that PLK-1 and PLK-2 have overlapping targets has been described for other processes as well (Nishi et al., 2008; Chase et al., 2000). Therefore, PLK-2 may have some affinity for known PLK-1 docking motifs. *In vitro* studies have shown that PLK-1 has a preferential binding for phosphoserine/threonine-containing sequence motifs (Elia et al., 2003), and an especially strong affinity for the consensus sequence `S[pS/pT][P/X]`.

Multiple sequence alignment was performed on the amino acid sequences of the PC proteins, which are required for PLK-2 recruitment to the chromosome ends, and it was found that there is a conserved alignment of sub-sequences `STP` and `ISEI` between all four PC proteins (Figure S1). When the threonine is phosphorylated, `STP` constitutes the PLK-1 core consensus polo-box domain binding motif (Elia et al., 2003). The `ISEI` region is not a previously identified PLK-1 docking motif; however PLK-1 and PLK-2 do not completely overlap in their targets (van de Weerdt et al., 2008). So it is possible that `ISEI` constitutes a previously unknown phosphoserine/threonine docking site for PLK-2. These sequences were further supported as potential PLK-2 docking motifs through experiments where worms which expressed HIM-8^{T64A} or HIM-8^{me4} failed to recruit PLK-2 (*data not shown)*. The *him-8(me4)* allele replaced the serine in the `ISEI` motif within HIM-8 with a non-phosphorylatable residue (S85F). The *him-8(T64A)* allele replaced the threonine with a non-phosphorylatable residue

(T64A) (Harper et al., 2011; Labella, 2012; Kim et al., 2015). Further investigations of the possible PLK-2 docking motifs would provide insight into potential PLK-2 phosphorylation targets since polo-like kinases tend to phosphorylate the proteins to which they physically bind (Petronczki et al., 2008).

Discovering possible PLK-2 phosphorylation motifs

There is evidence for a PLK-2 phosphorylation motif within the human neuronal cells (Franchin et al., 2014). Otherwise, very little is known about how PLK-2 targets its substrates and which motifs it preferentially phosphorylates within the germline. There are currently no confirmed PLK-2 germline direct targets.

In order to uncover the mechanism by which PLK-2 regulates chromosome motion and homologous chromosome pairing, we set out to find proteins that are phosphorylated by PLK-2 and are involved in accurate chromosome segregation. To answer this query, we took advantage of the advances in, and sophistication of, quantitative phosphoproteomics technology (Oda et al., 2001; Mann et al., 2002; Listgarten and Emili, 2005; Ong and Mann, 2005; Savitski et al., 2011) in order to compare the phosphoproteome of three *C. elegans* strains. One of the strains was a wild type worm. The other two animals each expressed a different mutant form of PLK-2: PLK-2^{vv44} and PLK-2^{K65M}. As discussed in Chapter I, *plk-2(vv44)* is a hypomorphic allele that contains a mutation in the activation domain of PLK-2. PLK-2^{vv44} is still able to phosphorylate other proteins *in vitro* (Labella et al., 2011). In the TZ nuclei of *plk-2(vv44)* mutants, chromosome ends are still able to move dynamically. However, *plk-2(vv44)* worms have high rates of chromosome mis-segregation and are highly defective in homologous chromosome pairing (Labella et al., 2011). In *plk-2(K65M)* worms, PLK-2's kinase domain is rendered inactive by a mutation in its ATP binding domain (Lee et al. 1995). In the TZ of *plk-*

2(K65M) mutants, chromosome end movement is greatly decreased and there are high rates of chromosome mis-segregation (Labella et al., 2011; Labella, 2012) (Table 1).

Since *plk-2(K65M)* mutants express a kinase-dead form of PLK-2, we were particularly interested in determining which phosphorylation sites were significantly enriched or depleted in *plk-2(K65M)* worms compared to wild type animals. These protein phosphorylation sites will be further tested *in silico* and *in vivo* as candidates for being potential PLK-2 targets. Furthermore, we wish to see if the list of predicted PLK-2 target proteins are enriched for the putative PLK-2 docking motifs: `ISE`, `SSP` or `STP`. If they are, it would be worthwhile to further test these potential docking motifs *in vivo*.

Experimental Procedures

Mass spectrometry

Mass spectrometry and analysis were outsourced to the MRC Clinical Science Centre. An overview of their procedure is as follows. Phosphoproteins were extracted and enriched using phosphopeptide precipitation. The enriched phosphoprotein fractions were then separated on a 10 % acrylamide gel for 20 minutes at 80V, and then stained overnight with Coomassie Blue. Bands were excised from the gel and subjected to overnight trypsin digestion at 37°C. Phosphopeptides were then extracted. Dried phosphopeptides were suspended in 0.1 % trifluoroacetic acid (Silva, et al., 2014). They were then subjected to LC-MS analysis using an Ultimate 3000 nano HPLC machine coupled to a LTQ-Orbitrap-Velos mass spectrometer. The estimated phosphopeptide abundance levels were inferred from the LC chromatograms. Peptide sequences were inferred from MS spectra using the MaxQuant-Andromeda bioinformatics suite (Cox and Mann, 2008; Cox et al., 2011). The proteins the peptides came from were identified through alignment against the *C. elegans* FASTA database downloaded from WormBase (WormBase, 2016). The estimated false discovery rate for protein identification was set to 1 % (Elias and Gygi, 2007). A target-decoy approach using the reverse model was used to calculate posterior error probabilities for protein modification. A Mascot Delta Score was used to evaluate post translational modification estimates (Savitski et al., 2011).

Identification of duplicate peptides

For each protein, its peptides were locally aligned alongside each other using the *pairwiseAlignment* function from the **Biostrings** package (Pagès et al., 2016). If the local

identity of the comparison was 100 %, the abundance data for the peptides were merged together.

See *searchForDuplicates.R* for details (R v3.3.1) (https://github.com/damedebugger/Thesis).

Differential phosphopeptide expression statistical analysis

Functions from the **limma** package were used in order to assess statistical differential expression between the strains (Ritchie et al., 2015). The function *lmFit* was used to fit a linear model of abundance to each peptide. As additional input, it took a design matrix whose columns indicated which of the MS dataset columns represented *plk-2*, *plk-2(vv44)* or *plk-2(K65M)* replicates. A contrast matrix was also built, which contained the comparisons we wished to make between the genotypes (*plk-2(vv44)* vs *plk-2* and *plk-2(K65M)* vs *plk-2)*. This was input into the function *contrasts.fit* which compared the fitted coefficients for the contrasts of interest. The resulting standard errors and *t*-statistics were then moderated using the function *eBayes*, which implemented a simple empirical Bayes. *eBayes* computed a common variance, which was evaluated using the entire dataset. It then computed a shrinkage of each peptide's individual residual sample variance towards the common variance. This resulted in a more stable inference of differential expression for peptides that had a smaller number of replicates. The linear models and other formulas are described in Smyth (2005).

Details in *proteinRatioSignificance.R* (R v3.3.1) (https://github.com/damedebugger/Thesis).

Docking motif enrichment

Full protein sequences were obtained from UniProt's proteome database for *C. elegans* (UniProt Consortium, 2014). Duplicate protein sequences were removed. The number of protein sequences which contained each motif were counted. The number of protein sequences

without each motif were then inferred. The sequences which belonged to proteins with differentially regulated post translational modifications were marked. Fisher's exact test was performed to assess if the set the sequence belonged to (differentially regulated or not differentially regulated) impacted the proportion of full protein sequences which contained a motif. Contingency tables were made with the use of the *CrossTable* function from the **gmodels** package (Warnes et al., 2015). The Fisher's exact test was run using the *fisher.test* function from the **stats** package (R Core Team, 2015). Details of implementation are contained in *dockingMotifEnrichment.R* (R v3.3.1) (https://github.com/damedebugger/Thesis).

Results

Evaluating which phosphorylation residues are enriched or depleted in *plk-2* mutants

We wanted to discover which of the proteins that were involved in homologous chromosome pairing were being phosphorylated by PLK-2. We collaborated with MRC Clinical Science Centre to perform two phosphoenrichment Mass Spectrometry experiments (termed MS1 and MS2) which compared the phosphoproteomes of wild type, *plk-2(vv44)* and *plk-2(K65M)* worms. First, phosphorylated segments of proteins, termed phosphopeptides, were evaluated for their relative abundance level. Then, their sequence was determined. Finally, the location of the phosphorylation residue was predicted. For each phosphopeptide detected, there were two technical replicates per strain (Table 2). MS1's dataset contains 480 phosphopeptides (305 unique) which represent 243 proteins. MS2's dataset contains 3438 phosphopeptides (2736 unique) which represent 1364 proteins.

We were interested in the effect of PLK-2 kinase activity on the level of phosphorylation of protein segments. To that end, we focused on differences in phosphopeptide abundance in *plk-2(vv44)* mutants compared to wild type worms and in *plk-2(K65M)* mutants compared to wild type worms. Preliminarily, we wanted to assess the range of fold changes in our system, evaluate how *plk-2(vv44)* mutants compared with *plk-2(K65M)* mutants and distinguish any differences in fold change distributions between MS1 and MS2. We hypothesized that since the *plk-2(K65M)* allele expresses a kinase-dead form of PLK-2, we'd see a larger relative decrease in abundance for phosphopeptides in *plk-2(K65M)* worms than in *plk-2(vv44)* mutants. We calculated the log ratio, for each replicate of each phosphopeptide, of *plk-2(vv44)* mutants over wild type worms and *plk-2(K65M)* mutants over wild type worms and plotted the resulting

distributions (Figure 1). The majority of phosphopeptides detected by the MSs had fold changes ranging from -2 to +2 in abundance level between genotypes. We favoured the idea that phosphopeptides with fold changes beyond that range would be of higher interest. In MS1, extreme abundance changes were more common in *plk-2(K65M)* mutants vs wild type worms (Figure 1B) than in *plk-2(vv44)* mutants vs wild type worms (Figure 1A). In MS2, it was the opposite (Figures 1C, D). Also of interest was that both of MS1's log ratio distributions have three local maxima, while MS2's distributions have at most two. Additionally, MS1 had a higher presence of phosphopeptides with higher fold changes (>±15) (Figures 1A, B). Due to the differences in the fold change distributions and in the sizes of the datasets, we decided not to combine the two MSs and instead treated them as separate experiments.

One instance of a high magnitude of fold change in a phosphopeptide between a mutant strain and wild type worm, is not sufficient evidence that a protein is a PLK-2 target. In order to evaluate which phosphopeptides were potentially regulated by PLK-2, we wanted to determine for which phosphopeptides there was a significantly larger variation in abundance between two strains than within the strains. We decided to use **limma**, a statistical tool designed for assessing differential expression for microarray datasets with lower numbers of technical replicates (Smyth, 2005). It calculates a common standard error from the variation within the entire dataset, which can be used to improve estimates for variances for proteins (or phosphopeptides) that have fewer replicates. However, it has been shown to work optimally for datasets that have at minimum three replicates per phosphopeptide (Schwämmle et al., 2013). Both of our MSs had only two replicates per phosphopeptide. In order to obtain a better estimation of the variance of abundance, we combined the replicates for all of the duplicate phosphopeptides within the dataset. This made our average replicate

per phosphopeptide sequence 3.6 in MS1 and 2.5 in MS2. The proportion of phosphopeptides which had 4 replicates after the merge was 27 % for MS1 and 17 % for MS2. We ran a **limma** analysis on the merged MS1 and MS2; it was used to determine which phosphopeptides had a differential abundance between the mutant strains and wild type which was significantly different than 0. Cumulatively, 278 phosphopeptides (from 244 proteins) were found to be upregulated in *plk-2(K65M)* compared to wild type. 43 % of these were also upregulated in *plk-2(vv44)* compared to wild type. 379 phosphopeptides (from 323 proteins) were found to be downregulated in *plk-2(K65M)* compared to wild type. Of these, 23 % were found to be also downregulated in *plk-2(vv44)* compared to wild type (Figures 2A, B, E, F). In both MS1 and MS2, more proteins were phospho-depleted in *plk-2(K65M)* mutants than phospho-enriched which is what we would expect since PLK-2^{K65M} has a non-functioning kinase domain. There is a high proportion of upregulated phosphopeptides though, which leads to the hypothesis that PLK-2 might regulate a phosphatase.

Based on the results of the **limma** analysis and the fold change distributions (Figure 1), we proposed that the focus should be on phosphopeptides that had an adjusted *p*-value less than 0.05 from the **limma** test and an average fold change whose absolute value was greater than 2 in *plk-2(K65M)* or *plk-2(vv44)* mutants compared to wild type (Figures 2C, D, G, H). The **limma** test assisted us in excluding some phosphopeptide candidates which had a large fold change but a high variance in abundance (Figures 2C, D, G, H; included phosphopeptides are in blue, excluded are in grey). Phosphopeptides which had a significant result from the **limma** analysis and an average fold change greater than 2 between the mutant and the wild type worm were predicted to be <u>enriched</u>. Significant phosphopeptides which had an average fold change lower than -2 between the mutant and wild type strains were categorized as <u>depleted</u>.

Evaluation of the limma analysis and final processing of the list of predicted PLK-2 targets

In order to evaluate the quality of our analysis, we compared the results for the 60 phosphopeptides which appeared in both MS1 and MS2 (Table 3). We assessed if there was an agreement on whether the phosphopeptide was enriched, depleted or not differentially expressed in the mutant strains compared to wild type worms. MS1 and MS2 agreed 73 % of the time on how the phosphopeptide was differentially abundant in *plk-2(K65M)* mutants compared to wild type and had matching results 85 % of the time for how the phosphopeptide's abundance differed in *plk-2(vv44)* mutants compared to wild type worms. All of the mismatches involved a phosphopeptide obtaining the result that it's differentially regulated based on one MS and not differentially regulated based on the other. There were no mischaracterizations where a phosphopeptide's test result was upregulation for one MS and then downregulation for the other. Likewise, most of the agreements involved a non-differentially regulated phosphopeptide getting characterized as such for both MSs. Only 1 of the phosphopeptides was characterized as differentially regulated in both MSs. Nevertheless, the high agreement between MSs increases our confidence in the experiment and follow-up analysis.

The Gene Ontology (GO) consortium is a collaborative work which endeavours to provide a consistent biological annotation for gene products on the basis of biological processes proteins are involved in, molecular functions of proteins and the cellular components proteins localize to (Ashburner et al., 2000). With the **PANTHER Classification System** (Mi et al., 2013) we were able to access the GO annotations database (AmiGO *v2.4.24*) and use it to summarize our candidates biologically. In order to assess the biological significance of our

candidate lists, we performed a GO enrichment analysis on our lists and plotted the GO terms which were significantly enriched ($p < 0.05$) after a Bonferroni multiple hypothesis correction (Figure 3). We found a significant enrichment of meiotic and cell cycle annotations (Figure 3, in bold) in all of our candidate lists, which increased confidence that our experiment wielded potential PLK-2 target proteins.

The enrichment of obviously unrelated categories, especially in the list of candidates differentially regulated in *plk-2(vv44)* animals (Figures 3J, K, L, M, N, O), revealed the level of noise in our candidate list. We decided to further filter the candidate lists using the GO annotation database (Amigo *v.2.2.24*). Since we were looking for proteins involved in cytoskeletal-driven dynamic chromosome motion during prophase I of meiosis, we selected proteins that were annotated with GO terms related to meiosis or the cytoskeleton. The final list of predicted PLK-2 targets contains 126 phosphopeptides from 89 proteins (Table 4).

Predicted PLK-2 docking motifs `ISE` and `STP` occur less frequently in the *C. elegans* proteome than among the proteins which have depleted phosphorylation in *plk-2(K65M)* mutants

Next, we wished to evaluate if our proteins which might be directly regulated by PLK-2 contained predicted PLK-2 docking motifs at a relatively higher frequency than one would expect. We conducted several Fisher's exact tests to see if there was enrichment of docking motif sequences in candidates that contained phosphopeptides, which were less abundant in *plk-2(K65M)* mutants (Table 4) relative to the *C. elegans* proteome. We focussed on phosphopeptides which were depleted in *plk-2(K65M)* worms because PLK-2^{K65M} has a non-functioning kinase domain. Thus phosphopeptides depleted in *plk-2(K65M)* mutants compared to wild type worms have a higher likelihood of being direct PLK-2 targets. We found statistical

evidence for the enrichment of the potential PLK-2 docking motifs `ISE` and `STP` in our list of candidates which were phosphodepleted in *plk-2(K65M)* mutants (Table 4) relative to the *C. elegans* proteome (Table 5 and Figure S2). We did not find statistical support for the motif `SSP` (Table 5). From this we can conclude that it would be worthwhile to test whether `ISE` or `STP` are potential PLK-2 docking motifs *in vivo*.

Discussion

We have provided evidence that PLK-2 kinase activity promotes dynamic chromosome motion during leptotene-zygotene (Chapter I). In order to better understand how PLK-2 regulates these processes, we sought to identify possible PLK-2 phosphorylation targets. To that end, we conducted two proteomics experiments, which quantified the effect of PLK-2 on the *C. elegans* phosphoproteome. We analysed how the abundances of 2982 phosphopeptides differed between *plk-2(vv44)* and *plk-2(K65M)* mutants compared to wild type worms and identified for which of the phosphorylation sites there was evidence of differential abundance due to PLK-2 kinase activity using the **limma** R package. We then further prioritized the list to the 126 most likely candidates using GO annotations. We also performed a comparison of the relative frequency of the motifs (`ISE`, `STP` and `SSP`) in the full sequences of our PLK-2 target candidates versus the *C. elegans* proteome. Our results support the theory (proposed by Labella, 2012) that the motifs `ISE` and `SSP` are indeed PLK-2 docking motifs.

An unintuitive finding was the high number of phosphosites, which were more abundant in *plk-2(K65M)* mutants. Currently, it is unknown whether PLK-2 regulates a phosphatase but our results support the possibility. Additionally, the high enrichment of annotations related to actin and myosin is in contradiction of the current school of thought that chromosome motion in the *C. elegans* nematode is driven primarily by microtubules (Baudrimont et al., 2010; Wynne et al., 2012). Our results support the need for further investigation of the contribution of actin related forces to dynamic chromosome motion in *C. elegans* animals.

The residue S32 of lmn-1 has already been discovered to be a PLK-2 dependent phosphorylation site by the Jantsch lab using CRISPR-Cas9 mutagenesis (*unpublished data*). These results support the conclusions of our experiment since S32 came out in both MS1 and

MS2 as a residue that is more phosphorylated in *plk-2(vv44)* mutants than in wild type worms. However, since this phosphopeptide was only observed as differentially abundant in *plk-2(vv44)* mutants, and not in *plk-2(K65M)* animals, this means that it would be a poor strategy to completely ignore phosphopeptides which are differentially expressed only in *plk-2(vv44)* mutants.

It is important to take into account differences between MS1 and MS2 and potential biases that exist within them when deciding which candidates to pursue. The samples given for the conducting of MS1 were much lower in volume than those given for MS2. In both MS1 and MS2, the lowest bound of abundance for a phosphopeptide was 1, which is equivalent to a log abundance of 0. However, in MS1 the abundance values jumped from 1 to a value two magnitudes higher while in MS2, the values rose much more gradually by an interval of 0.001 units. This large gap between low and high abundance values in MS1 is what resulted in the fold change distributions having three local maxima (Figure 1). Table 3 suggests that the MS1 dataset is biased towards phosphopeptides which are less abundant in *plk-2(K65M)* mutants and not differentially regulated in *plk-2(vv44)* mutants. Due to the local maxima at high fold change values in MS1's fold change distributions (Figures 1A, B), it is likely only detecting the phosphopeptides as differentially abundant which have a large variance in abundance.

A limitation of this experiment is the low number of technical replicates. Usually, experiments designed to evaluate differential expression or abundance combine the results for peptides from the same protein in order to increase the amount of information on the variation of expression for each protein. However, since we're interested in the variation of the level of a post-translational modification, which may increase on one part of a protein and decrease on another, we could not use that method. We have merged all of the information

for peptides, but still we have 83 % lower average replicate number for MS2 than is recommended for a **limma** analysis. This could be why we have such a large number of phosphopeptides which are differentially regulated in *plk-2(vv44)* mutants. We predict that the false positive rate is likely to be higher than 5 %, due to insufficient information about the variance of post-translational modification for most peptides.

In conclusion, we proposed a list of 126 candidate phosphopeptides from 89 proteins. Further processing will be needed to prioritize candidates and then to confirm them. This list provides an informed starting point and guide for that future work.

We recommend constructing a criterion for prioritizing candidates and then validating them *in vivo* using the CRISPR-Cas9 mutagenesis technique to mutate predicted serine phosphosites to alanine and threonine phosphosites to valine (Hsu et al., 2014). Based on our technical analysis, we suggest prioritizing candidates that are differentially phosphorylated in *plk-2(K65M)* mutants compared to wild type worms (but we caution against ignoring the ones differentially phosphorylated solely in *plk-2(vv44)* mutants), have a higher number of replicates in the dataset, have been associated with previous meiotic phenotypes, and are expressed in the germline. We also recommend further testing of the predicted PLK-2 docking motifs (`ISE` and `STP`) *in vivo.*

Additional *in silico* work would involve performing a motif analysis, in order to detect enrichment of any phosphorylation motif (Annan et al., 2009). We currently do not know what PLK-2's phosphorylation motif is, and knowledge of it would greatly assist in prioritizing candidates and in expanding our understanding of its mechanistic model. We can additionally input our differentially regulated phosphopeptides into software which detects consensus

motifs of other kinases, in order to further narrow our list to phosphorylation sites that are more likely to be PLK-2 dependent.

The dataset would be further bolstered if an additional MS experiment could be run using a different protease other than trypsin. This will result in the identification of other peptides and reveal sites of phosphorylation modification that may have been missed.

References:

Alsheimer, M. (2008). The dance floor of meiosis: evolutionary conservation of nuclear envelope attachment and dynamics of meiotic telomeres Meiosis (Vol. 5, pp. 81-93): Karger Publishers.

Annan, R. B., Lee, A. Y., Reid, I. D., Sayad, A., Whiteway, M., Hallett, M., & Thomas, D. Y. (2009). A biochemical genomics screen for substrates of Ste20p kinase enables the in silico prediction of novel substrates. PloS one, 4(12), e8279.

Ashburner, M., Ball, C. A., Blake, J. A., Botstein, D., Butler, H., Cherry, J. M., Davis, A. P., Dolinski, K., Dwight, S. S., Eppig, J. T., & Harris, M. A. (2000). Gene Ontology: tool for the unification of biology. Nature genetics, 25(1), 25-29.

Baudrimont, A., Penkner, A., Woglar, A., Machacek, T., Wegrostek, C., Gloggnitzer, J., Fridkin, A., Klein, F., Gruenbaum, Y., & Pasierbek, P. (2010). Leptotene/zygotene chromosome movement via the SUN/KASH protein bridge in Caenorhabditis elegans. PLoS Genet, 6(11), e1001219.

Chase, D., Serafinas, C., Ashcroft, N., Kosinski, M., Longo, D., Ferris, D. K., & Golden, A. (2000). The polo-like kinase PLK-1 is required for nuclear envelope breakdown and the completion of meiosis in Caenorhabditis elegans. GENESIS-NEW YORK-WILEY LISS-, 26(1), 26-41.

Cheng, K. Y., Lowe, E. D., Sinclair, J., Nigg, E. A., & Johnson, L. N. (2003). The crystal structure of the human polo-like kinase-1 polo box domain and its phospho-peptide complex. The EMBO journal, 22(21), 5757-5768.

Cox, J., & Mann, M. (2008). MaxQuant enables high peptide identification rates, individualized ppb-range mass accuracies and proteome-wide protein quantification. Nature biotechnology, 26(12), 1367-1372.

Cox, J., Neuhauser, N., Michalski, A., Scheltema, R. A., Olsen, J. V., & Mann, M. (2011). Andromeda: a peptide search engine integrated into the MaxQuant environment. Journal of proteome research, 10(4), 1794-1805.

Elia, A. E., Cantley, L. C., & Yaffe, M. B. (2003). Proteomic screen finds pSer/pThr-binding domain localizing Plk1 to mitotic substrates. Science, 299(5610), 1228-1231.

Elias, J. E., & Gygi, S. P. (2007). Target-decoy search strategy for increased confidence in large-scale protein identifications by mass spectrometry. Nature methods, 4(3), 207-214.

Franchin, C., Cesaro, L., Pinna, L. A., Arrigoni, G., & Salvi, M. (2014). Identification of the PLK2-dependent phosphopeptidome by quantitative proteomics. PloS one, 9(10), e111018.

Harper, N. C., Rillo, R., Jover-Gil, S., Assaf, Z. J., Bhalla, N., & Dernburg, A. F. (2011). Pairing centers recruit a Polo-like kinase to orchestrate meiotic chromosome dynamics in C. elegans. Developmental cell, 21(5), 934-947.

Hiraoka, Y., & Dernburg, A. F. (2009). The SUN rises on meiotic chromosome dynamics. Developmental cell, 17(5), 598-605.

Hsu, P. D., Lander, E. S., & Zhang, F. (2014). Development and applications of CRISPR-Cas9 for genome engineering. Cell, 157(6), 1262-1278.

Kim, Y., Kostow, N., & Dernburg, A. F. (2015). The chromosome axis mediates feedback control of CHK-2 to ensure crossover formation in C. elegans. Developmental cell, 35(2), 247-261.

Labella, S. (2012). Characterization of the functions of Polo-like kinase 2 during meiotic chromosome pairing in C. elegans. (Biology), McGill University.

Labella, S., Woglar, A., Jantsch, V., & Zetka, M. (2011). Polo kinases establish links between meiotic chromosomes and cytoskeletal forces essential for homolog pairing. Developmental cell, 21(5), 948-958.

Lee, K. S., Yuan, Y., Kuriyama, R., & Erikson, R. L. (1995). Plk is an M-phase-specific protein kinase and interacts with a kinesin-like protein, CHO1/MKLP-1. Molecular and Cellular Biology, 15(12), 7143-7151.

Listgarten, J., & Emili, A. (2005). Statistical and computational methods for comparative proteomic profiling using liquid chromatography-tandem mass spectrometry. Molecular & cellular proteomics, 4(4), 419-434.

Mann, M., Ong, S. E., Grønborg, M., Steen, H., Jensen, O. N., & Pandey, A. (2002). Analysis of protein phosphorylation using mass spectrometry: deciphering the phosphoproteome. Trends in biotechnology, *20*(6), 261-268.

Mi, H., Muruganujan, A., Casagrande, J. T., & Thomas, P. D. (2013). Large-scale gene function analysis with the PANTHER classification system. Nature protocols, 8(8), 1551-1566.

Nishi, Y., Rogers, E., Robertson, S. M., & Lin, R. (2008). Polo kinases regulate C. elegans embryonic polarity via binding to DYRK2-primed MEX-5 and MEX-6. Development, 135(4), 687-697.

Oda, Y., Nagasu, T., & Chait, B. T. (2001). Enrichment analysis of phosphorylated proteins as a tool for probing the phosphoproteome. Nature biotechnology, 19(4), 379-382.

Ong, S. E., & Mann, M. (2005). Mass spectrometry–based proteomics turns quantitative. Nature chemical biology, 1(5), 252-262.

Pagès, H., Aboyoun, P., Gentleman, R., & DebRoy, S. (2016). Biostrings: String objects representing biological sequences, and matching algorithms. R package version 2.40.2.

Penkner, A., Tang, L., Novatchkova, M., Ladurner, M., Fridkin, A., Gruenbaum, Y., Schweizer D., Loidl, J., & Jantsch, V. (2007). The nuclear envelope protein Matefin/SUN-1 is required for homologous pairing in C. elegans meiosis. Developmental cell, 12(6), 873-885.

Penkner, A. M., Fridkin, A., Gloggnitzer, J., Baudrimont, A., Machacek, T., Woglar, A., Csaszar, E., Pasierbek, P., Ammerer, G., & Gruenbaum, Y. (2009). Meiotic chromosome homology search involves modifications of the nuclear envelope protein Matefin/SUN-1. Cell, 139(5), 920-933.

Petronczki, M., Lénárt, P., & Peters, J.-M. (2008). Polo on the rise—from mitotic entry to cytokinesis with Plk1. Developmental cell, 14(5), 646-659.

R Core Team (2015). R: A language and environment for statistical computing. R Foundation for Statistical Computing, Vienna, Austria. URL https://www.R-project.org/.

Ritchie, M.E., Phipson, B., Wu, D., Hu, Y., Law, C.W., Shi, W., & Smyth, G.K. (2015). limma powers differential expression analyses for RNA-sequencing and microarray studies. Nucleic Acids Research, 43(7), pp. e47.

Sato, A., Isaac, B., Phillips, C. M., Rillo, R., Carlton, P. M., Wynne, D. J., Kasad R. A., & Dernburg, A. F. (2009). Cytoskeletal Forces Span the Nuclear Envelope to Coordinate Meiotic Chromosome Pairing and Synapsis. Cell, 139(5), 907-919. doi:http://dx.doi.org/10.1016/j.cell.2009.10.039

Savitski, M. M., Lemeer, S., Boesche, M., Lang, M., Mathieson, T., Bantscheff, M., & Kuster, B. (2011). Confident phosphorylation site localization using the Mascot Delta Score. Molecular & cellular proteomics, 10(2), M110. 003830.

Schwämmle, V., León, I. R., & Jensen, O. N. (2013). Assessment and improvement of statistical tools for comparative proteomics analysis of sparse data sets with few experimental replicates. Journal of proteome research, 12(9), 3874-3883.

Silva, N., Ferrandiz, N., Barroso, C., Tognetti, S., Lightfoot, J., Telecan, O., Encheva, V., Faull, P., Hanni, S., & Furger, A. (2014). The fidelity of synaptonemal complex assembly is regulated by a signaling mechanism that controls early meiotic progression. Developmental cell, 31(4), 503-511.

Smyth, G. K. (2005). Limma: linear models for microarray data Bioinformatics and computational biology solutions using R and Bioconductor (pp. 397-420): Springer.

UniProt Consortium. (2014). UniProt: a hub for protein information. Nucleic acids research, gku989.

van de Weerdt, B. C., Littler, D. R., Klompmaker, R., Huseinovic, A., Fish, A., Perrakis, A., & Medema, R. H. (2008). Polo-box domains confer target specificity to the Polo-like kinase family. Biochimica et Biophysica Acta (BBA)-Molecular Cell Research, 1783(6), 1015-1022.

Warnes, G. R., Bolker, B., Lumley, T., & Johnson, R. C. (2015). gmodels: Various R Programming Tools for Model Fitting. R package version 2.16.2.

WormBase web site, http://www.wormbase.org, release WS253, date 2016.

Wynne, D. J., Rog, O., Carlton, P. M., & Dernburg, A. F. (2012). Dynein-dependent processive chromosome motions promote homologous pairing in C. elegans meiosis. The Journal of cell biology, 196(1), 47-64

Table 1

	Chromosomes move during Prophase I	Accurate homologous chromosome pairing
plk-2	✓	✓
plk-2(vv44)	✓	×
plk-2(K65M)	×	×

Table 1. PLK-2 is a kinase which regulates chromosome motion and accurate homologous chromosome pairing in *C. elegans* germline nuclei.

A summary of the key phenotypes of the *C. elegans* strains which were submitted for phosphoproteomics analysis. For evidence of assertions within the table see Chapter I and Labella (2012).

Table 2

UniProt.ID	prot.name	peptide	*plk-2* A	*plk-2* B	*plk-2(vv44)* A	*plk-2(vv44)* B	*plk-2(K65M)* A	*plk-2(K65M)* B
V6CJD7	dys-1	KDDMVQLEMAKNMIIPSLK	3913	1	1	1	1	1
P46549	kin-18	LYLTQMVQVVPK	5383	1	1	1	1	1
Q22436	sqst-1	IQQPQTIKGINKTVITR	7054	1	1	1	1	1
G5EDA1	rsa-2	ITIDHFRNVATLHRNSK	6829	1	1	1	1	1

Table 2. A sample of the MS datasets.

In the peptide column is the sequence detected by the MS. *plk-2 A*, *plk-2 B*, etc have the normalized expression levels which were inferred by Liquid Chromatography before passing through the MS. *A* contains the replicate *A* values. *B* holds the replicate *B* values. Not shown is a pep.mod column which holds the post-translation modifications and their positions within the peptide which were detected by the MS. Sample pep.mod value for the peptide in row 1: [12] Deamidated (NQ)|[17] Phospho (ST), where [n] is the position n within the peptide and the post-translational modification follows.

Figure 1

A

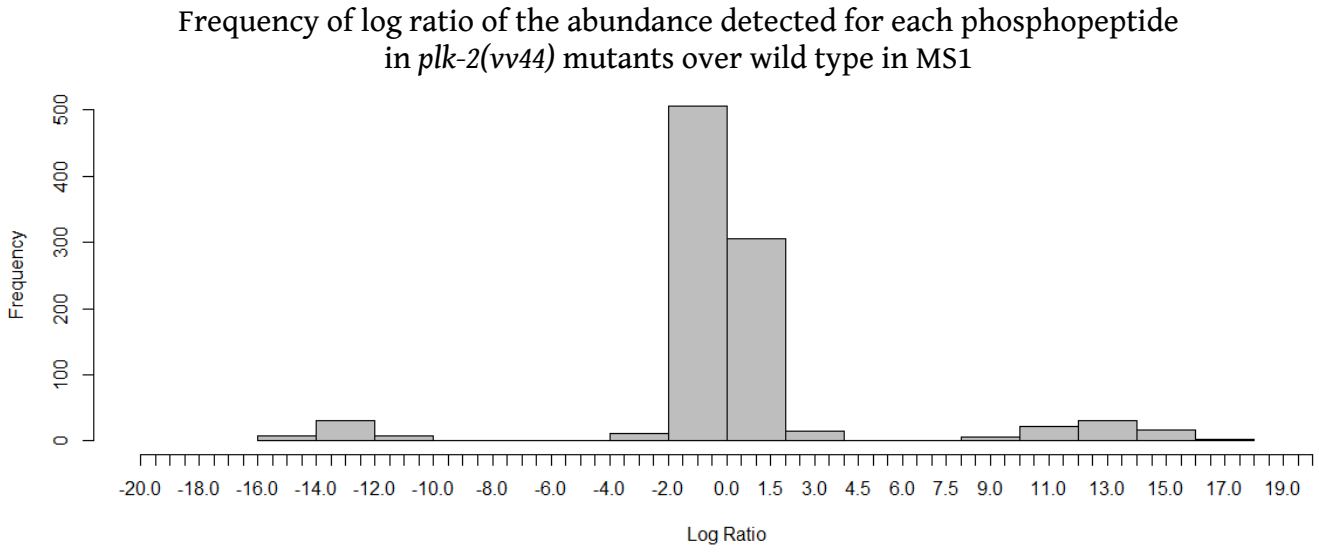
Frequency of log ratio of the abundance detected for each phosphopeptide in plk-2(vv44) mutants over wild type in MS1
Frequency
0
100
200
300
400
500
-20.0 -18.0 -16.0 -14.0 -12.0 -10.0 -8.0 -6.0 -4.0 -2.0 0.0 1.5 3.0 4.5 6.0 7.5 9.0 11.0 13.0 15.0 17.0 19.0
Log Ratio

B

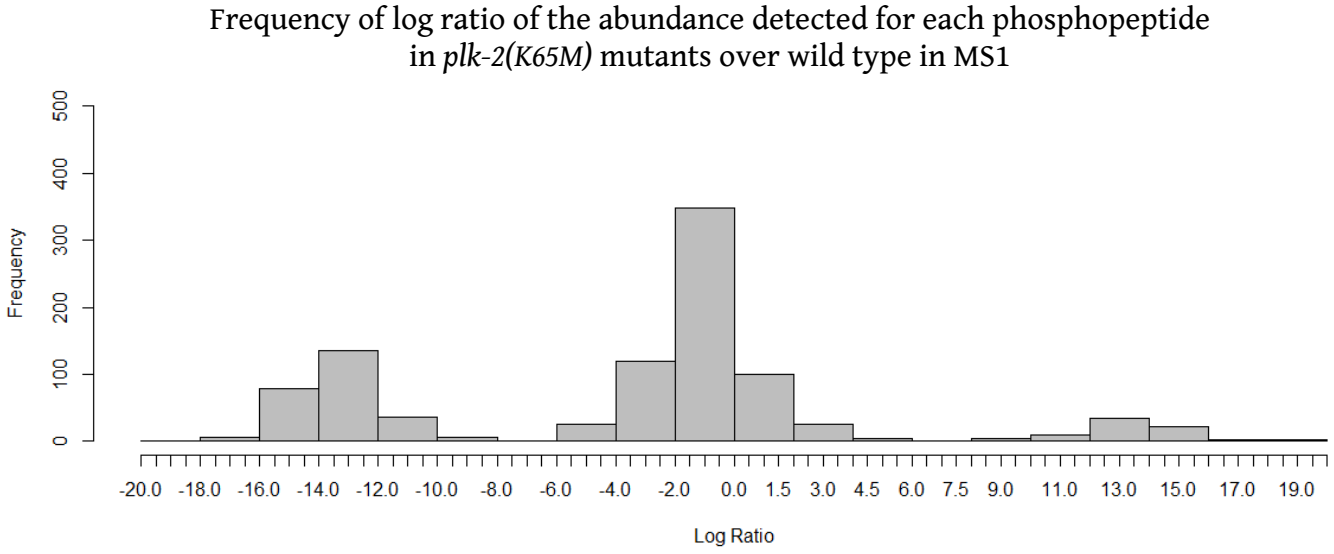
Frequency of log ratio of the abundance detected for each phosphopeptide in plk-2(K65M) mutants over wild type in MS1
Frequency
0
100
200
300
400
500
-20.0 -18.0 -16.0 -14.0 -12.0 -10.0 -8.0 -6.0 -4.0 -2.0 0.0 1.5 3.0 4.5 6.0 7.5 9.0 11.0 13.0 15.0 17.0 19.0
Log Ratio

Frequency of log ratio of the abundance detected for each phosphopeptide in *plk-2(vv44)* mutants over wild type in MS2

C

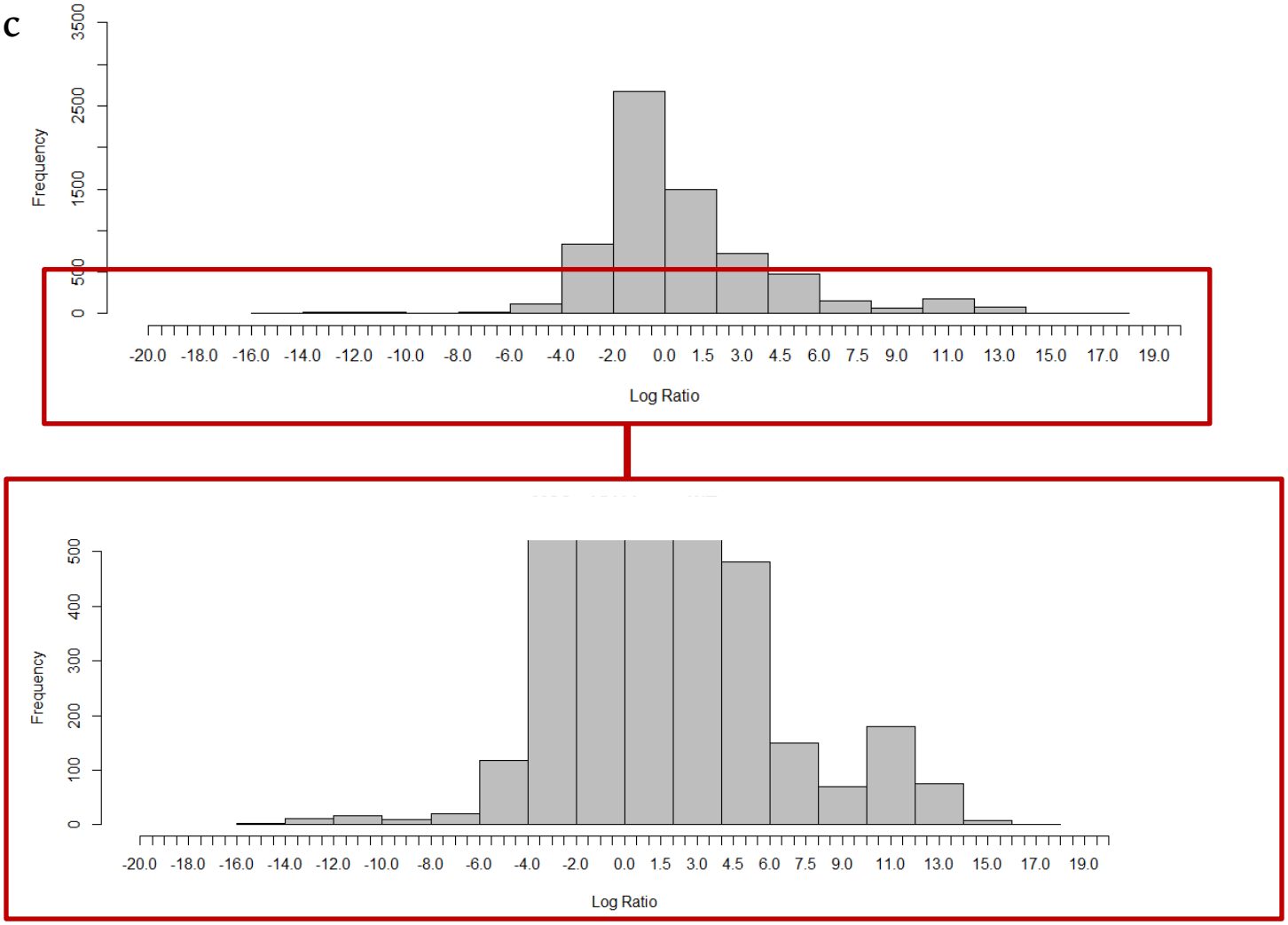

Frequency of log ratio of the abundance detected for each phosphopeptide in *plk-2(K65M)* mutants over wild type in MS2

D

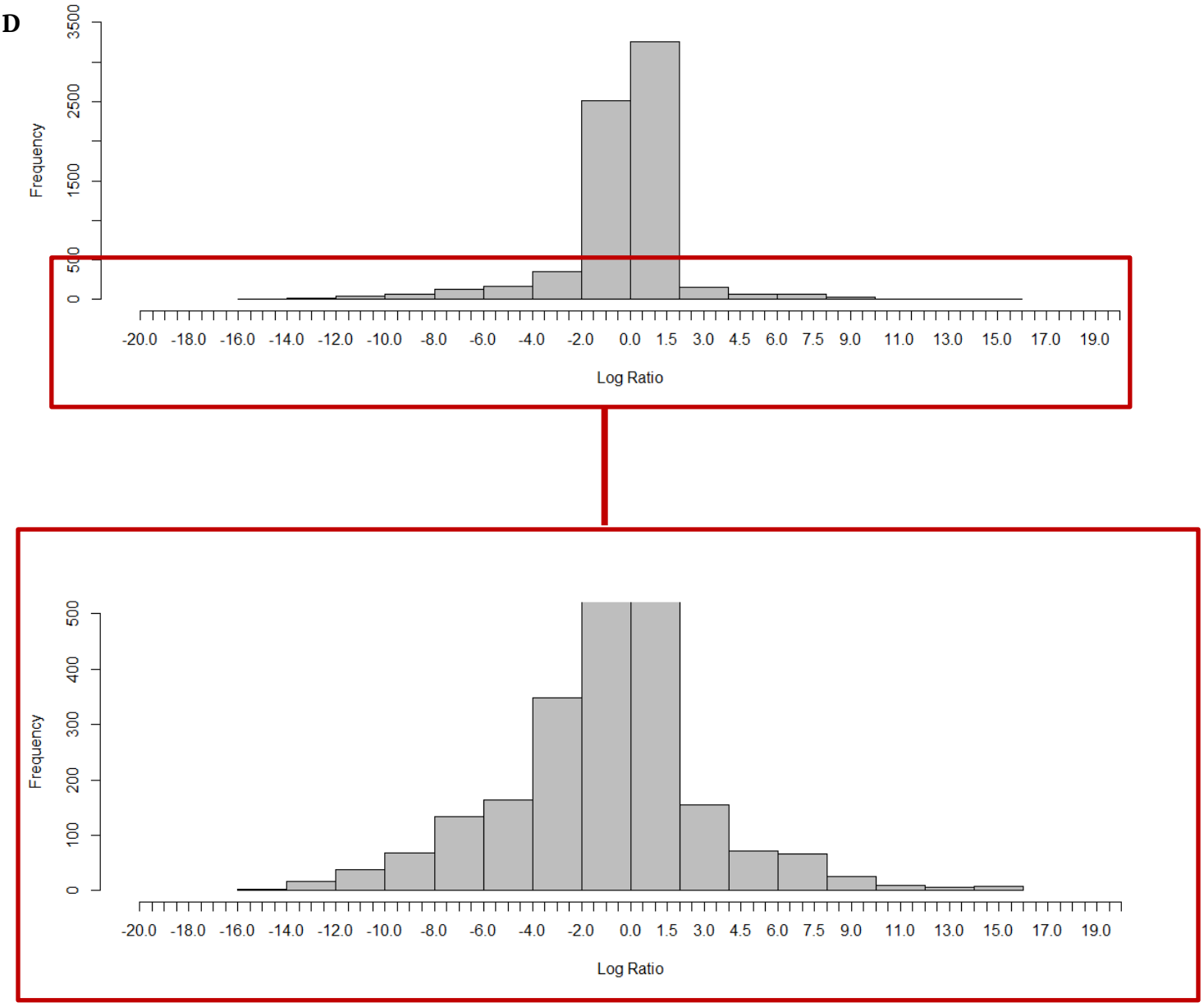

Figure 1. Due to the differences in the log ratio distributions between MS1 and MS2, the two experiments were not combined and instead were analyzed separately.

For each MS, the phosphopeptide abundances of *plk-2(vv44)* and *plk-2(K65M)* mutants for replicate *x* were divided by the abundance levels for that phosphopeptide in replicate *x* of wild type worms. The $\log_2$ of this ratio was taken. This method was repeated for each replicate and phosphopeptide. The frequency of log ratios was plotted in order to compare the distributions. (A) Log ratio distribution for *plk-2(vv44)* mutant phosphopeptide abundance over wild type in MS1. Most phosphopeptides were not differentially regulated in *plk-2(vv44)* mutants compared to wild type. Distribution appears to have local maxima at fold changes of -13, -1 and +13. (B) Log ratio distribution for *plk-2(K65M)* mutant phosphopeptide abundances over wild type in MS1. More phosphopeptides are differentially regulated in *plk-2(K65M)* mutants compared to wild type than they are in *plk-2(vv44)* mutants compared to wild type in MS1. Distribution appears to have local maxima at fold changes of -13, -1 and +13. (C) Log ratio distribution for *plk-2(vv44)* mutant phosphopeptide abundance over wild type in MS2. The zoomed in *y*-axis is shown to allow for easier comparison with the MS1 log ratios. Distribution has a global maxima at -1 and a small local maxima at +12. (D) Log ratio distribution for *plk-2(K65M)* mutant phosphopeptide abundance over wild type in MS2. The zoomed in *y*-axis is shown to allow for easier comparison with the MS1 log ratios. Distribution has one global maxima at +1. Fewer phosphopeptides are differentially regulated in *plk-2(K76M)* mutants compared to wild type than in *plk-2(vv44)* mutants compared to wild type in MS2.

Figure 2

A

Number of peptides which are phospho-enriched compared to wild type worms in MS1

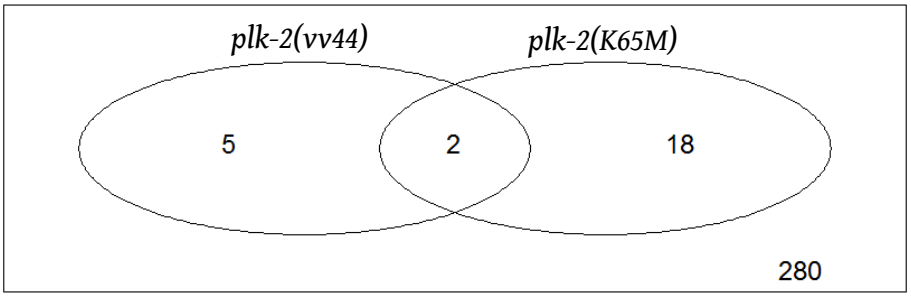

B

Number of peptides which are phospho-depleted compared to wild type worms in MS1

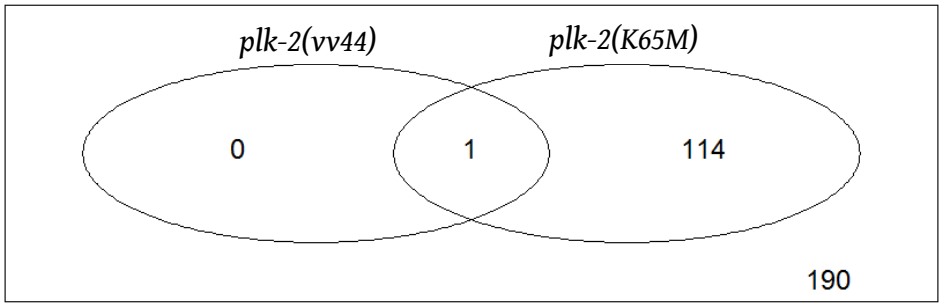

C

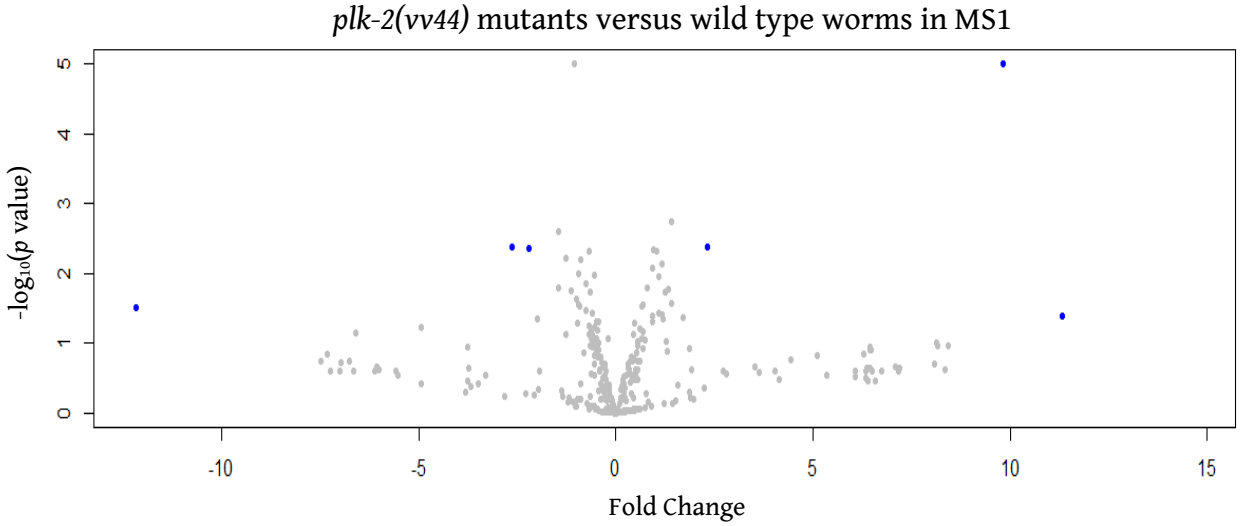
plk-2(vv44) mutants versus wild type worms in MS1
-log10(p value)
0
1
2
3
4
5
-10
-5
0
5
10
15
Fold Change

D

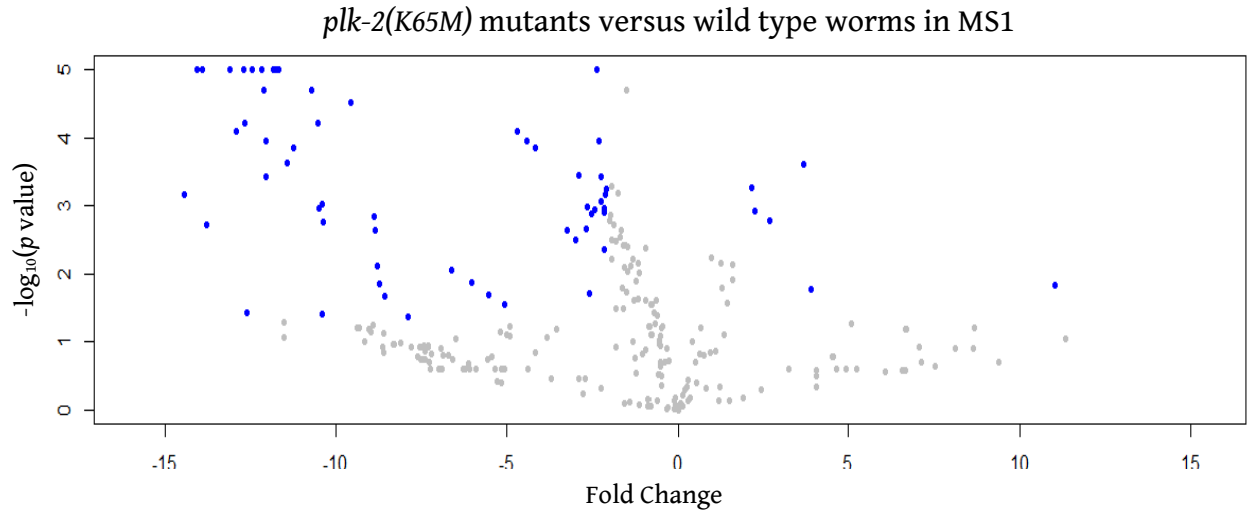
plk-2(K65M) mutants versus wild type worms in MS1
-log10(p value)
0
1
2
3
4
5
-15
-10
-5
0
5
10
15
Fold Change

E

Number of peptides which are phospho-enriched compared to wild type worms in MS2

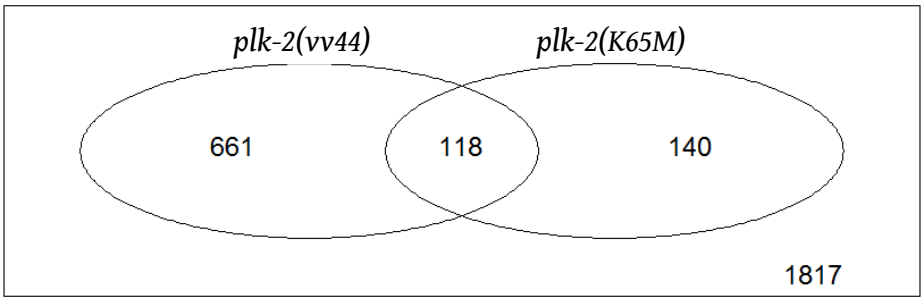

F

Number of peptides which are phospho-depleted compared to wild type worms in MS2

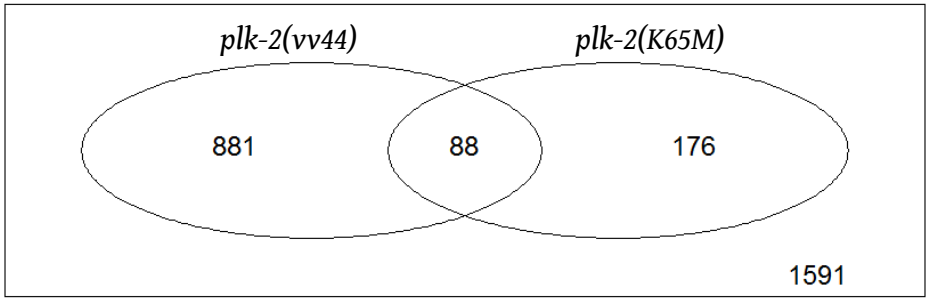

G

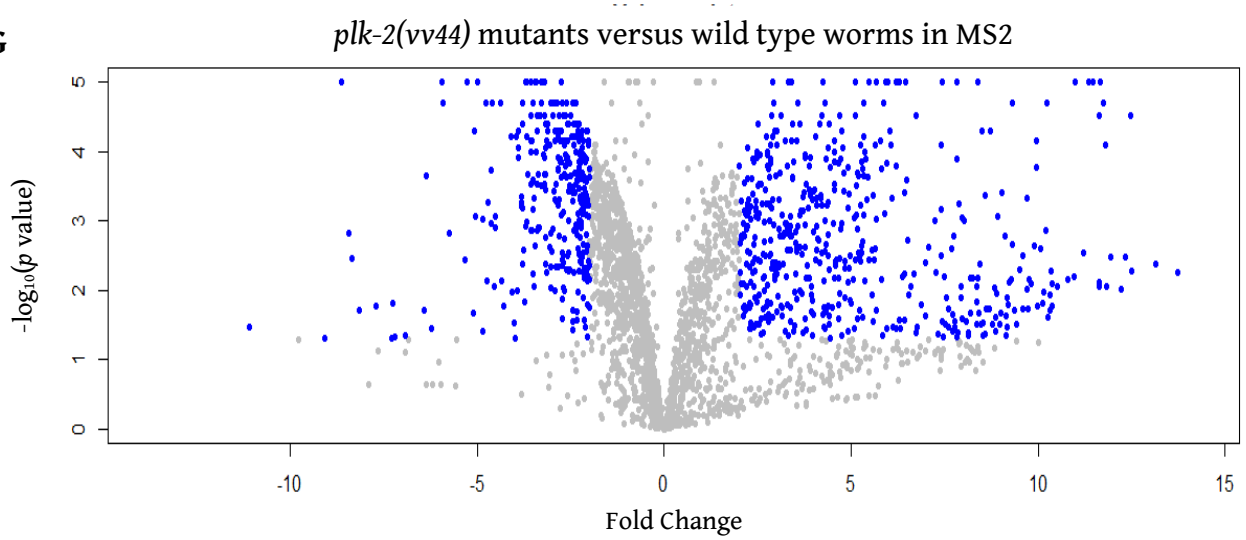
plk-2(vv44) mutants versus wild type worms in MS2
-log10(p value)
0
1
2
3
4
5
-10
-5
0
5
10
15
Fold Change

H

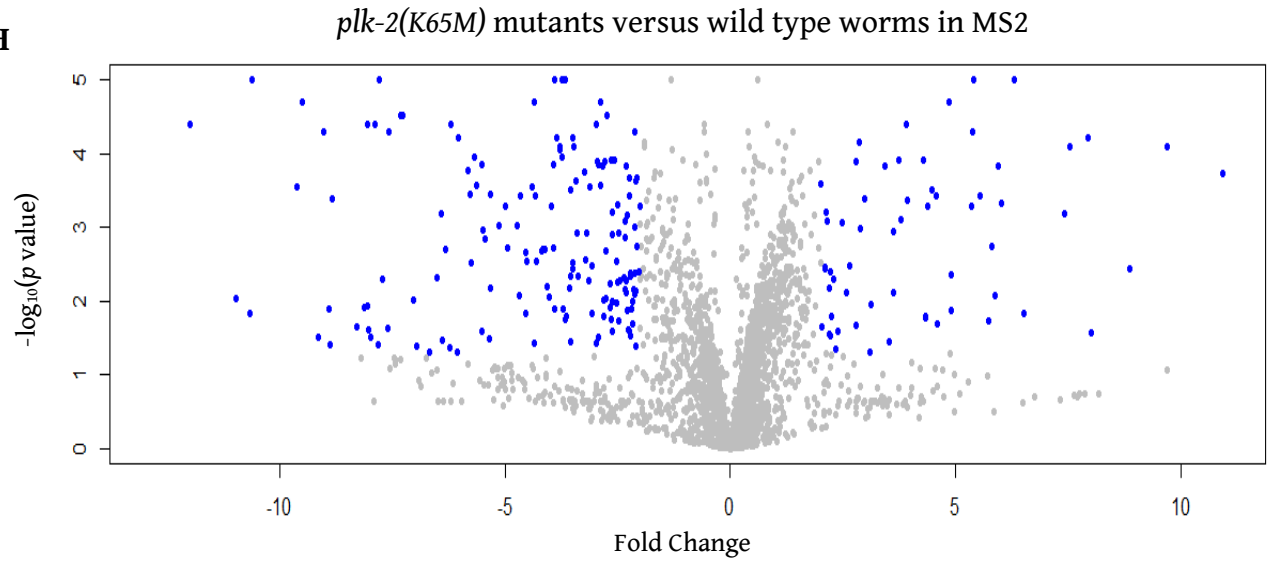
plk-2(K65M) mutants versus wild type worms in MS2
-log10(p value)
0
1
2
3
4
5
-10
-5
0
5
10
Fold Change

Figure 2. Overview of the limma analysis performed on MS1 and MS2.

The software tool **limma** was used to distinguish which phosphopeptides were differentially expressed in the worms which expressed a mutant form of PLK-2 compared to worms which expressed PLK-2^{WT}. (A) The number of phosphopeptides which were enriched in *plk-2(vv44)* or in *plk-2(K65M)* worms compared to wild type in MS1. The overlap contains the number of phosphopeptides which were enriched in both. (B) The number of phosphopeptides which were depleted in *plk-2(vv44)* and *plk-2(K65M)* worms compared to wild type in MS1. The overlap contains the number of phosphopeptides which were depleted in both. (E) The number of phosphopeptides which were enriched in *plk-2(vv44)* and *plk-2(K65M)* worms compared to wild type in MS2. The overlap contains the number of phosphopeptides which were enriched in both. (F) The number of phosphopeptides which were depleted in *plk-2(vv44)* and *plk-2(K65M)* worms compared to wild type in MS2. The overlap contains the number of phosphopeptides which were depleted in both. More phosphopeptides were found to be depleted than found to be enriched in *plk-2(K65M)* mutants compared to wild type worms for both MSs. Very few phosphopeptides were detected as differentially regulated in *plk-2(vv44)* mutants compared to wild type worms in MS1. In MS2, a much larger amount were found to be differentially regulated in *plk-2(vv44)* mutants compared to wild type worms than in *plk-2(K65M)* mutants compared to wild type worms. (C), (D), (G) and (H) contain the volcano plots which show the relationship between the measure of effect of the PLK-2 mutation on phosphorylation and the likelihood of a phosphopeptide being considered as differentially abundant between the two strains. The peptides highlighted in blue had a fold change greater than 2 or less than -2 and were found to be statistically differentially regulated by **limma**.

Table 3

Phosphopeptide is	Symbol
Enriched	
Depleted	
Not differentially expressed	

Gene Name	Peptide	*plk-2(K65M)* vs *plk-2*		*plk-2(vv44)* vs *plk-2*	
		MS1	MS2	MS1	MS2
C04G2.8	SPSLVVVISPSPR				
C37C3.2	EAEEETEEESDDEIAFGGDVK				
C46G7.2	AASFTNLTYIK				
C49H3.9	ATDSINEILNYGQSSTSPQKR				
cdk-1	IGEGTYGVVYK				
cec-5	AASDDDEEEEPVATK				
cec-5	RAETSDEEDEDEEDEKEAPK				
dao-5	KSSPFR				
eef-1B.1	TWASAGGSAPAAAAADGDDFDLFGSDDEEEDAEK				
F17A9.2	SDFKPFDFTAEDDSD				
F18C12.3	IVAPVSEDENDDDESSSFFLPK				
F19F10.9	KLADSDEEDSAASFVNK				
F53F8.5	SVSPIDK				
fib-1	VSVDDGAGSIEYR				
fln-2	HTPQHSSEQIK				
fln-2	QDDIDEVSRNASFPSAPTINYNERSDEVSNYNR				
gei-7	AGSVVNRIPEAADLLEK				
gld-1	SSVMTPTSLDGDNSPRK				
hmg-11	SPVAKSPVASSSADASPK				
hmg-12	AQTPAADTDAIDTASSPVKK				
hmg-12	NLAADTDAIDTASSPVKK				
hmg-12	NPSADAGSPLVK				
hmg-12	RENSANDSPANTNDVDIVSSPVKR				

hmg-12	SAIDAFFDGSD				
hsr-9	DSTPDGHIVDSSVITK				
isp-1	EVVQTLVSYKAMAADQRALASIEINMADIPEGK				
K07F5.14	LFDSEDENDKDEEEDFEIK				
K08F4.2	EVAKTPQKPQLAQQPPQQR				
K12D12.1	KAAGSDDEDDESFVVAPR				
larp-1	SGEEDSASGDEQQYWSR				
lem-2	RLSPVYKPSPVPK				
let-418	RDSDAPDSDQEFEAFIK				
let-504	EGSMSPTPILPEHIK				
lmn-1	SANSSLSNNGGGDDSFGSTLLETSR				
mbk-1	IYQYIQSR				
myo-5	STSGVFGPR				
nol-1	QKADGDDSDDDNNAPMK				
pqn-59	SLSPQPPLPSVAPVK				
R08D7.1	VIKPEPLSPDNSPPR				
R148.3	SQLPFGAESPSDQEK				
rack-1	KEIEELKPEIASSGSSR				
ran-3	MDTSEVELPNDNVNEQGNKTPR				
rnp-5	RPSPSPPRR				
rps-8	LDSGNFSWASEQTTR				
rsp-8	GHSPTPGQYMGDR				
T19C3.4	IEELDENSDTDLQK				
T27F2.1	APPSPPAPVMHSPPR				
tag-18	VTSYPNLSTVR				
tcc-1	KAQDAAPAPASAAPAAPNAPTPTAQQQPSPK				
unc-15	SPSQAAFGAPFGSMSVADLGSLTR				
unc-23	NNCELCPEQETDGDPSPLTSPITEGKPK				
unc-54	ASASVAPGLQSSASAAVIR				
unc-95	TISPQPSHQQFESYQWTTESR				
vig-1	NNTPFNASDDAFPALGAK				
vit-1	NQLCGLCGNNDDESTNEFYTSDNTETKDIEEFHR				
Y14H12B.1	LQLSDDEAPPSSPSLNLSTR				
Y71F9AL.9	HATSQSSITSSVGADSGVNLSPTHK				
zbp-1	DGSALEKMDQLGTIAPISNSNRASPK				
zbp-1	KLDETDSGCEGVASGDHPQEFLEDNATINSSDAIEEKPKPVSER				
ZK370.4	AVSFTDLAAAMSK				
	Number of matches	44		51	
	Number of non-matches	16		9	

Table 3. Comparison of the limma results for the phosphopeptides which came up in both mass spectrometry experiments shows a 73 % agreement for change in abundance in *plk-2(K65M)* mutants compared to wild type and an 85 % agreement for change in abundance in *plk-2(vv44)* mutants compared to wild type. Phosphopeptides were designated as enriched or depleted. They were labelled as enriched if they had an adjusted *p*-value less than 0.05 from the **limma** test with multiple hypothesis correction and if they had a fold change larger than 2. They were considered depleted if they had an adjusted *p*-value less than 0.05 from the **limma** analysis with multiple hypothesis correction and a fold change lower than -2. The categorizations of phosphopeptides from MS1 and MS2 that had a 100% local alignment were compared.

Figure 3

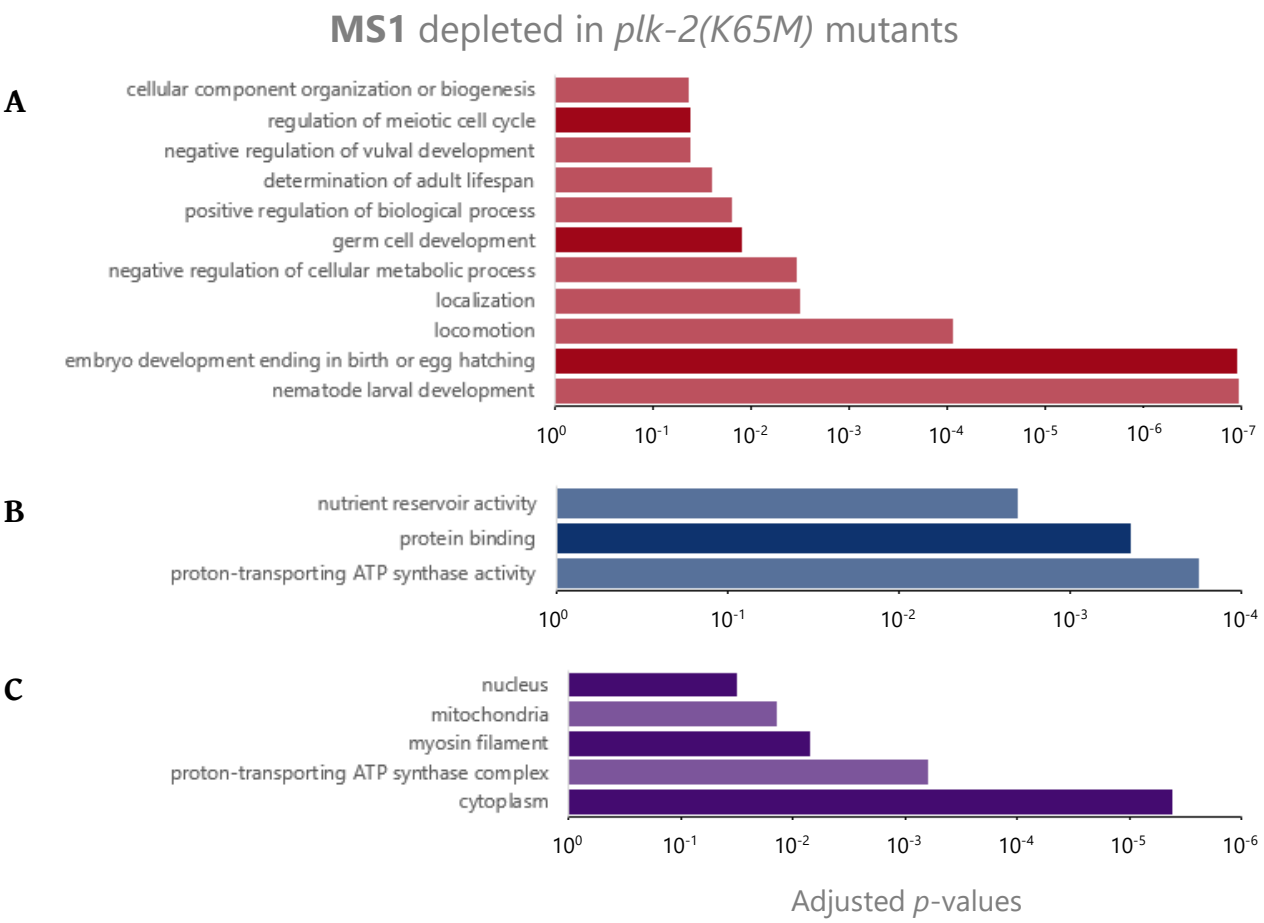
MS1 depleted in plk-2(K65M) mutants
A
cellular component organization or biogenesis
regulation of meiotic cell cycle
negative regulation of vulval development
determination of adult lifespan
positive regulation of biological process
germ cell development
negative regulation of cellular metabolic process
localization
locomotion
embryo development ending in birth or egg hatching
nematode larval development
10^0 10^-1 10^-2 10^-3 10^-4 10^-5 10^-6 10^-7
B
nutrient reservoir activity
protein binding
proton-transporting ATP synthase activity
10^0 10^-1 10^-2 10^-3 10^-4
C
nucleus
mitochondria
myosin filament
proton-transporting ATP synthase complex
cytoplasm
10^0 10^-1 10^-2 10^-3 10^-4 10^-5 10^-6
Adjusted p-values

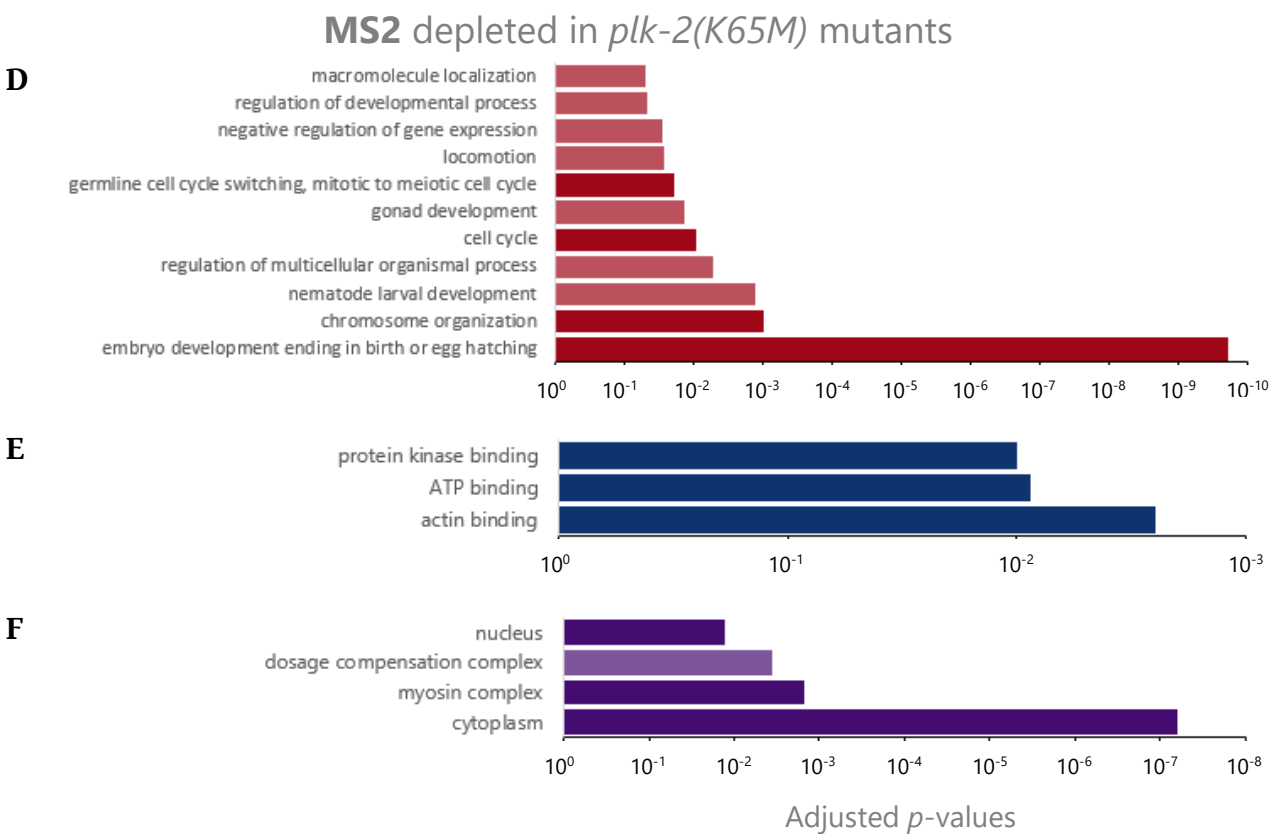
MS2 depleted in plk-2(K65M) mutants
D
macromolecule localization
regulation of developmental process
negative regulation of gene expression
locomotion
germline cell cycle switching, mitotic to meiotic cell cycle
gonad development
cell cycle
regulation of multicellular organismal process
nematode larval development
chromosome organization
embryo development ending in birth or egg hatching
10^0 10^-1 10^-2 10^-3 10^-4 10^-5 10^-6 10^-7 10^-8 10^-9 10^-10
E
protein kinase binding
ATP binding
actin binding
10^0 10^-1 10^-2 10^-3
F
nucleus
dosage compensation complex
myosin complex
cytoplasm
10^0 10^-1 10^-2 10^-3 10^-4 10^-5 10^-6 10^-7 10^-8
Adjusted p-values

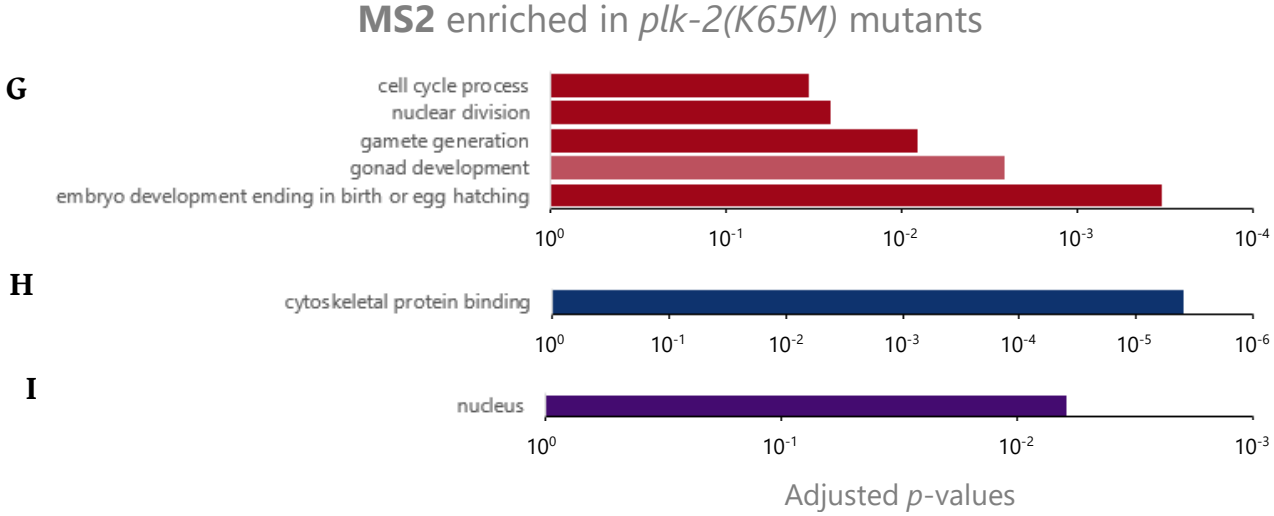
MS2 enriched in plk-2(K65M) mutants
G
cell cycle process
nuclear division
gamete generation
gonad development
embryo development ending in birth or egg hatching
10^0 10^-1 10^-2 10^-3 10^-4
H
cytoskeletal protein binding
10^0 10^-1 10^-2 10^-3 10^-4 10^-5 10^-6
I
nucleus
10^0 10^-1 10^-2 10^-3
Adjusted p-values

MS2 depleted in *plk-2(vv44)* mutants

J

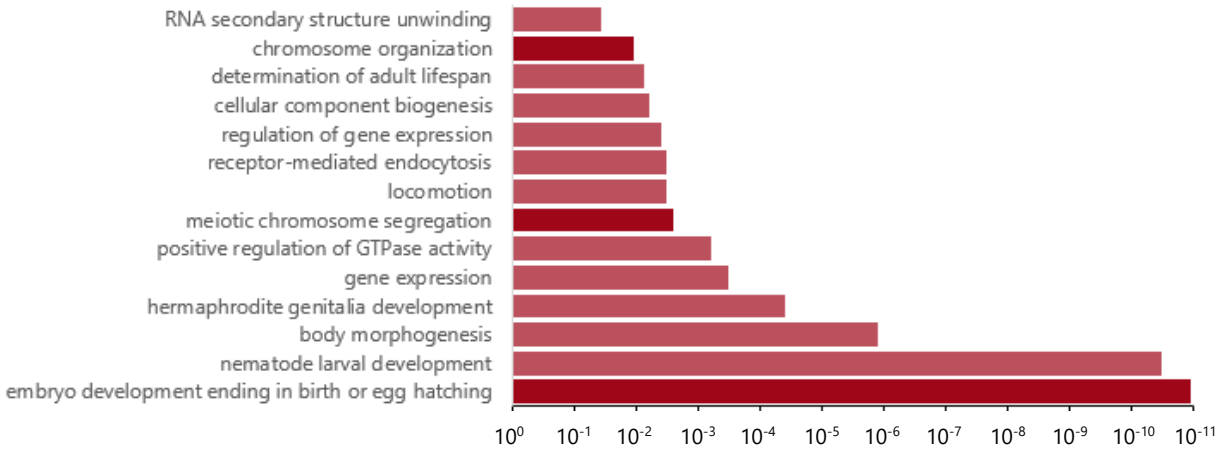

K

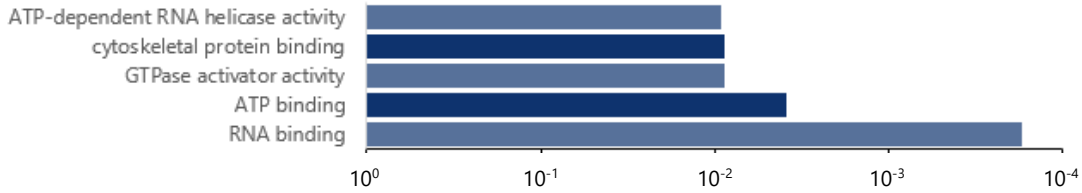

L

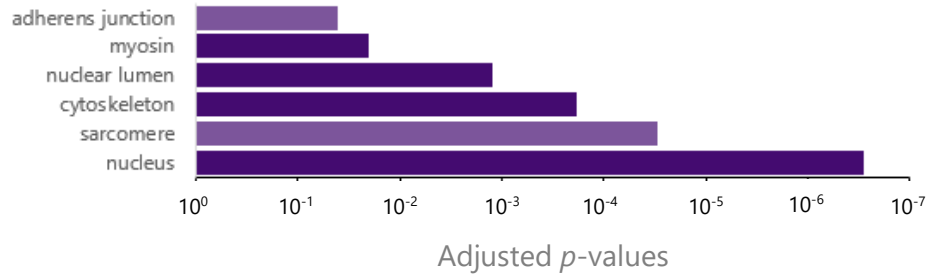

M

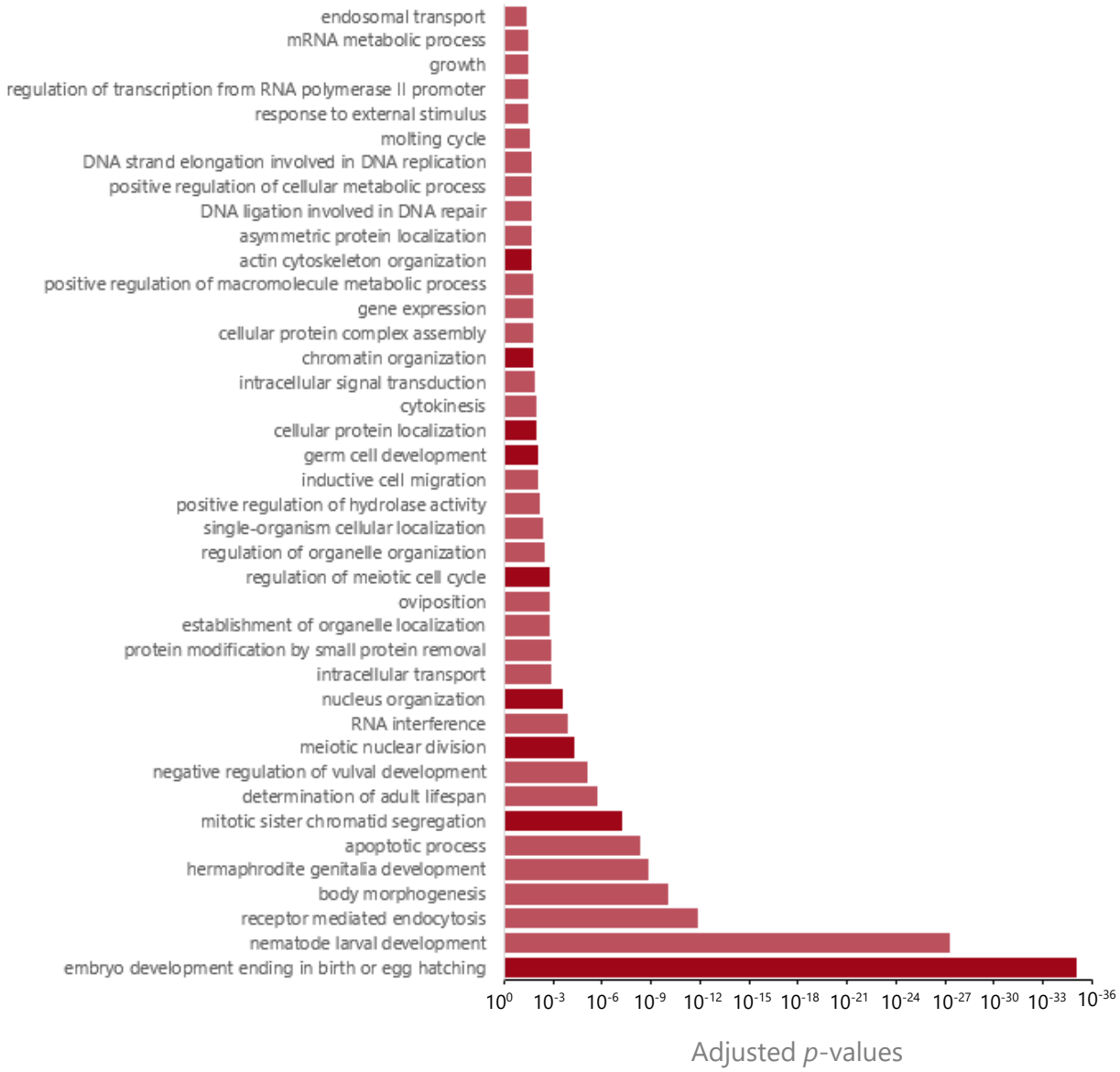
MS2 depleted in plk-2(vv44) mutants
endosomal transport
mRNA metabolic process
growth
regulation of transcription from RNA polymerase II promoter
response to external stimulus
molting cycle
DNA strand elongation involved in DNA replication
positive regulation of cellular metabolic process
DNA ligation involved in DNA repair
asymmetric protein localization
actin cytoskeleton organization
positive regulation of macromolecule metabolic process
gene expression
cellular protein complex assembly
chromatin organization
intracellular signal transduction
cytokinesis
cellular protein localization
germ cell development
inductive cell migration
positive regulation of hydrolase activity
single-organism cellular localization
regulation of organelle organization
regulation of meiotic cell cycle
oviposition
establishment of organelle localization
protein modification by small protein removal
intracellular transport
nucleus organization
RNA interference
meiotic nuclear division
negative regulation of vulval development
determination of adult lifespan
mitotic sister chromatid segregation
apoptotic process
hermaphrodite genitalia development
body morphogenesis
receptor mediated endocytosis
nematode larval development
embryo development ending in birth or egg hatching
10^0 10^-3 10^-6 10^-9 10^-12 10^-15 10^-18 10^-21 10^-24 10^-27 10^-30 10^-33 10^-36
Adjusted p-values

N

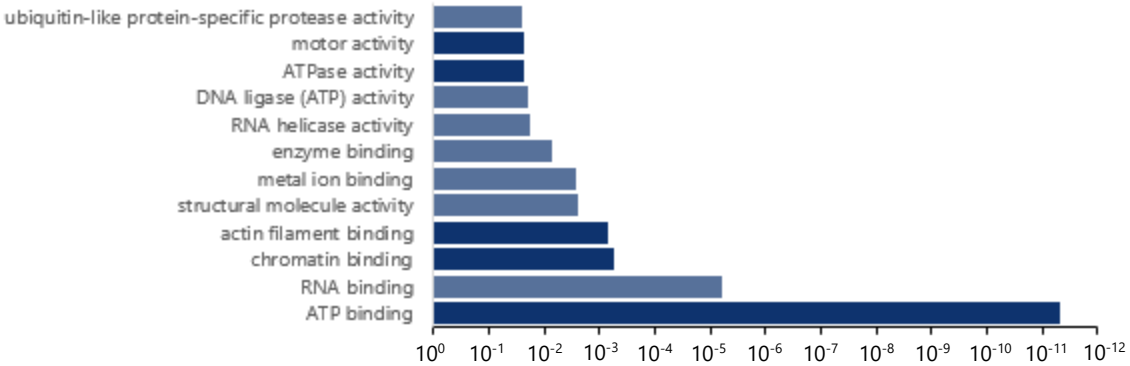
ubiquitin-like protein-specific protease activity
motor activity
ATPase activity
DNA ligase (ATP) activity
RNA helicase activity
enzyme binding
metal ion binding
structural molecule activity
actin filament binding
chromatin binding
RNA binding
ATP binding
10^{0} 10^{-1} 10^{-2} 10^{-3} 10^{-4} 10^{-5} 10^{-6} 10^{-7} 10^{-8} 10^{-9} 10^{-10} 10^{-11} 10^{-12}

O

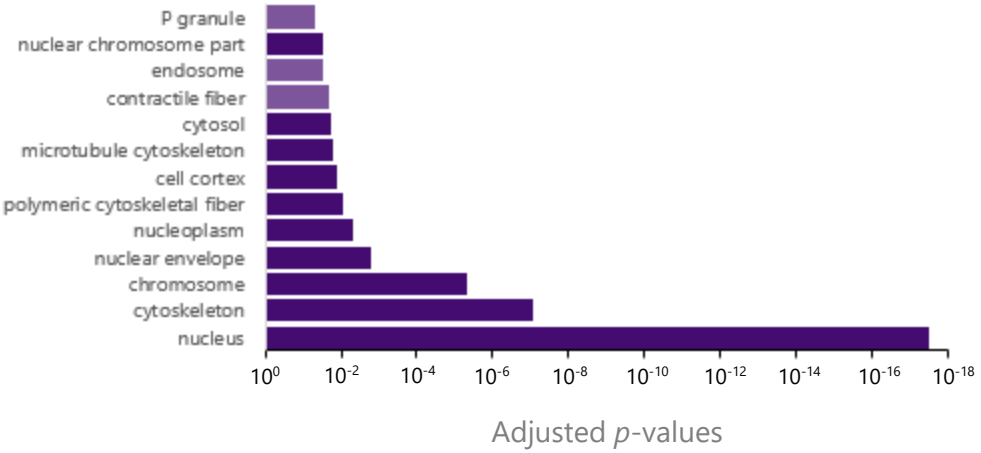
P granule
nuclear chromosome part
endosome
contractile fiber
cytosol
microtubule cytoskeleton
cell cortex
polymeric cytoskeletal fiber
nucleoplasm
nuclear envelope
chromosome
cytoskeleton
nucleus
10^{0} 10^{-2} 10^{-4} 10^{-6} 10^{-8} 10^{-10} 10^{-12} 10^{-14} 10^{-16} 10^{-18}
Adjusted *p*-values

Figure 3. The GO terms which were significantly enriched in our respective candidate lists.

In order to assess the biological significance of our candidates, a GO enrichment analysis (Ashburner et al., 2000) was performed using the **PANTHER Classification System** (Mi et al., 2013). The GO terms which were significantly enriched ($p < 0.05$) after Bonferroni multiple hypothesis correction are shown. If a parent of a significantly enriched GO term was also significant only the child term is shown, except in the case of the cellular component graphs where the more general parent term (e.g. "nucleus", "cytoplasm", "nuclear envelope") is shown. (A), (D), (G), (J), (M) Biological processes GO graphs are coloured red. (B), (E), (H), (K), (N) Molecular function GO graphs are shown in blue. (C), (F), (I), (L), (O) Cellular component GO graphs are in purple. The bars for the categories of highest interest are darker for emphasis. There are no GO enrichment plots for the candidates which were enriched in *plk-2(K65M)* mutants in MS1 and for the ones that enriched and depleted in *plk-2(vv44)* mutants in MS1 due to low sample size. (A), (B) and (C) are the GO enrichment graphs for the 90 candidates which had phosphopeptides which were depleted in *plk-2(K65M)* mutants in MS1. (A) 14 proteins were unclassified. (B) 22 proteins were unclassified. (C) 24 proteins were unclassified. (D), (E) and (F) are the GO enrichment graphs for the 145 candidates which had phosphopeptides which were depleted in *plk-2(K65M)* mutants in MS2. (D) 39 proteins were unclassified. (E) 44 proteins were unclassified. (F) 51 proteins were unclassified. (G), (H) and (I) are the GO enrichment graphs for the 49 candidates which had phosphopeptides which were enriched in *plk-2(K65M)* mutants in MS2. (G) 13 proteins were unclassified. (H) 16 proteins were unclassified. (I) 16 proteins were unclassified. (J), (K) and (L) are the GO enrichment graphs for the 345 candidates which had phosphopeptides which were depleted in *plk-2(vv44)* mutants in MS2. (J) 78 proteins were unclassified. (K) 116 proteins were unclassified. (L) 108

proteins were unclassified. (M), (N) and (O) are the GO enrichment graphs for the 528 candidates which phosphopeptides which were enriched in *plk-2(vv44)* mutants in MS2. (M) 91 proteins were unclassified. (N) 137 proteins were unclassified. (O) 159 proteins were unclassified. The enrichment of meiotic and cell cycle related proteins increased our confidence in the biological significance of the list. However, the enrichment of obviously unrelated categories, especially in the list of candidates differentially regulated in *plk-2(vv44)* animals, showed the noise in the lists and revealed the need for further reduction of the candidate list. Enrichment of annotations such as "body morphogenesis" and "apoptosis" may seem unrelated but are not surprising considering that the PC proteins share those annotations (AmiGO *v2.4.24*). The high presence of annotations related to actin and myosin supports an investigation into the contribution of actin related forces to dynamic chromosome motion in *C. elegans* animals.

Table 4

Gene name	Phosphopeptide	Average Fold Change	GO
MS1: depleted in *plk-2(K65M)* mutants			
nos-3	ESSQKPIDPQEISDDQDDTVPDVPDQIVEQDNQSHK	-2.137	regulation of meiotic cell cycle [GO:0051445]
unc-84	SGRNSPNIFAK	-2.249	intermediate filament cytoskeleton [GO:0045111]
htp-3	APAVPITPTEPASPVESPVKEQPQK	-2.353	meiotic cell cycle [GO:0051321] meiotic chromosome segregation [GO:0045132]
R31.2	APTPAEDLSHYVK	-4.709	actin cytoskeleton [GO:0015629]
unc-15	SPSAALLKSPSQAAFGAPFGSMSVADLGSLTRLEDK	-8.847	actin cytoskeleton [GO:0015629]
unc-44	AGSISGQFQQQPLHGAGPEDNLEELVR	-10.381	meiotic cell cycle [GO:0051321]
F19F10.9	KLADSDEEDSAASFVNKMR	-11.228	regulation of meiotic cell cycle [GO:0051445]
npp-9	VTFGFGASAPAKEPLAQTSQFGGSLSGSPSTSSSIFGGGTPK	-11.417	meiosis I [GO: 0007127] microtubule cytoskeleton [GO:0015630]
Y41E3.11	SSSFTQQSPR	-11.779	regulation of meiotic cell cycle [GO:0051445]
myo-3	SSSNARFL	-12.874	actin cytoskeleton [GO:0015629]
gld-1	SSVMTPTSLDGDNSPR	-13.258	regulation of meiotic cell cycle [GO:0051445]
smc-4	AVNEKFDGSDGEDDDSDLFSLQLPSRPDFLTKPNR	-13.273	regulation of meiotic cell cycle [GO:0051445]
R31.2	NVAAAAAVAGVAGLGYYVYVKK	-13.287	actin cytoskeleton [GO:0015629]
rnp-5	RRSPMGGR	-13.928	regulation of meiotic cell cycle [GO:0051445]
ben-1	SGPFGQLFRPDNFVFGQSGAGNNWAK	-14.313	microtubule cytoskeleton [GO:0015630]
cls-2	NGSPPRRPSATEAFPAEMQR	-14.959	meiotic cell cycle [GO:0051321] meiotic spindle organization [GO:0000212] microtubule cytoskeleton [GO:0015630]
MS1: enriched in *plk-2(K65M)* mutants			
Y65B4BR.5	EVKEPQVDVSDDSDNEAVEQELTEEQR	3.9	meiotic chromosome segregation [GO:0045132]
unc-23	NNCELCPEQETDGDPSPLTSPITEGKPK	13.243	meiotic cell cycle process [GO:1903046]

MS1: enriched in *plk-2(vv44)* mutants			
lmn-1	SANSSLSNNGGGDDSFGSTLLETSR	10.589	intermediate filament cytoskeleton [GO:0045111]
MS2: depleted in *plk-2(K65M)* mutants			
myo-3	HGDSVAELTEQLETLQK	-2.249	actin cytoskeleton [GO:0015629]
hum-4	IFNMSSNAESIVFGGESGSGKSYNVFKAFK	-2.728	actin cytoskeleton [GO:0015629]
capg-1	KPLVEEDALEILKSPPR	-2.834	germline cell cycle switching, mitotic to meiotic cell cycle [GO:0051729] meiotic chromosome segregation [GO:0045132]
kin-18	SRPSDTIQELIQRTKNMVLELDNFQYK	-2.871	regulation of meiotic cell cycle [GO:0051445]
unc-87	GDSQKLMTNFGTPRNTNTR	-2.928	actin cytoskeleton [GO:0015629]
D2045.5	EFANIHKYLETLEYK	-2.966	germline cell cycle switching, mitotic to meiotic cell cycle [GO:0051729]
nmy-2	RTPGLIGHR	-3.46	actin cytoskeleton [GO:0015629] microtubule cytoskeleton [GO:0015630]
pab-1	ITGMMLEIDNSELIMMLQDSELFRSKVDEAASVLVSAQK	-3.495	germline cell cycle switching, mitotic to meiotic cell cycle [GO:0051729]
myo-6	LCSAIMHIGNSTFKQKPR	-3.505	actin cytoskeleton [GO:0015629]
spd-5	TSNQKCAQPHYTSPTRQLLHESTMAVDAIVQK	-4.148	microtubule cytoskeleton [GO:0015630]
smc-4	EMIAQEKQYPNFPSSNEISK	-4.405	germline cell cycle switching, mitotic to meiotic cell cycle [GO:0051729]
unc-44	EFQDEEYPRPESPAEIFPIPSSEQQSEEPHIVK	-4.421	meiotic nuclear division [GO:0007126]
dpy-26	KIRPADVVPETIMTKIGAHIDDIVNK	-4.512	meiotic nuclear division [GO:0007126] meiotic chromosome segregation [GO:0045132]
rsa-2	RNSATPEASPSSDQYFTPEPADDEFVTPSTSK	-5.674	meiotic nuclear division [GO:0007126] microtubule cytoskeleton [GO:0015630]
D2045.5	SYCFMVMTLLGKDLMAHK	-6.298	germline cell cycle switching, mitotic to meiotic cell cycle [GO:0051729]

aak-2	SSPGGETSTKQQQELK	-7.36	germline cell cycle switching, mitotic to meiotic cell cycle [GO:0051729]
nab-1	RHSIQNLELIELR	-8.048	actin cytoskeleton [GO:0015629]
unc-44	EMTENQSPPEDVMMLSDIREESEAEDMSIR	-11.983	meiotic nuclear division [GO:0007126]
MS2: enriched in *plk-2(K65M)* mutants			
fln-1	IIQQNTFTR	2.019	meiotic nuclear division [GO:0007126] actin cytoskeleton [GO:0015629]
Y46G5A.4	RMTQNPNYYNLQGTTHR	2.098	regulation of meiotic cell cycle [GO:0051445]
ani-1	ETTPNMKENAENSLNSFK	2.117	meiotic nuclear division [GO:0007126] microtubule cytoskeleton [GO:0015630]
smc-4	TENAQFIIISLR	2.66	regulation of meiotic cell cycle [GO:0051445]
mtr-4	TTDVFEGSIIR	3.614	regulation of meiotic cell cycle [GO:0051445]
smk-1	DSVAVSPK	3.917	meiotic chromosome segregation [GO:0045132]
dnc-1	NSESTSRMVR	5.544	actin cytoskeleton [GO:0015629] microtubule cytoskeleton [GO:0015630]
rsa-2	IDKLTQAQLAIHQLVSSQPFSGDPYNQR	7.889	meiotic nuclear division [GO:0007126] microtubule cytoskeleton [GO:0015630]
MS2: depleted in *plk-2(vv44)* mutants			
myo-3	KASVGILDK	-2.048	actin cytoskeleton [GO:0015629]
lig-4	EYGDSSMAIGKLSSRIHSFFNK	-2.147	meiotic cell cycle [GO:0051321]
dao-5	AASSSSDSSDDEKKPVAKPTSAK	-2.157	meiotic chromosome segregation [GO:0045132]
gck-1	DDHRFTDTILRTTNVQSAIQR	-2.202	meiotic cell cycle [GO:0051321]
gld-1	MPSCTTPTYGVSTQLESQSSESPSR	-2.205	meiotic cell cycle [GO:0051321]
htp-3	MDEDVANESIR	-2.231	meiotic chromosome segregation [GO:0045132]
ifc-2	AQSPVTSPVFK	-2.238	intermediate filament cytoskeleton [GO:0045111]
mog-5	TTQMTQYAIEAGLGRRGK	-2.309	regulation of meiotic nuclear division [GO:0040020]

tba-8	DVNAAISSVKAK	-2.332	microtubule cytoskeleton [GO:0015630]
lig-4	TAQAIASNSCTVLKPAWLER	-2.341	meiotic cell cycle [GO:0051321]
F15G9.1	EVSSAASLFANDNGNETENR	-2.444	actin cytoskeleton [GO:0015629]
vbh-1	TDSGINFDK	-2.605	regulation of meiotic nuclear division [GO:0040020]
myo-6	NMMSDKENQSMLITGESGAGKTENTK	-2.613	actin cytoskeleton [GO:0015629]
F26B1.2	VGAAINGTDSPK	-2.642	meiotic chromosome segregation [GO:0045132]
ben-1	LSNPTYGDLNHLVSVTMSGVTTCLRFPGQLNADLRK	-2.723	microtubule cytoskeleton [GO:0015630]
tpxl-1	APSVPRPPHNSVTR	-2.729	microtubule cytoskeleton [GO:0015630]
gld-4	NEDSRLSSSQQPSTSTPR	-2.783	meiotic cell cycle [GO:0051321]
him-4	AFDDTQLNVYGGSSRR	-2.788	meiotic chromosome segregation [GO:0045132]
frm-5.1	ESSPFTDFDDVPPPPVAPETPAPAQNR	-2.848	meiotic chromosome segregation [GO:0045132]
scc-3	VNYTDMAAGNNSVEKEPVFR	-2.936	meiotic chromosome segregation [GO:0045132]
top-1	SVVSNHHSNGNGNSTVYDTNGNDEIK	-3.055	meiotic chromosome segregation [GO:0045132] microtubule cytoskeleton [GO:0015630]
dnc-1	MANLNSQIQDQK	-3.277	actin cytoskeleton [GO:0015629] microtubule cytoskeleton [GO:0015630]
dpy-28	DSSTVENLMKAMNGVTEK	-3.39	meiotic chromosome segregation [GO:0045132]
ttn-1	ASSSAATAR	-3.448	actin cytoskeleton [GO:0015629]
xnd-1	AVTPPPILER	-3.467	meiotic chromosome segregation [GO:0045132]
klp-4	QEVAITNMLTKK	-3.577	microtubule cytoskeleton [GO:0015630]
srgp-1	QMTASIETR	-3.704	meiotic chromosome segregation [GO:0045132]
unc-84	SAYMKLTNYQQAPMETIHVR	-3.779	intermediate filament cytoskeleton [GO:0045111]
ifa-4	VQEIHTQNSRNCLEQNYAREEVK	-3.819	intermediate filament cytoskeleton [GO:0045111]
cyk-4	SILGPVTTSPATPLLAR	-4.063	meiotic cell cycle [GO:0051321] microtubule cytoskeleton [GO:0015630]

aspm-1	IVLQEMSSLGVPTDNVNAESIVGGKK	-4.629	meiotic cell cycle [GO:0051321] microtubule cytoskeleton [GO:0015630]
R08D7.1	HDSDNSPPRNR	-4.75	meiotic chromosome segregation [GO:0045132]
zyx-1	TYRANLQQLAQPKTR	-5.106	actin cytoskeleton [GO:0015629]
R31.2	ESTPMVTGDAVNMSEER	-5.755	actin cytoskeleton [GO:0015629]
evl-14	ETNGVSPKK	-8.637	meiotic chromosome segregation [GO:0045132]
myo-5	ANKGNQLMADLWADYATQEDVAAAAKDGK	-13.211	actin cytoskeleton [GO:0015629]
set-2	NFESLQQSSVYQTNSFRNPR	-13.744	meiotic chromosome segregation [GO:0045132]
MS2: enriched in *plk-2(vv44)* mutants			
F10C1.8	IYGRNAGEINLTPDSIVMESHASWGQGR	2.033	intermediate filament cytoskeleton [GO:0045111]
smc-4	TENAQFIIISLR	2.102	regulation of meiotic cell cycle [GO:0051445]
ifa-1	GNVSIHEASPDGK	2.163	meiotic cell cycle [GO:0051321] intermediate filament cytoskeleton [GO:0045111]
ebp-1	LRTIEVICQDNESIGNVEVNR	2.206	microtubule cytoskeleton [GO:0015630]
atx-2	RSNNHNNGTGWSVNDMFAANEKMNVVSTFK	2.22	meiotic cell cycle [GO:0051321]
unc-104	EGANINKSLTTLGLVISKLAEESTK	2.241	microtubule cytoskeleton [GO:0015630]
kca-1	NPAINEDGSDDEYSLVPLR	2.274	meiotic cell cycle [GO:0051321] microtubule cytoskeleton [GO:0015630]
lmn-1	LNLTQEAPQNTSVHHVSFSSGGASAQR	2.288	intermediate filament cytoskeleton [GO:0045111]
dpy-26	KIRPADVVPETIMTKIGAHIDDIVNK	2.305	meiotic chromosome segregation [GO:0045132]
cls-2	NLDMTPVKSPSTR	2.341	meiotic chromosome segregation [GO:0045132] microtubule cytoskeleton [GO:0015630]
Y19D2B.1	VSFIPFHNVCMLSDTTAIAEAWSRLDYK	2.416	microtubule cytoskeleton [GO:0015630]
icp-1	NAAYSGTPR	2.489	meiotic cell cycle [GO:0051321]
F17C11.10	APSPTVESLNEDQTNDGDESSSR	2.495	meiotic chromosome segregation [GO:0045132]
myo-6	LCSAIMHIGNSTFKQKPR	2.548	actin cytoskeleton [GO:0015629]

wip-1	EQFRTMRPLRPANDVKPTMYRR	2.61	actin cytoskeleton [GO:0015629]
paa-1	TAVIEGLHSSLTDLHVDEQDSVR	2.666	microtubule cytoskeleton [GO:0015630]
smk-1	KGDSPEYNDVSSTSNEEK	2.741	meiotic chromosome segregation [GO:0045132]
ttn-1	AESDDMGVYVCSATSVAGVDSTSSMVMIA KTTGTDSHLVIAQTADEK	2.897	actin cytoskeleton [GO:0015629]
aak-2	SSPGGETSTKQQQELK	2.902	regulation of meiotic cell cycle [GO:0051445]
prp-8	SGMSHDEDQLIPNLYRYIQPWEAEFVDSV R	2.967	meiotic chromosome segregation [GO:0045132]
hcp-1	DVPQSPVLPVK	3.113	meiotic chromosome segregation [GO:0045132] microtubule cytoskeleton [GO:0015630]
pab-1	ITGMMLEIDNSELIMMLQDSELFRSKVDE AASVLVSAQK	3.19	regulation of meiotic cell cycle [GO:0051445]
nab-1	RHSIQNLELIELR	3.208	actin cytoskeleton [GO:0015629]
kin-18	SRPSDTIQELIQRTKNMVLELDNFQYK	3.278	regulation of meiotic cell cycle [GO:0051445]
chc-1	EMIGDQQQVVIIDLADTANPTR	3.627	microtubule cytoskeleton [GO:0015630]
lig-4	EDTIFVAKHEEGSK	3.656	meiotic cell cycle [GO:0051321]
nmy-1	DRLSEEEQQNEK	3.807	actin cytoskeleton [GO:0015629]
npp-9	NIFSKPSILQPAPGTPK	3.836	microtubule cytoskeleton [GO:0015630]
smk-1	LEDETETEVESVDGGQEEK	3.953	meiotic chromosome segregation [GO:0045132]
mat-1	DIILNTSMVRLQLGRACFEQSEYR	4.093	meiotic cell cycle [GO:0051321]
coh-1	GETPLR	4.132	meiotic chromosome segregation [GO:0045132]
hcp-1	STKAMMDQEEHLAELVAKIESR	4.166	meiotic chromosome segregation [GO:0045132] microtubule cytoskeleton [GO:0015630]
unc-54	ALESMQASLETEAKGKAELLR	4.249	actin cytoskeleton [GO:0015629]
dnc-1	NSESTSRMVR	4.298	actin cytoskeleton [GO:0015629]
frm-5.1	NSLVPSR	4.347	meiotic chromosome segregation [GO:0045132]
unc-87	EEQPNATMETKVTGQGQPKR	4.377	actin cytoskeleton [GO:0015629] microtubule cytoskeleton [GO:0015630]

gld-2	IHLYRSAGTAPGGYTQCPSPYK	4.386	meiotic cell cycle [GO:0051321]
usp-48	CSDDVCDQCRQMEVDAQNGSENMRGLVR	4.387	regulation of meiotic cell cycle [GO:0051445]
D2045.5	SYCFMVMTLLGKDLMAHK	4.463	regulation of meiotic cell cycle [GO:0051445]
unc-15	SPSQAAFGAPFGSMSVADLGSLTR	4.56	actin cytoskeleton [GO:0015629]
let-92	RTPDYFL	4.561	meiotic cell cycle [GO:0051321] microtubule cytoskeleton [GO:0015630]
nmy-2	RTPGLIGHR	4.677	actin cytoskeleton [GO:0015629] microtubule cytoskeleton [GO:0015630]
scc-3	TKASMLFDSNLMDGFVQLLTGMADSQVR	4.827	meiotic chromosome segregation [GO:0045132]
smk-1	TEELSPK	5.005	meiotic chromosome segregation [GO:0045132]
capg-1	HAPTDQPGVDAYKQMLISMLMNVFYQK	5.333	meiotic chromosome segregation [GO:0045132]
Y46G5A.4	RMTQNPNYYNLQGTTHR	5.359	regulation of meiotic cell cycle [GO:0051445]
unc-44	HAISPSVASEVLSSHDDELAAHFVAESFEK	5.426	meiotic cell cycle [GO:0051321]
hum-1	IPVMGNVINQLNNMNLSGNGNSPAGRGPPPAR	5.561	actin cytoskeleton [GO:0015629]
cls-2	MLAGIVSEPNLSNAEIKSLGAVLNRLLGESTNQIVLESISSFVK	5.671	meiotic cell cycle [GO:0051321] microtubule cytoskeleton [GO:0015630]
myo-3	SRSEAERELEELTER	5.968	actin cytoskeleton [GO:0015629]
him-4	AFMSPIHQEFVGRDLNLSCTVESASAYTIYWVK	6.041	meiotic chromosome segregation [GO:0045132]
smc-4	EMIAQEKQYPNFPSSNEISK	6.069	regulation of meiotic cell cycle [GO:0051445]
smk-1	DSVAVSPK	6.206	meiotic chromosome segregation [GO:0045132]
mlc-4	ATSNVFAMFDQAQIQEFK	6.515	meiotic cell cycle [GO:0051321] actin cytoskeleton [GO:0015629]
snx-1	RFSDFLGLHGK	7.556	meiotic cell cycle [GO:0051321]
Y41E3.11	EHSEHSYDALQQTQK	8.352	regulation of meiotic cell cycle [GO:0051445]
mtr-4	FDGSDNRYITSGEYIQMAGRAGR	8.583	regulation of meiotic cell cycle [GO:0051445]
nmy-1	INFDMSGYISGANIEFYLLEK	8.777	actin cytoskeleton [GO:0015629]

top-1	SKGAEKSKPSTSK	9.432	meiotic chromosome segregation [GO:0045132] microtubule cytoskeleton [GO:0015630]
unc-15	ADLSVQVIALTDRLEDAEGTTDSQIESNR	9.504	actin cytoskeleton [GO:0015629]
zyg-9	KIDPIMPGTLEARMPQEDEAVVVR	10.272	meiotic cell cycle [GO:0051321] microtubule cytoskeleton [GO:0015630]
rnp-5	MSPMR	10.325	regulation of meiotic cell cycle [GO:0051445]
rsa-2	IDKLTQAQLAIHQLVSSQPFSGDPYNQR	11.14	meiotic cell cycle [GO:0051321] microtubule cytoskeleton [GO:0015630]
dpy-28	APPPAQSDEDDSDSDDAPAAPRSAARR	11.318	meiotic chromosome segregation [GO:0045132]
ttn-1	LSNVSFKVSASEGKVFETR	12.036	actin cytoskeleton [GO:0015629]

Table 4. List of predicted PLK-2 targets.

Phosphopeptides which had a significant adjusted *p*-value (< 0.05) from the **limma** test and a fold change greater than 2 were considered enriched. Phosphopeptides which had a significant adjusted *p*-value (< 0.05) from the **limma** test and a fold change less than -2 were considered depleted. These lists were further filtered for phosphopeptides which belonged to proteins that were annotated with a GO term related to meiosis or the cytoskeleton using the **PANTHER Classification System** (Amigo *v2.2.24*) (Mi et al., 2013). Candidates were organized based on which MS they were isolated from, in which mutant strain they were found to be differentially regulated and whether they were enriched or depleted in that strain. To obtain the average fold changes for a phosphopeptide, the average of the log ratios of abundance in the mutant referenced over wild type were calculated. The final candidate list contains 126 phosphopeptides from 89 proteins.

Table 5

Enriched for motif?	ISE	SSP	STP
adjusted *p*-values	$p < 0.05$	$p > 0.05$	$p < 0.05$

Table 5. There is statistical support for an enrichment of the predicted PLK-2 docking motifs, `ISE` and `STP`, in the set of proteins which in the list of predicted PLK-2 targets which are depleted in *plk-2(K65M)* worms compared to wild type.

Fisher's exact test was used to compare the frequency of the predicted PLK-2 docking motifs (Figure S1) in the full sequences from our list of predicted PLK-2 targets from MS1 and MS2 which are depleted in *plk-2(K65M)* mutants (Table 4) compared to the prevalence of the motifs within the entire *C. elegans* proteome (contingency tables are in Figure S2). The *p*-values were adjusted using the FDR multiple hypothesis correction.

Supplemental Figures **Figure S1**

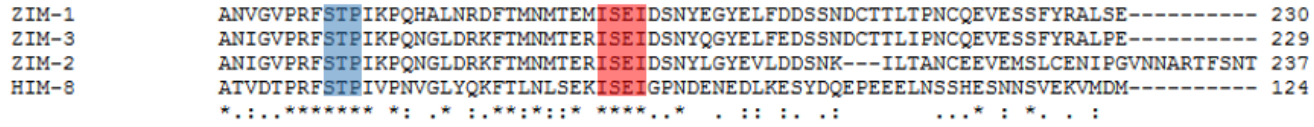

Figure S1, related to Table 5. Multiple sequence alignment of the *C. elegans* PC proteins shows conserved regions which are predicted PLK-2 docking sites.

Multiple sequence alignment was performed using **M-coffee** with the *Mclustalw_msa*, *Mmuscle_msa* and *Mt_coffee_msa* settings. Sequences for each protein were obtained from WormBase (2016). Predicted PLK-2 docking sites are highlighted in blue and red. Symbols beneath sequences depict the level of conservation. "." means low conservation. ":" means medium conservation. "*" means high conservation. A blank space underneath the sequence means no conservation.

Figure S2

Protein Sequence Sets	with ISE	without ISE	Row Total
Depleted in *plk-2(K65M)*	9 32.14 %	19 67.86 %	28
Proteome – depleted in *plk-2(K65M)*	3180 11.97 %	23393 88.03 %	26573
Column Total	3189	23412	26601
p-value	$p < 0.00413$		
p-adjusted	$p < 0.012390$		

Protein Sequence Sets	with SSP	without SSP	Row Total
Depleted in *plk-2(K65M)*	8 28.57 %	20 71.43 %	28
Proteome – depleted in *plk-2(K65M)*	3917 14.74 %	22656 85.26 %	26573
Column Total	3925	22676	26601
p-value	$p < 0.056$		
p-adjusted	$p < 0.056$		

Protein Sequence Sets	with STP	without STP	Row Total
Depleted in *plk-2(K65M)*	8 28.57 %	20 71.43 %	28
Proteome – depleted in *plk-2(K65M)*	3439 12.94 %	23134 87.06 %	26573
Column Total	3447	23154	26601
p-value	$p < 0.02231$		
p-adjusted	$p < 0.033465$		

Figure S2, related to Table 5. Contingency tables used for the Fisher's exact tests which aimed to evaluate whether there was statistical support for an enrichment of each predicted PLK-2 motif in the protein sets resulting from the MSs.